Wearable Antennas and Wireless Sensing Systems for e-Textile Applications

A thesis submitted to The University of Manchester for the degree of

Doctor of Philosophy

in the Faculty of Science & Engineering

2021

Yutong Jiang

School of Engineering/Department of Electrical & Electronic Engineering

Contents

List of Figures

List of Tables

List of Abbreviations

AC	Alternating Current
ADS	Advanced Design System
BAN	Body Area Network
BSN	Body Sensor Network
CMOS	Complementary Metal–Oxide–Semiconductor
CRLH	Composite Right/Left-Handed
DC	Direct Current
EBG	Electromagnetic Band-Gap
ECG	Electrocardiogram
EEG	Electroencephalograms
EHF	Extremely High Frequency
EM	Electromagnetic
EMG	Electromyography
EMI	Electromagnetic Interference
GSM	Global System for Mobile Communications
HF	High Frequency
IC	Integrated Circuit
IFF	Identify Friend or Foe
IoT	Internet of Things
ISM	Industrial, Scientific and Medical
LTE	Long Term Evolution
MBAN	Medical Body Area Network

NFC	Near Field Communication
PC	personal computer
PDPU	Personal Data Processing Unit
P-FCB	Planar Fashionable Circuit Board
Q	Quality
RF	Radio Frequency
RFID	Radio Frequency Identification
SCMs	Sensor Communication Modules
UHF	Ultra-High Frequency
WBAN	Wireless Body Area Network

Abstract

Smart textile or electro-textile (e-textile) is defined as fabrics constructed entirely or partially by electrically conductive material, which can be integrated with clothing as a part of body-worn electronics. The main features of e-textile that make it so desirable are its flexibility, durability and high corrosion resistance as a type of daily carry-on electronic device. Over the past decade, e-textile antennas have gained tremendous attention. The close-body nature of such antennas possesses great potential in various fields such as daily communication, personal healthcare and body area networks (BANs). However, due to flexible structures of the e-textile, it can be easily affected by body movements. Therefore, the challenges exist in the application of wearable antennas are the factors that are difficult to predict and control. The purpose of this thesis is to present comprehensive study into multiple types of e-textile integrated antennas and their real-life applications, including NFC antennas integrated body sensing device, RFID antennas and broadband monopole antennas integrated body-worn energy harvesting systems. This thesis is comprised of three main research areas.

The first area of this work focuses on the development of novel e-textile embroidered wearable near-field communication RFID antennas, which includes antenna design through full electromagnetic wave simulation, fabrication with conductive treads and textile substrates and measurements under various circumstances such as mechanical bending and human body effects. The measurement results show that the proposed NFC antenna is able to operate under significant degree of bending as well as direct skin contact attributed to its broad operating bandwidth. Distinguished from conventional NFC antennas, e-textile NFC antennas are ensured to be capable of communicating at desired operating frequency of 13.56 MHz while placed on almost any place on clothes. Based on this design, a smart textile integrated wireless powered near field communication (NFC) body temperature and sweat sensing system has also been developed. In this research, temperature and sweat sensors are embedded and powered by an e-textile NFC antenna enabling battery-free and wireless sensing operation. The proposed device is seamlessly integrated with close-fitting garments and the sensor data can be acquired with NFC readers and smart phones, which achieves real-time health monitoring in a convenient and non-intrusive way. The sensor data can be accessed with maximum read distance of 6 cm. The on-body accuracy of the temperature and sweat sensors is measured as ±0.14°C and ±0.2%, respectively. The proposed device aims to

provide ubiquitous wireless and battery-free connectivity for daily healthcare and wellbeing monitoring.

The second area includes design, fabrication and measurements of e-textile integrated antennas for various applications. Two designs are presented in this part. The first one is a machine embroidered wearable e-textile wideband UHF RFID tag antenna. The antenna read distance is above 6.5 m between 860 MHz and 960 MHz. The tag reading has been tested both in air and on body where the maximum read distance are 7.23 m and 4.71 m, respectively. The second design is a novel e-textile integrated wideband monopole antenna that aims to be applied in body-worn RF energy harvesting systems. The proposed antenna is constructed with silver coated conductive threads woven into cotton substrate. A novel dual circular patch structure is introduced to achieve a wide operating bandwidth which covers GSM bands (range 870.4-915 MHz and 1.7-1.9 GHz), LTE bands (range 0.79–0.96 GHz; 1.71–2.17 GHz; and 2.5–2.69 GHz) and Wi-Fi frequencies (2.4 and 3.6 GHz).

The last area under investigation is to develop a functional on-body ambient RF energy harvesting system by combining an e-textile antenna array with a multiband low-input rectifier. The antenna array is constructed with two identical broadband monopole antennas, which achieves relatively high gain and efficiency at most occupied ambient RF frequency bands. A compact six-band rectifier is integrated with the textile antenna with corresponding working frequencies. Experimental results show that the harvesting device performs stably with low input power down to -20dBm, and it is able to generate highest DC power of -11.67 dBm with a wireless power source at a single frequency (0.9 GHz).

This work has successfully demonstrated design and performance of a number of novel e-textile fabricated antennas and antenna-based electronics (wireless sensors and RF energy harvester). The challenges over this topic such as human body effects and external forces that might be taken by the antennas have been discussed and overcome. This work is believed to be a great contribution to the field of wearable electronics.

Declaration

No portion of the work referred to in the thesis has been submitted in support of an application for another degree or qualification of this or any other university or other institute of learning.

All published papers included in this thesis have been given permission to be reused.

Copyright Statement

i. The author of this thesis (including any appendices and/or schedules to this thesis) owns certain copyright or related rights in it (the "Copyright") and he has given The University of Manchester certain rights to use such Copyright, including for administrative purposes.

ii. Copies of this thesis, either in full or in extracts and whether in hard or electronic copy, may be made only in accordance with the Copyright, Designs and Patents Act 1988 (as amended) and regulations issued under it or, where appropriate, in accordance with licensing agreements which the University has from time to time. This page must form part of any such copies made.

iii. The ownership of certain Copyright, patents, designs, trademarks and other intellectual property (the "Intellectual Property") and any reproductions of copyright works in the thesis, for example graphs and tables ("Reproductions"), which may be described in this thesis, may not be owned by the author and may be owned by third parties. Such Intellectual Property and Reproductions cannot and must not be made available for use without the prior written permission of the owner(s) of the relevant Intellectual Property and/or Reproductions.

iv. Further information on the conditions under which disclosure, publication and commercialisation of this thesis, the Copyright and any Intellectual Property and/or Reproductions described in it may take place is available in the University IP Policy (see http://www.campus.manchester.ac.uk/medialibrary/policies/intellectual-property.pdf), in any relevant Thesis restriction declarations deposited in the University Library, The University Library's regulations (see http://www.manchester.ac.uk/library/aboutus/ regulations) and in The University's policy on presentation of Theses.

Acknowledgement

First of all else, I would express my sincere gratitude to my main supervisor Professor Zhirun Hu, who has provided me invaluable support, advise and opportunities throughout my Ph.D. study. You have always been encouraging and generous, and you've always believed in the best in me. I have learned so much from you both academically and personally. It is a great honour to be your student, and I could never achieve where I am without you. Secondly, I would like to thank my second supervisor Professor Henry Yi Li, for the generous support and academic guidance you have given to me.

I would also like to thank my parents, who have always supported and encouraged me. Your help, understanding and faith in me make me feel loved all the time. Thank you for always being proud of me even when I make mistakes, and I am grateful for everything you've done.

Special thanks are paid to my brilliant and lovely colleagues and friends, Dr. Kewen Pan, Dr. Ting Leng, Miss Yixian Fang and Miss Xinyao Zhou, for always being there for me and all the enjoyable moments. Particularly I would like to thank Miss Lulu Xu, for all her help during my experiments. Many thanks should also be paid to Mr. Derrick Bradshaw from the PCB workshop for always being nice to me and fabricating my circuits efficiently and perfectly.

Last but not least, the financial support from UK Engineering and Physical Research Council, EU Graphene Flagship Program and the EEE Department of The University of Manchester is gratefully acknowledged.

List of Publication

[1] “e-Textile embroidered wearable near-field communication RFID antennas”
Y. Jiang, L. Xu, K. Pan, T. Leng, Y. Li, L. Danoon, Z. Hu
IET Microwaves, Antennas & Propagation, vol. 13, no. 1, pp. 99-104, 2019
doi: 10.1049/iet-map.2018.5435.

[2] "Smart Textile Integrated Wireless Powered Near Field Communication Body Temperature and Sweat Sensing System"
Y. Jiang, K. Pan, T. Leng and Z. Hu
IEEE Journal of Electromagnetics, RF and Microwaves in Medicine and Biology, vol. 4, no. 3, pp. 164-170, Sept. 2020
doi: 10.1109/JERM.2019.2929676.

[3] "A Novel e-textile Integrated Wideband Monopole Antenna for Body-worn Energy Harvesting Systems"
Y. Jiang, T. Leng, Y. Fang, L. Xu, K. Pan and Z. Hu,
2019 IEEE MTT-S International Microwave Symposium (IMS), Boston, MA, USA, 2019, pp. 1057-1059
doi: 10.1109/MWSYM.2019.8700860.

[4] "Machine Embroidered Wearable e-textile Wideband UHF RFID Tag Antenna"
Y. Jiang, T. Leng, Y. Fang, Z. Hu and L. Xu
2019 IEEE International Symposium on Antennas and Propagation and USNC-URSI Radio Science Meeting, Atlanta, GA, USA, 2019, pp. 643-644
doi: 10.1109/APUSNCURSINRSM.2019.8889354.

[5] "On the design of metamaterial radar absorber applying AMC by controlling surface resistance"
Y. Fang**, Y. Jiang**, K. Pan and Z. Hu
2019 IEEE International Symposium on Antennas and Propagation and USNC-URSI Radio Science Meeting, Atlanta, GA, USA, 2019, pp. 1327-1328

doi: 10.1109/APUSNCURSINRSM.2019.8888926.

[6] "Dual Band Graphene Nanoflakes Printed Compact Monopole Antenna for Low Cost WIFI Applications"
T. Leng, K. Pan, **Y. Jiang**, Z. Hu, H. OUSLIMANI and M. A. Abdalla
2019 IEEE International Symposium on Antennas and Propagation and USNC-URSI Radio Science Meeting, Atlanta, GA, USA, 2019, pp. 1287-1288
doi: 10.1109/APUSNCURSINRSM.2019.8889034.

[7] "Graphene Printed UWB Monopole Antenna for Wireless communication applications"
K. Pan, T. Leng, **Y. Jiang**, Y. Fang, X. Zhou, M. A. Abdalla, H. Ouslimani, Z. Hu
2019 IEEE International Symposium on Antennas and Propagation and USNC-URSI Radio Science Meeting, Atlanta, GA, USA, 2019, pp. 1739-1740
doi: 10.1109/APUSNCURSINRSM.2019.8888805.

Chapter 1 Introduction

1.1. Motivation of this work

Nowadays, body worn electronics have been vastly developed in order to catch up with ever increasing data usage and achieve ultimately convenient, secure and personal services. Such devices are applied in numerous of fields, such as personal media, health monitoring, wireless data exchange and electronic bill payments. As it shows in Fig. 1-1, there are numerous types of wearable electronics due to the large available body area. Most of the body worn electronics, particularly those implanted on clothes, are expected to be light weight, durable, conformable and skin-friendly. During the past decade, increasing types of advanced materials, such as carbon materials, quantum dot light-emitting diodes and metal nanowires, have been contributed to wearable electronics [1]-[4].

Fig. 1-1. Wearable electronics [5].

E-textile integrated electronics, as a general concept of combining electronic device with closing-fitting garments, have been widely developed over recent years. The definition of e-textile (or smart textile) is fabrics that enable digital components and electronics to be embedded in them, which is normally formed with conductive yarns and applied within daily clothing. The close-fitting property of e-textile electronics is especially desirable in forms of antennas and body sensors for fields of emergency first-responder personnel such as military, hospital and astronauts [6-8].

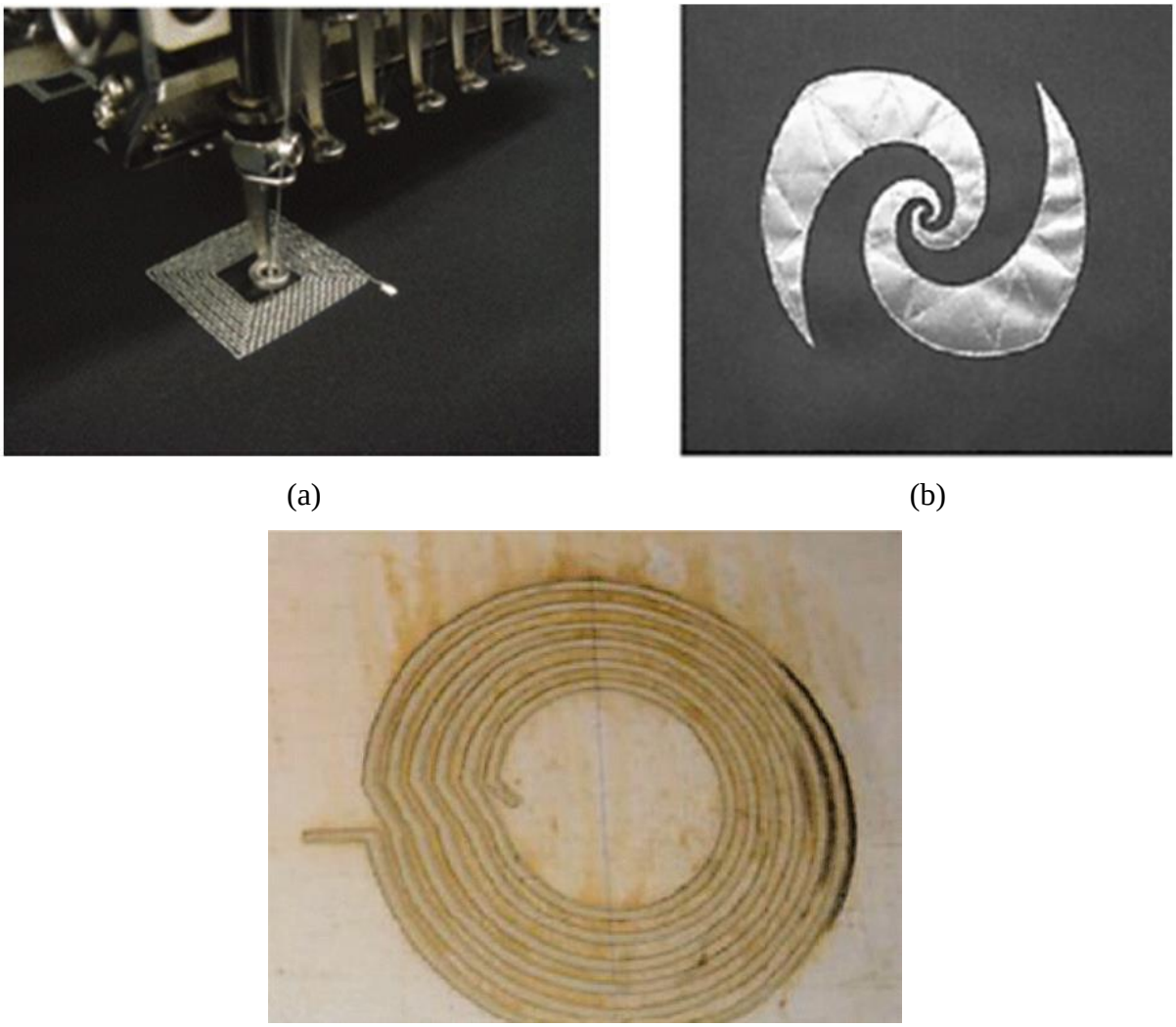

(a) (b)

(c)

Fig. 1-2. Fabrication methods of e-textile antennas: (a) conductive yarns (b) metal-coated fabric patches (c) Silver-printed inductive coil on cotton fabric [6].

The most common fabrication methods for e-textile antenna circuits are conductive yarn embroidery, metal-coated fabric patches integration and ink-jet metal printing as it presents in Fig. 1-2, where conductive yarn embroidery is considered particularly suitable for both

antenna fabrication and sensor implantation due to the ease of structure modification, high durability and toughness towards external forces.

For the convenience provided by e-textile based wearable electronics in modern life and their real-time application which makes great contribution to Internet of Things (IoT), it has been desirable to introduce new and advanced closed-body electronics into our daily life in a more sufficient and subtle way. This work is innovated by the idea of integrating electrically conductive threads with fabric of daily clothing using machine embroidery, which functions as wearable antennas and electronic devices based on antennas, such as wireless sensing systems and even wearable power generator.

In the design process of e-textile antennas, the most challenging aspect is that the device may become electrically unstable under external forces due to its conformable structure. Therefore, the most suitable designs to start with are NFC and UHF RFID antennas for their small sizes and wide range of applications. On the other hand, the large available body area on the back of clothing is suitable for implanting far-field radiating broadband e-textile antennas with larger sizes since this part of the body take minimum effects from skin contacts and body movements, where e-textile RF energy harvesters (rectennas) can be applied. The greatest challenge exists in developing e-textile integrated far-field rectennas is the antenna efficiency can be compromised due the extra power loss within conductive threads. At present, there are no reported designs that focus on RF energy harvesting using purely e-textile embroidered broadband antennas.

So far, about 211 journal paper and 826 conference papers have been published in IEEEXPLORE about textile antennas, among which there is only 1 conference paper focused on e-textile NFC antennas, 22 journal papers and 96 conference papers for RFID tags and 2 conference papers for e-textile RF energy harvesters [9]. However, very few of these papers are based on conductive thread embroidery. As a newly-developing topic in wearable electronics, novel antennas structures, detailed antenna properties and performance are expected to be studied for e-textile integration.

1.2. Aim and objectives

The aim of this work is to design and fabricate novel e-textile integrated antennas as well as to develop wearable devices based on these antennas which can be applied into daily life. The objectives of the research in this thesis are:

- To develop an e-textile NFC antenna that is suitable for daily wearing, for which antenna structure, textile material selection, manufacturing process and antenna performance under various circumstances should all be considered.
- To achieve a relatively wide operating bandwidth for an NFC antenna.
- To analyse the performance of an NFC antenna response to external forces such as bending and pressure.
- To verify how the read distance of e-textile RFID and NFC antennas respond to skin and clothe contact.
- To integrate e-textile NFC antenna and compact wearable sensing device for wireless battery-free near field sensing applications.
- To increase the voltage acquired from an e-textile NFC antenna in order to power external sensors.
- To develop an e-textile embroidered UHF RFID tag antenna with relatively wide operation bandwidth.
- To develop a broadband e-textile antenna that covers multiple ambient power frequency bands, which can be applied into a wearable energy harvesting system.
- To take advantage of the large body area for applying a highly functional e-textile RF energy harvester.
- To develop a functional wearable RF ambient energy harvesting devices for low power electronic applications.
- To achieve a minimum usage of e-textile material while maintaining the antenna performance for a low cost application.

1.3. Thesis outline

This thesis contains 8 chapters that mainly focus on design, simulation, fabrication and measurements of e-textile integrated NFC antennas, RFID antennas, and broadband

monopole antennas along with the developed applications based on these antennas. Chapter 1 presents the background of this work, motivation and objectives of the research in this thesis. In Chapter 2, an overview of wearable electronics for body worn communication with a detailed literature review of the state-of-art development of electronic textile, antenna designs, rectenna designs and body sensors for these applications is presented. Chapter 3 describes the methodology applied in this work, including design procedures and experiments that are not fully covered in the publications. The detailed findings are presented in Chapters 4 to 7 in forms of scientific publications.

- Chapter 4 presents the development of a novel e-textile integrated NFC antenna. The antenna is designed based on the parameters of selected textile material for antenna body and substrate and simulated through full electromagnetic wave model. The proposed antenna is fabricated with silver coated conductive thread and cotton and measured with both VNA and NFC reader for S-parameters and read distance. The antenna measurements under mechanical bending and human skin contact shows that it performs properly while placed on skin as well as under significant bending angle due to its relatively wide operating bandwidth.
- Chapter 5 presents a smart textile integrated wireless powered NFC body temperature and sweat sensing system which is developed based on the NFC antenna discussed in Chapter 4. The proposed sensing device composed a temperature sensor and a sweat sensor integrated with an e-textile NFC antenna where the sensor data can be acquired simultaneously. Since the temperature sensor is built in the microchip matched to the NFC antenna, a voltage booster is connected between the sweat sensor and the antenna in order to produce a steady voltage source. Distinguished from conventional wearable sensors, the proposed wearable sensing system provides anytime wireless connectivity for point-of-care and battery-free operation.
- Chapter 6 discusses the development of two types of machine embroidered e-textile antennas. The first part presents an e-textile fabricated wideband UHF RFID tag antenna. The antenna is designed to be matched to the RFID chip between 860 and 960 MHz. The read range of the tag has been measured in air, with vicinity to human body and on sleeve. Although the tag performance can be affected as it is placed closely to human body, it still can be read within a steady distance at the desired frequency range. The second part presents a novel e-textile monopole antenna which is designed for energy harvesting applications. The antenna body is designed in a shape of combination of two

circular patches, which is able to operate in a wide bandwidth (0.5 to 5 GHz). Both simulated and measured radiation patterns of the antenna at various frequency range are presented and discussed. The proposed antenna is considered suitable as a receiving antenna to be applied in an energy harvesting device which aims for ambient RF power in frequency bands that includes GSM bands (range 870.4-915 MHz and 1.7-1.9 GHz), LTE bands (range 0.79–0.96 GHz; 1.71–2.17 GHz; and 2.5–2.69 GHz) and Wi-Fi frequencies (2.4 and 3.6 GHz).

- Chapter 7 presents the development of a novel wearable energy harvesting system constructed with a pure e-textile broadband dual antenna array and a compact six-band rectifier. The textile antennas are seamlessly integrated with skin friendly cotton substrate, which is wearable for relatively large body area in order to harvest ambient RF energy. The operating bandwidth of the proposed device covers the most occupied RF power generating frequency bands. This system aims for providing constant DC power for body sensors, which has the potential to be applied in various fields as a part of body area network.

At last, Chapter 8 summarises the major contributions of this thesis. The limitations and future work based on this research are discussed.

1.4. References

[1] Wang, Chunya et al. "Advanced Carbon For Flexible And Wearable Electronics". Advanced Materials, vol 31, no. 9, 2018, p. 1801072. Wiley, doi:10.1002/adma.201801072.

[2] Kim, Jaemin et al. "Ultrathin Quantum Dot Display Integrated With Wearable Electronics". Advanced Materials, vol. 29, no. 38, 2017, p. 1700217. Wiley, doi:10.1002/adma.201700217.

[3] Hong, Sukjoon et al. "Highly Stretchable And Transparent Metal Nanowire Heater For Wearable Electronics Applications". Advanced Materials, vol. 27, no. 32, 2015, pp. 4744-4751. Wiley, doi:10.1002/adma.201500917.

[4] Lee, Seulah et al. "Stretchable Electronics: Ag Nanowire Reinforced Highly Stretchable Conductive Fibers For Wearable Electronics (Adv. Funct. Mater. 21/2015)". Advanced Functional Materials, vol. 25, no. 21, 2015, pp. 3105-3105. Wiley, doi:10.1002/adfm.201570139.

[5] Manners, David. "Quicklogic Upgrades Sensor Hub". Electronics Weekly, 2020, https://www.electronicsweekly.com/news/business/finance/quicklogic-upgrades-sensor-hub-2014-09/.

[6] Jung-Sim Roh, Yong-Seung Chi & Tae Jin Kang. “Wearable textile antennas”. Smart Textiles, vol 3, no. 3, 2010, pp. 135-153, International Journal of Fashion Design, Technology and Education, doi: https://doi.org/10.1080/17543266.2010.521194

[7] Lina M Castano and Alison B Flatau. “Smart fabric sensors and e-textile technologies: a review”. Smart Mater, vol. 23, no. 5, 2014, IOP, doi: https://doi.org/10.1088/0964-1726/23/5/053001

[8] Stoppa, Matteo, and Alessandro Chiolerio. "Wearable Electronics And Smart Textiles: A Critical Review". Sensors, vol 14, no. 7, 2014, pp. 11957-11992. MDPI AG, doi:10.3390/s140711957.

[9] IEEE Xplore Search Results". Ieeexplore.Ieee.Org,2020, https://ieeexplore.ieee.org/search/searchresult.jsp?newsearch=true&queryText=textile%20antenna. Accessed 20 Feb 2020.

Chapter 2 Literature Review

2.1. RFID Antennas

The first idea of radio frequency identification (RFID) technology can be tracked back to World War II. The Germans discovered a method of changing the radio signal reflected back from the German planes in order to identify these planes from enemy aircrafts. Afterwards, the British developed the first active identify friend or foe (IFF) system based on this method. The implanted transmitter on each British plane began to broadcast a signal back that identified the aircraft as friendly once it received signals from radar stations on the ground. This system established the basic concept and the two main types of RFID technology: when a signal is sent to a transponder, it responds with either reflecting back a signal (passive system) or broadcasting a signal (active system) [1].

(a) (b)

Fig. 2-1. Examples of RFID tags: (a) active [8] (b) passive [9].

Examples of active and passive RFID devices are presented in Fig. 2-1. Active RFID devices, such as the transponders attached to aircrafts mentioned above, require a power source (most commonly an integrated battery). Therefore, the lifetime of the tags is limited to the stored energy. In commodity markets, passive RFID tags have raised more interest due to their battery-free operation, indefinite life-time and small sizes [2]. Till this day, RFID technology

has been applied in diverse industries, such as shipment tracking, inventory control [3], healthcare [4] and distributed sensors [5]. This technology is still evolving to become more sufficient and worldwide with the development of mobile platforms [6] and Internet of Things (IoT) [7].

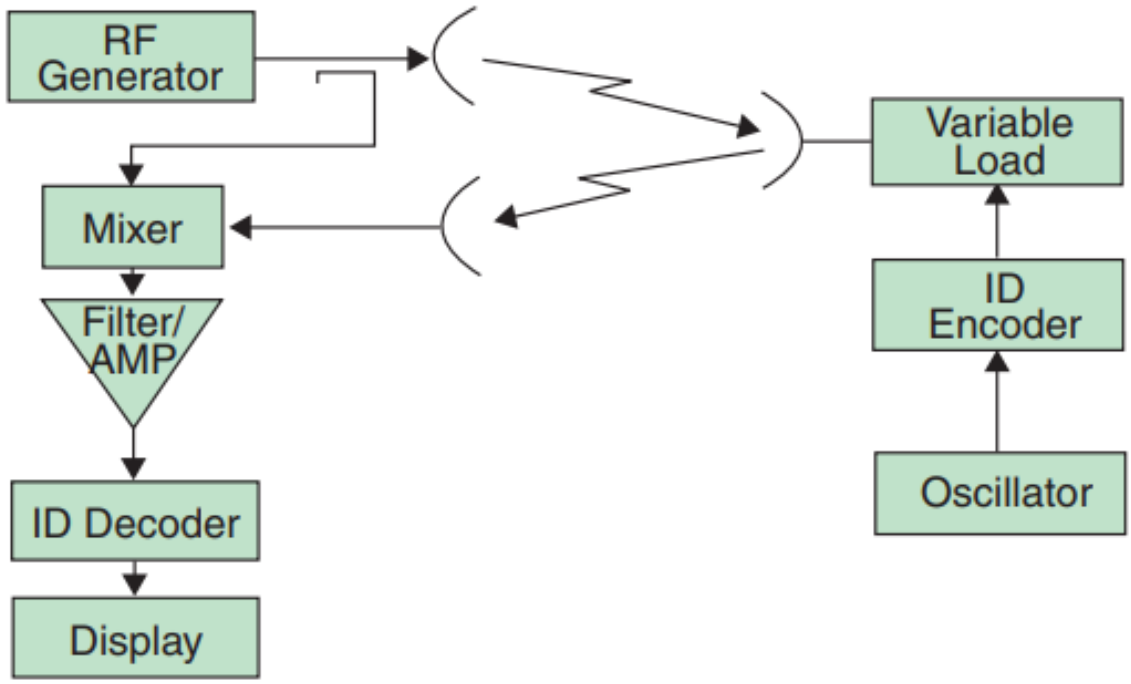

Fig. 2-2. Functional blocks for reading data from a backscatter RFID tag: left: reader; right: tag [11].

In RFID technology, several frequency bands have been standardized: Low-frequency (LF, 125-134 kHz) and high-frequency (HF, 13.56 MHz) systems are the most developed and globally applied technology, which are based on quasi-static magnetic flux coupling between the reader's and tag's coils. The devices operate in the high-frequency band (13.56 MHz) are also called near field communication (NFC) tags, which will be further introduced in Section 2.2. Ultra-high-frequency (UHF, 860-960 MHz) and microwave (2.4 GHz and 5.8 GHz), as emerging technologies, employ electromagnetic interaction among true antennas and permit longer communication distance [10]. A typical RFID system can be defined by the principle of modulated backscatter as it presents in Fig. 2-2. The tag reading of this system operates as follows: after the tag receives an unmodulated signal sent by the reader, it reads its internal memory of stored data and changes the loading on the tag antenna in a coded manner corresponding to the stored data, and the signal modulated with this coded information is then reflected from the tag and acquired by the reader [11].

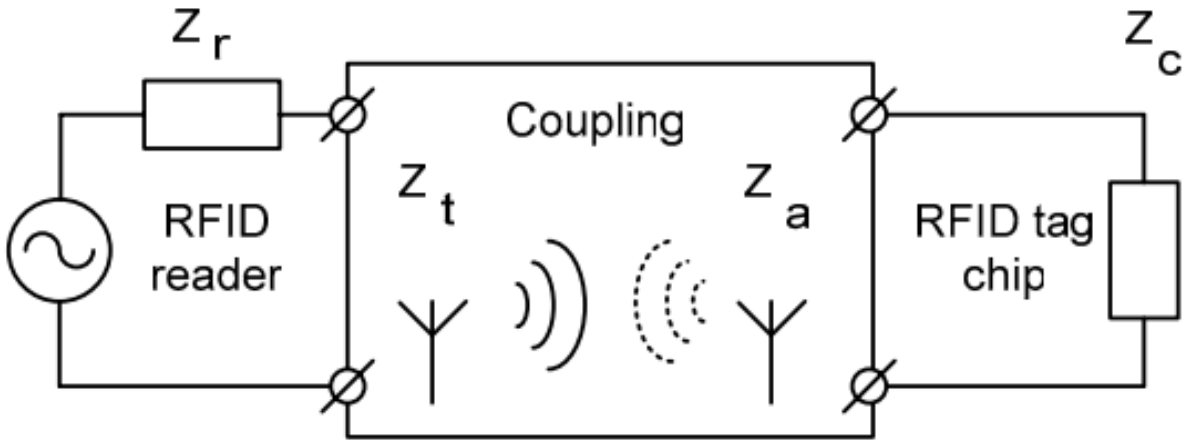

Fig. 2-3. Antenna coupling for general RFID [12]: $Z_r = R_r + jX_r$ is the reader output impedance (usually 50 Ω), $Z_t = R_t + jX_t$ is the transmitting antenna impedance, $Z_a = R_a + jX_a$ is the tag antenna impedance, and $Z_c = R_c + jX_c$ is the chip impedance.

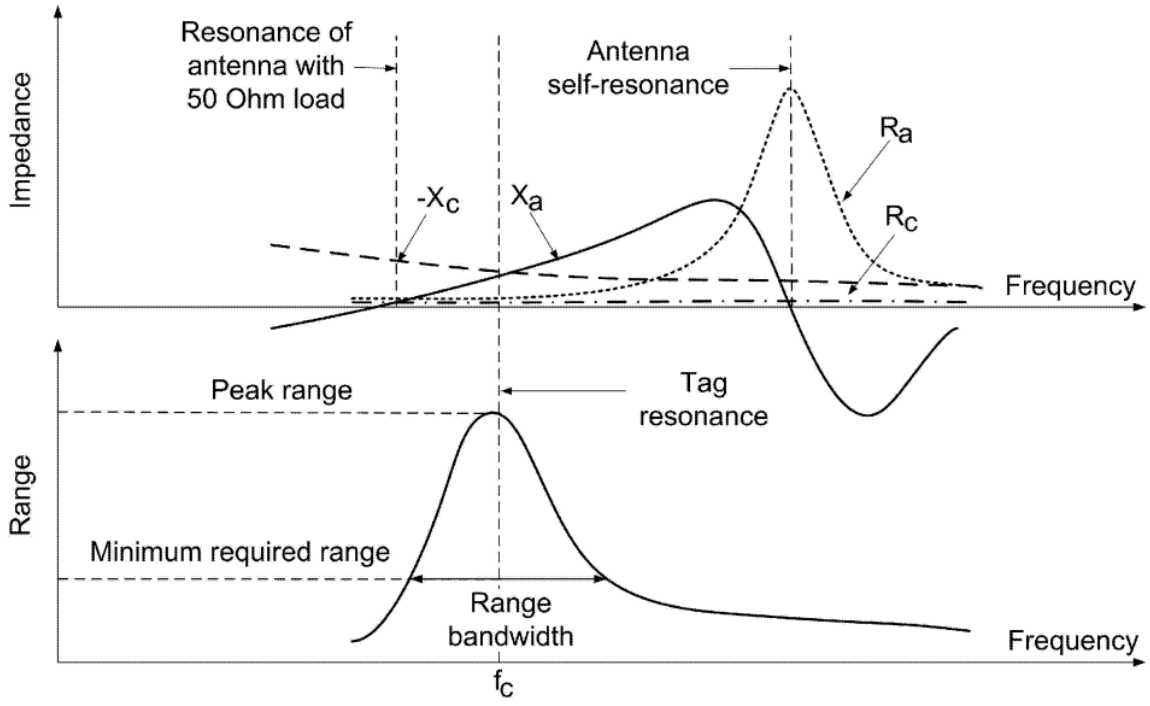

Fig. 2-4. Antenna impedance, chip impedance, and range as functions of frequency for a typical RFID tag [20].

The antenna coupling mechanism for general RFID can be represented with a conventional linear two-port network as it presents in Fig. 2-3 where the coupling coefficient is the transmission loss between two ports [12]. For UHF RFID antennas (860-960 MHz) with desirable read range, the most essential part of the design is the conjugate matching between

the antenna impedance and the tag impedance. As shown in Fig. 2-4, a typical dipole RFID antenna is capacitive at low frequencies and becomes inductive as it reaches radiative region where it can be matched with the chip capacitance. Consequently, the read range and the bandwidth of the matched antenna can be determined.

In recent years, with the development of wireless body area networks (WBAN), the integration of UHF RFID antennas with e-textile materials has been brought to sight [13]-[15], aiming to realize truly wearable and real-time applications such as body sensors [16] [17], smart clothing [18] and indoor positioning and localization [19]. In this work, an e-textile integrated UHF RFID antenna will be presented in Chapter 6, and the design, properties and measurements will be discussed in detail.

2.2. NFC antennas

During the past decade, as smart phones have been developed with NFC reading functions, Near Field Communication (NFC) has become a necessity in daily short-range communication smartphone scanning alongside with a variety of typical applications, such as ID cards, credit cards, itemized commodities and hotel room keys [21].

The main function of an NFC system is the contactless communication between the NFC tag and the reader as a wireless short-distance information acquirement. The first development of NFC can be traced back to the year of 1970 when it was initially named "Short-Range Radio-Telemetry for Electronic Identification Using Modulated Backscatter" [11]. This technology has been developed based on RFID (radio frequency identification) ever since. In 2004, Nokia cooperated with Sony and Philips and established the NFC Forum, promoting the security, ease of use, and popularity of near field communication. Afterwards, the first set of specifications for NFC tags was produced by the group in 2006 [24]. NFC tags are passive devices with small sizes, like a sticker, and the information of which is mostly read-only for the access of NFC readers and NFC compatible smart phones while certain tags allow read-and-write operation in the scanning process.

As an embranchment of RFID technology, NFC tags possess a shorter communication range for security reasons and they have developed along with NXP semiconductors (capacitive microchips) [25]. Fig. 2-5(a) presents a typical design of an NFC tag as a small-sized sticker, and a typical model of NXP diodes connected within the tag is shown in Fig. 2-5(b). The operating frequency of an NFC tag antenna is typically set at 13.56 MHz. A passive NFC tag

operates by the transmitted power from the reader [26]. As it is shown in Fig. 2-6, magnetic induction coupling is applied between the tag antenna and the reader antenna within a short distance to draw its necessary operating power for the IC chip on the tag from the reader's electromagnetic field. Circuits with high quality factors would significantly improve the efficiency of this power transfer [27]. NFC tag antennas possess a working distance that is typically around 10 cm and a data transfer rate around 424 Kbits/s for which the maximum value up to 848 Kbits/s [25].

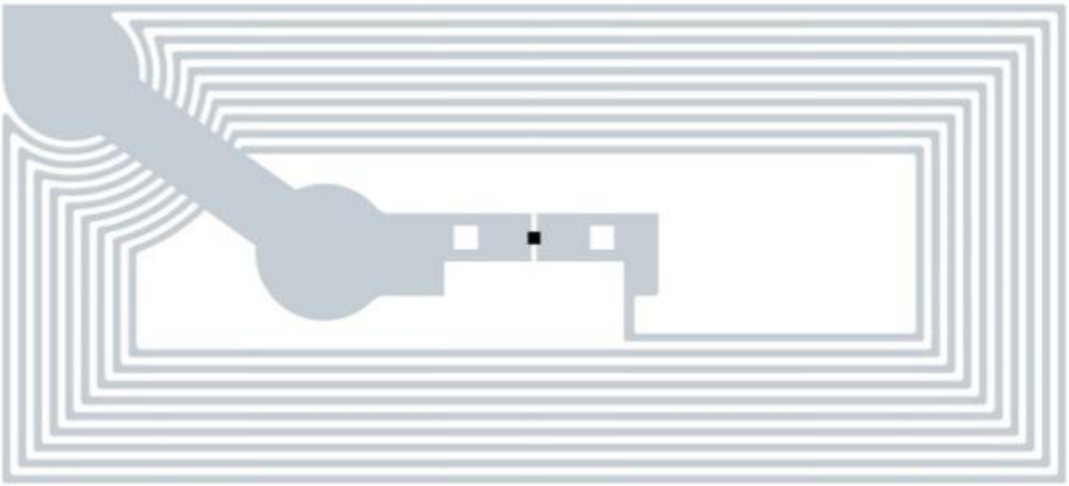

(a)

(b)

Fig. 2-5. (a) NFC antenna [22] (b) NXP diodes [23]

For a passive NFC tag, since there is no external battery attached, its read range depends on the minimum transmitted power that is needed to operate the tag circuitry. As a result, the main challenges in the design process are to minimize the power dissipated by the tag and to maximize the converting efficiency between the EM power from the reader and the DC power consumed by the tag [26].

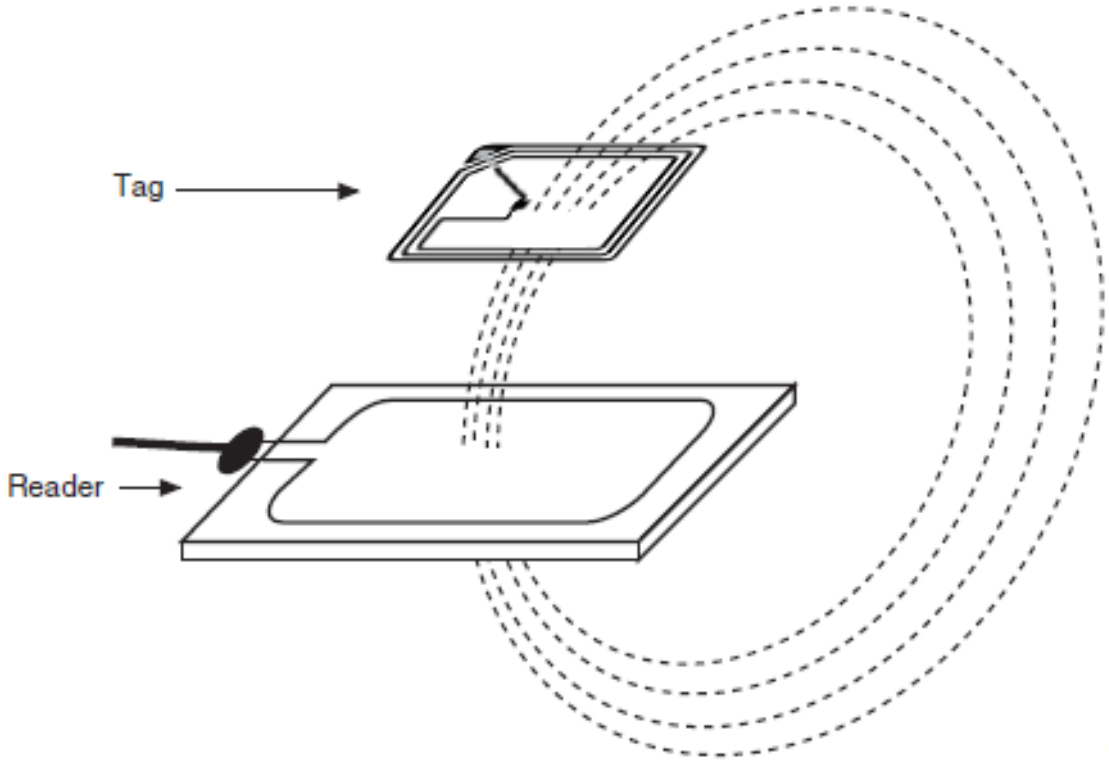

Fig. 2-6. Magnetic coupling between tag coil and reader coil.

Existing fabrication methods for NFC antennas, including chemical etching and screen printing have been working perfectly for mobile devices and simple electronics [28]. However, with the concept to apply NFC technology into everyday garments, the circuit design is expected to be light weight, flexible and most importantly, close fitting. In this case, the application of electro-textile has become a strong candidate as a method to achieve all the terms stated above.

Study of NFC antenna characteristics and the development of e-textile integrated NFC antennas will be demonstrated in detail in Chapter 4.

2.3. Wearable sensors

The concept of wireless body sensors has been developed over decades. Until this day, close-body sensors have become a powerful tool in health care applications that aim for prevention and early detection of diseases, providing maintenance for chronic conditions and fitness control, such as piezo sensors on the wrist for blood pressure testing [29] and shoe-mounted sensor system applicable for both health monitoring and sport performance with functional sensors attached [30]. A fully developed health care system based on such sensors is called a wireless body area network (WBAN) [31], which possesses great potential to interact with internet of things (IoT) and create new opportunities for the society [32] [33]. The popularization of close-body sensors is a great step forward in preventive healthcare since it constantly raises the users' awareness of their health status. In [34]-[36], WBANs consisting multiple sensors that detect medical signals such as electrocardiogram (ECG) and electroencephalograms (EEG) have been presented. The sensors are integrated with sensor communication modules (SCMs) in order to be connected with a personal data processing unit (PDPU) which passes the data to a PC or local network as it is shown in Fig. 2-7.

Fig. 2-7. Body area network consists of multiple sensors [34]

For the purpose of wireless communication, wearable antennas have also been developed for WBANs. For example, in [37], a compact antenna working in medical body-area network (MBAN) band (2.36 GHz to 2.4 GHz) is introduced for wearable applications. One of the greatest challenges of body-worn antenna is the effects toward performance caused by human body, which is mainly due to loading effect of lossy tissue. Therefore, it has provided a solution to induce an adapted meta-surface as not only isolating ground plane but also the main radiator.

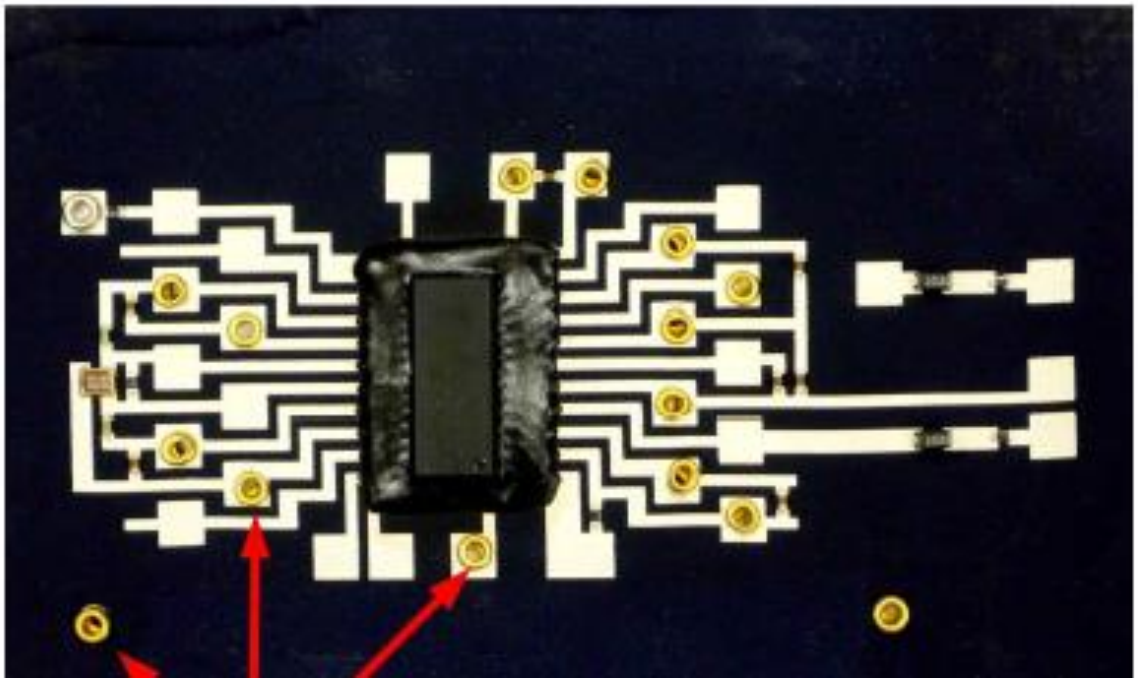

Fig. 2-8. P-FCB circuit [39].

For personal media applications, numerous of devices have been developed based on electronic textile and become a part of daily garments, such as clothing-based computers and MP3 systems [38]. [39] has proposed a textile MP3 player mainly composed by silkscreen printed circuit board on fabric patch, IC moulded with non-conductive epoxy and conductive adhesive connection as it presents in Fig. 2-8, for which the technology is adapted from planar fashionable circuit board (P-FCB).

During recent years, great interest has been raised in integrating sensors with daily worn textile materials since clothes are the most natural and necessary wearables in our daily life. However, in real-life applications, textile sensors usually face certain limitations since the deformable structure of textile can easily affect sensor performance under external forces such as bending and stretching. Among existing research of textile based sensors, mostly

aiming for monitoring pressure, body position electromyography (EMG) and heartbeat [40]-[43], the most desirable properties of such devices are not only the ability to provide a conveniently subtle way for real-time monitoring the patients' status without affecting one's daily life but also a straight forward instruction that benefits the users since they do not need to worry about placing the sensors [44] [45].

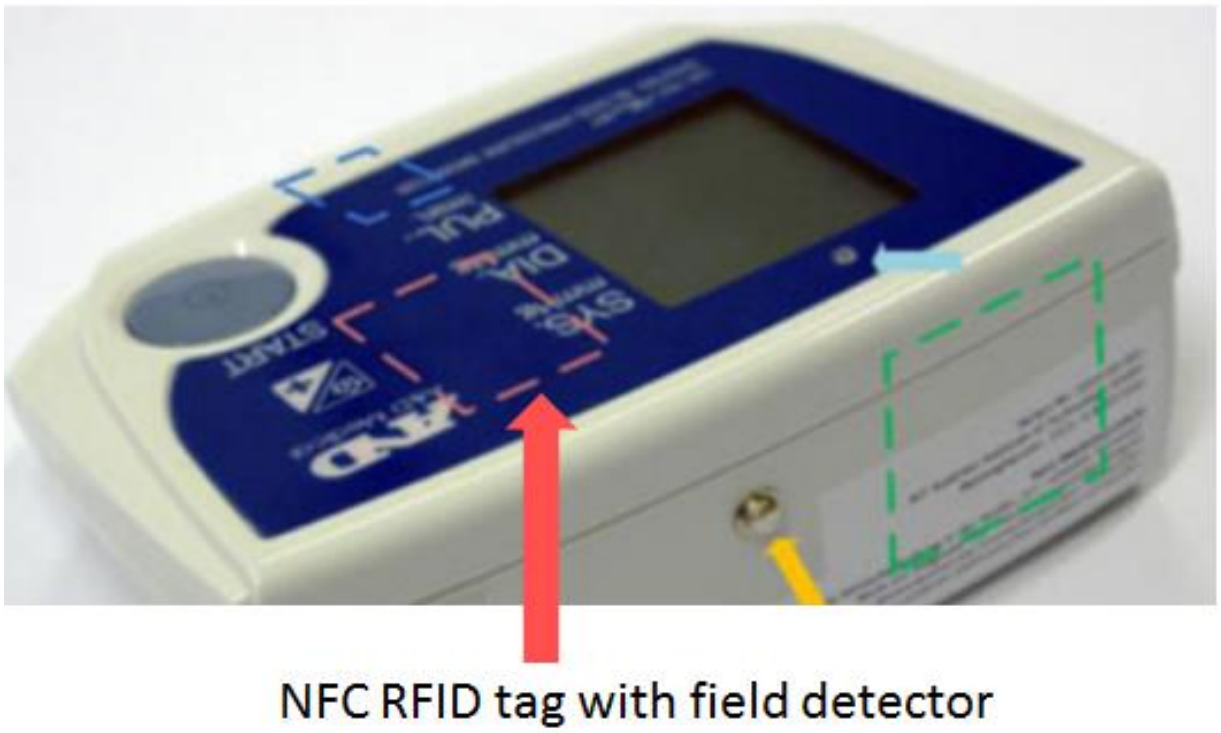

Fig. 2-9. Modified blood pressure meter with integrated μC with ECG amplifier, Bluetooth module and RFID tag with field detector [47].

Along with the development of wireless communication, NFC has been considered being one of the potential solutions in wireless health and wellbeing monitoring applications for its low cost, low power consumption, relatively simple structure and better usability [46]. As presented in [47], NFC has been applied in a blood pressure testing system as a wireless switch that enables Bluetooth communication between blood-pressure meters and mobile phones for the benefits of remote data storage, as shown in Fig. 2-9. However, in general health care system, wearable NFC enabled sensors possess the potential to achieve much more than that. In this thesis, a novel battery-free smart textile NFC enabled body temperature and sweatiness sensing system for health and wellbeing monitoring has been developed. The concept of applying textile based temperature and humidity sensors is inspired by [48]. This development focuses on daily heath care, work-out monitoring, and

accessing personal health status associated with excessive fever and sweating symptoms which are often caused by various kinds of infection, inflammation and trauma [49]. The detailed development of this system will be presented in Chapter 5.

2.4. e-Textile integrated antennas

2.4.1. Smart textiles and wearable antennas

e-Textiles (also called smart textiles) are defined as conductive fabrics that can be integrated as a part of wearable electronics or enable digital components and electronics to be embedded in them. The idea of e-textile was firstly brought up in the 90's when the penetration of electronics in our daily life was rapidly growing and introducing crossover research with other areas, and the textile industry was one of them [50]. Although integrating electronics with daily clothing can be achieved by employing conventional electronic circuits, it is limited by the maximum available substrate size, substrate rigidity and fragility [51]. Textile materials, on the other hand, as a fundamental and transformational component of people's life for centuries, have been considered an attractive medium for electronic integration. Till this day, e-textile has been applied in numerous of areas for sensing, actuating, adopting, communicating, self-healing, self-powering, memorizing, learning, etc. [52].

In the past 20 years, e-textile integrated wearable antennas have been increasingly popular in both electronic and textile industry as a novel production from integrated smart textile. The most significant challenges in developing e-textile antennas are due to the soft and absorbent nature of the textile material, such as the orientation of the textile breaks the planar properties of the antenna circuit while encountering external forces and fibres absorbing moisture from the surrounding environment and changing its morphology properties [53]. In the state-of-art development, various types of textile antennas have been introduced in order to realize off-body far-field communications [54]-[59], some of these devices are particularly designed for special professions, such as patch antennas applied in protective clothing for firefighters. Moreover, [60] presents an e-textile antenna array manufactured with non-woven conductive fabric, and [61] illustrates embroidered antennas based on metamaterial substrates. Typical fabrication methods for e-textile antennas are presented in Fig. 2-10.

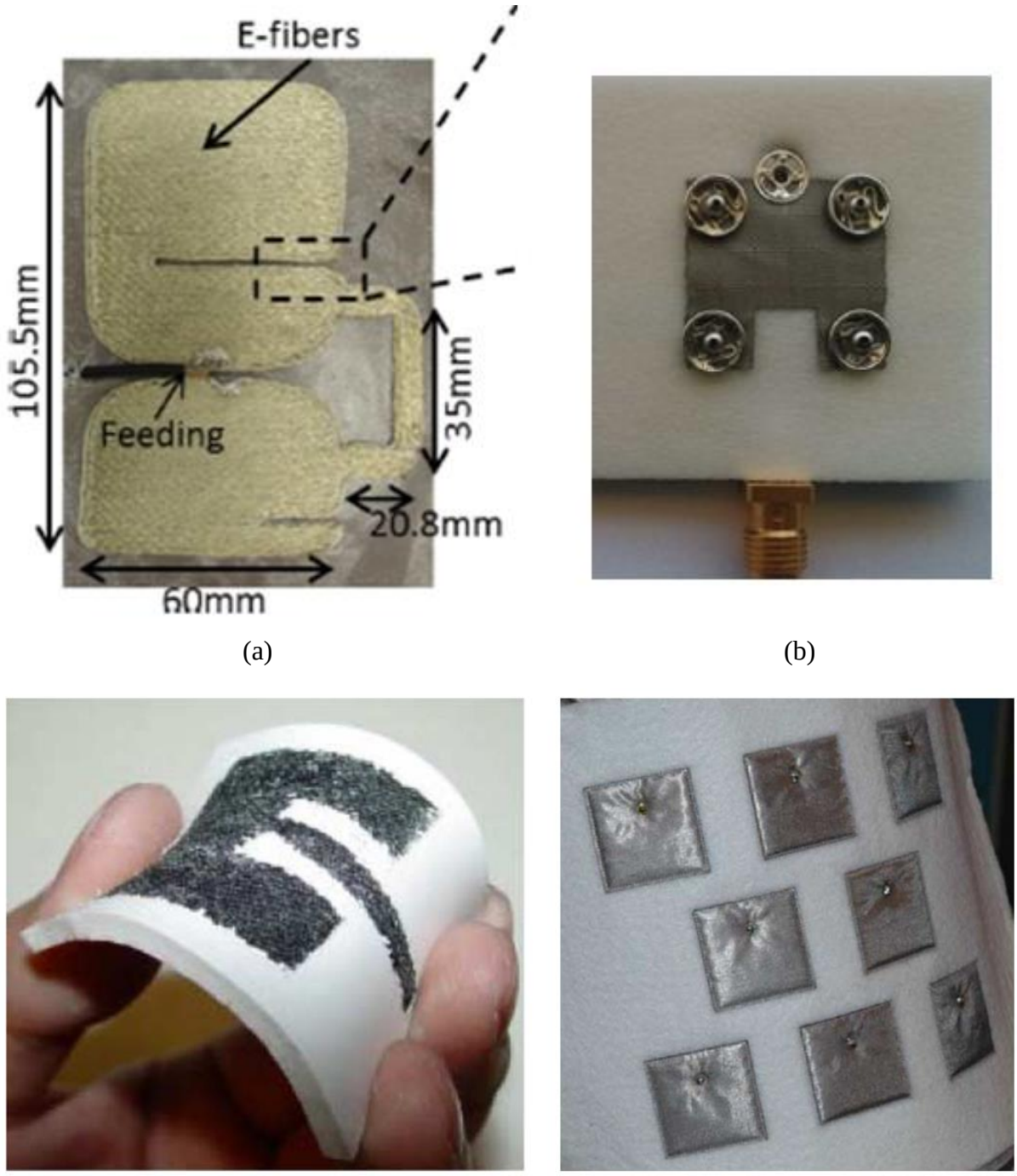

(a) (b)

(c) (d)

Fig. 2-10. Various fabrication methods for clothing integrated antennas (a) e-fibre textiles embroidered antenna [57] (b) Antenna loaded with a 2.45 GHz patch fabricated with metal-coated nylon RIPSTOP fabric as patch and ground plane and Cuming Microwave C-Foam PF-4 foam as substrate [58] (c) carbon nanotube coated e-textile printed on polymer-ceramic composites [59] (d) e-textile microstrip patch array with a conductive fabric affixed to a Nomex felt substrate [60].

Wearable UHF RFID tags have also been developed based on smart textiles for various applications, such as body sensing and health care [62]-[64]. In [65], an epoxy-coated copper fabric textile UHF RFID tag is introduced, and the reading range of which is tested before and after washing. It has been found that although the textile tag maintains a reading range of 7 m after 15 cycles of washing (8m before washing), the strong mechanical spinning still causes serious damage to the tag circuit and the microchip. Therefore, waterproofing and circuit protecting are considered as major objectives for future textile circuit design.

The most significant factor that differs the performance of e-textile antennas from conventional ones is the textile substrate which is mostly deformable and porous. Electrical permittivity ε is the most basic parameter for dielectrics, which is characterized with the material dielectric constant (ε_r) and the loss tangent ($\tan\delta$). Generally, the dielectric properties of textile material are affected by temperature, moisture, surface roughness and packing density of the fabrics [66] [67]. Most textiles possess fairly low dielectric constants and the fact that air fills up the gaps between fibres draws their permittivity closer to 1. For substrate materials, this property leads to less surface wave loss and therefore offers the antennas great potential to perform with high efficiency and gain [53]. The thickness of the textile substrate is also an essential factor for wearable antennas. As it reports in [55], the surface compression towards a textile patch antenna results in a working frequency shift in the return-loss characteristics. This raises another challenge that the performance of textile antennas could be unstable while facing substrate compression.

For textile antenna circuits, physical bending is also considered as an essential factor for the power propagation. Among existing work, antenna bending tests have been carried out in a number of researches such as [60], [68] and [69], which aim to observe how the antenna gain would be affected under external forces. In these researches, the antenna circuits are measured while bent around a cylinder with a certain radius (U bend method) in order to simulate their performance on arms, legs and shoulders as it presents in Fig. 2-11. The results from these experiments have shown that the resonant frequencies of all tested antennas would increase with the degree of bending, and the input-match bandwidth would also become slightly different. According to the measurement comparison in [68], patch antennas take more influence from bending in comparison to EBG antennas and U-slot antennas since the patch structure is more substrate-dependent, which are considered less suitable to be implanted in wearables.

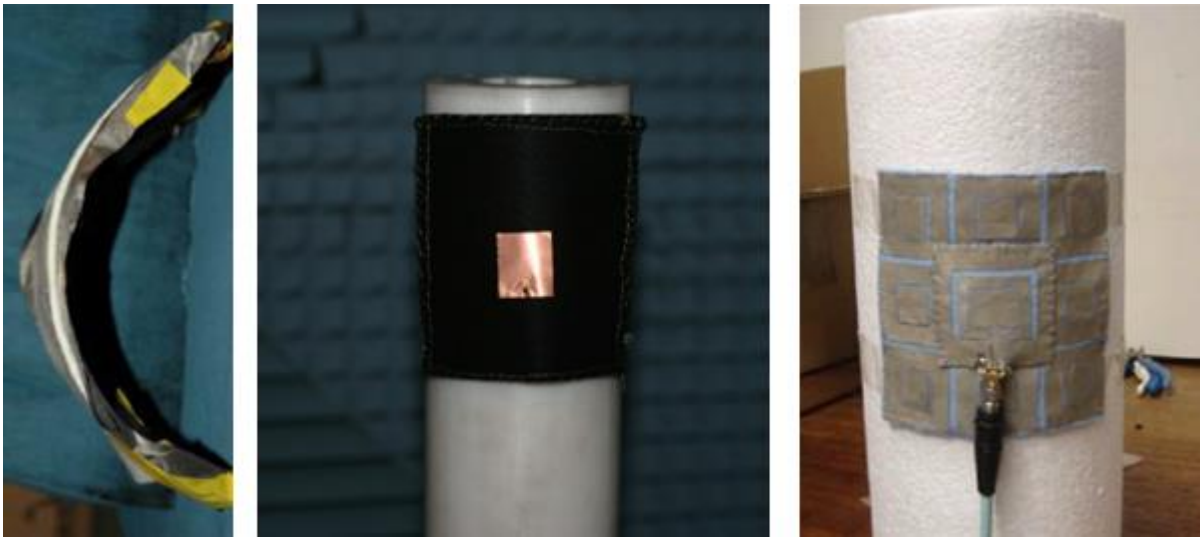

(a) (b) (c)

Fig. 2-11. Antenna bending tests set up of (a) e-textile microstrip patch array [62] (b) patch antenna on fabric substrate [68] (c) EBG textile antenna [69].

2.4.2. Conductive fibers and embroidery techniques

In recent years, conductive fibres (conductive threads) have become widely popular as a type of fundamental material for e-textile fabrication. e-textile produced with conductive thread is considered particularly suitable for planar close-body electronics such as electromagnetic interference (EMI) shielding, wearable antennas and health-monitoring sensors due to its low cost, high precision in shaping and great fitness to daily clothing [70].

The production of conductive threads can be easily achieved with a solid metal wire or common insulating threads with metal film coating up to 1μm thick. The downside of such methods is that the threads can be easily broken not only during the fabricating process but also under multiple bends and stretches [71]. Alternatively, conductive polymer and carbon nanotube have been applied as textile coatings in order to achieve high flexibility [72] [73]. However, the conductive polymer has been tested to be easily corroded in air and moisture. Moreover, due to the relatively high resistivity, none of these materials are considered the best choice for highly conductive wearable circuits.

Since the most desirable properties of conductive threads are high conductivity for circuit performance, high flexibility and toughness to withstand the embroidering process, researchers have developed a method of producing conductive threads by coating polyamide

threads with metallic nanoparticles such as silver, gold and platinum, among which silver has been most commonly used due to its reasonable price, low resistivity and high resistance towards corrosion. Naturally, conductive threads produced with this method would never achieve the same conductivity level with pure metal since the nanoparticle size leads to numerous of inter-particle junctions [74]. Such junctions can be reduced by replacing the nanoparticles with metallic nanowires [71].

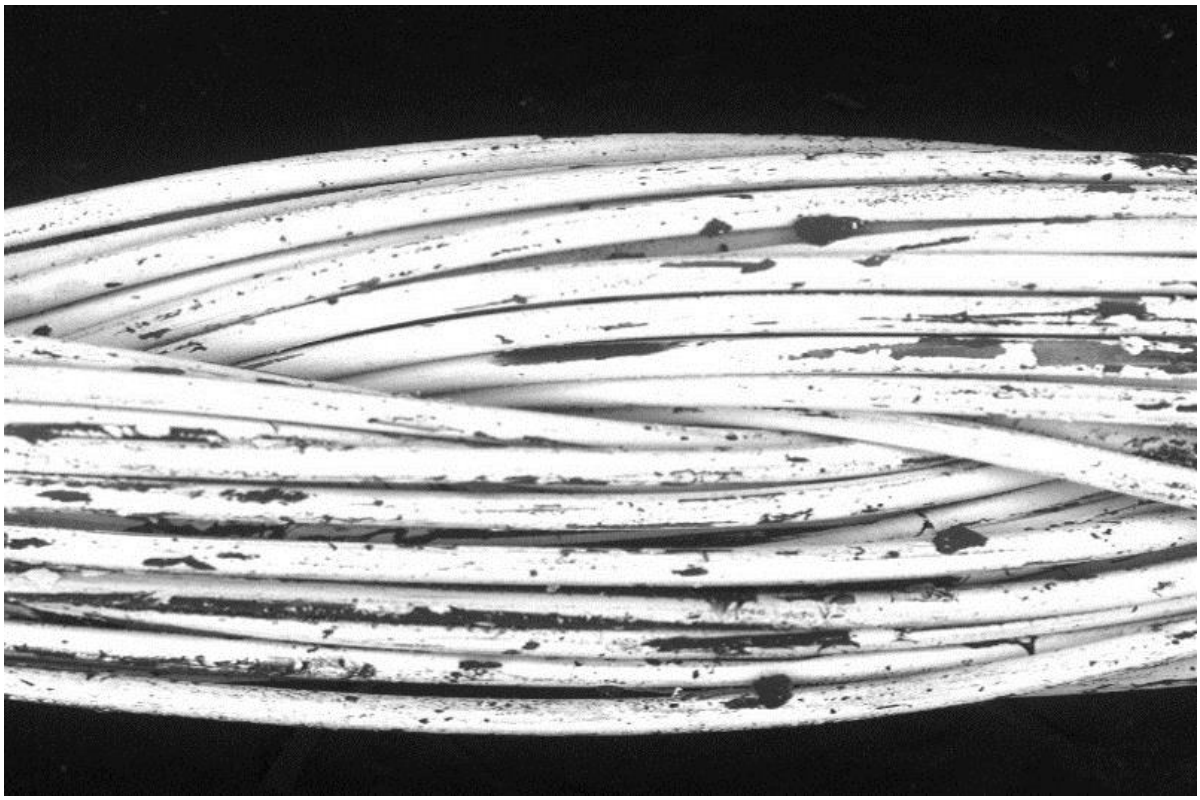

Fig. 2-12. Digital images of conductive yarns with 500× magnification.

Fig. 2-12 presents a magnified image of typical silver coated polymer conductive yarns. It can be seen that a single conductive thread is evenly constructed by numerous of extremely thin yarns, the purpose of which is to achieve stable resistance, strength and flexibility. On the other hand, it also gives the conductive threads a relatively loose structure that could be affected by stretching and compression.

As listed in Fig. 2-13, e-textile devices can be fabricated with conductive threads using various techniques, each of which provides specific features for different circuit properties [75]. Among all these methods, machine embroidery is considered the most suitable for body-worn antennas fabrication for the following reasons: I. The antenna shape can be precisely controlled; II. According to [76], one of the essential requirements for the

conductive fabrics of textile antennas is the sheet resistance must be homogeneous over the antenna area, which can be more easily achieved using an embroidery machine with high resolution; III. A relatively low sheet resistance of the conductive textile can be achieved by increasing the packing density of the conductive threads using machine settings.

Detailed fabrication and performance of machine embroidered e-textile antennas will be presented in Chapter 6 and Chapter 7. The average measured sheet resistance of the proposed antennas is 0.4 Ω/sq, which meets the standard of e-textile for antenna design [77].

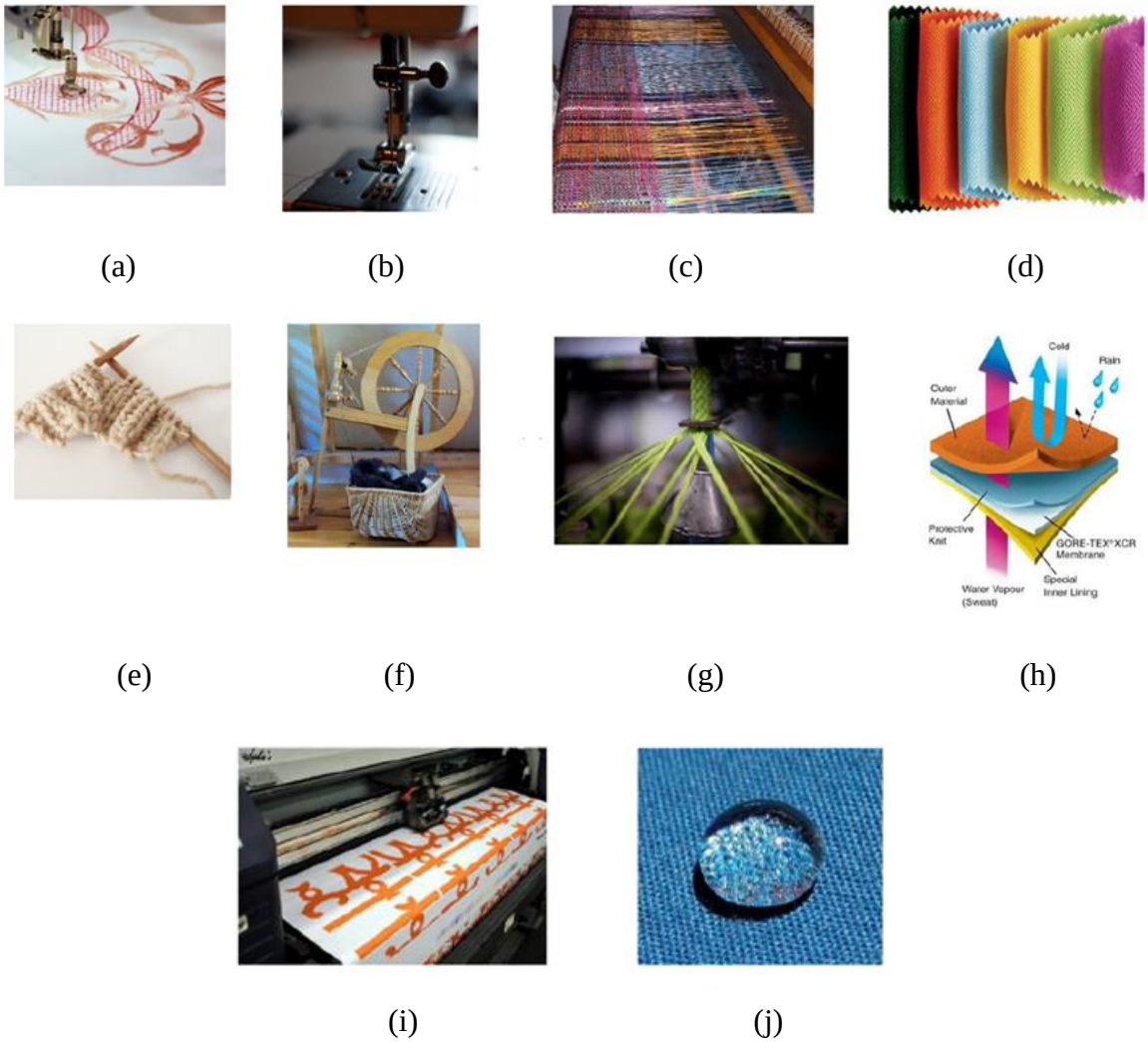

(a) (b) (c) (d)

(e) (f) (g) (h)

(i) (j)

Fig. 2-13. Different kinds of textile/fabric manufacturing and treatment. (a) Machine embroidery; (b) sewing; (c) weaving; (d) non-woven; (e) knitting; (f) spinning; (g) breading; (h) coating/laminating; (i) printing and (j) chemical treatment [75].

2.5. RF Energy harvesting

During recent years, the world has been facing a series of crucial energy-related issues mainly due to the high energy demand and enormous emission of carbon dioxide, such as climate change, ocean acidification, air pollution etc. In the meantime, RF energy harvesting has been raised as an alternative concept for solar converter since RF energy is widely available from numerous reliable electromagnetic resources. It is believed that collecting ambient RF power as DC power supply for low power consuming electronics would eventually reduce worldwide traditional electric energy consumption and environmental pollution [78].

Table 2-1. Peak ambient power level survey [79]

Application	Frequency (MHz)	Indoor		Outdoor	
		Power level (dBm)	Power Density ($\mu W/m^2$)	Power level (dBm)	Power Density ($\mu W/m^2$)
Broadcasting	150–600	-54	0.005	-27.6	2.18
GSM900 (MTx)	860–915	-28.41	34.5	-8.99	300
GSM900 (BTs)	925–960	-37.5	5.91	-19.87	290
GSM1800 (MTx)	1710–1785	-60.1	0.091	-43.3	4.37
GSM1800 (BTx)	1805–1880	-45.4	3.15	-40.89	8.9
3G (MTx)	1920–1980	-51.55	0.82	-31.07	91.9
3G (BTx)	2110–2140	-49	1.7	-21.45	100
Wi-Fi	2400–2500	-42.4	10.7	-47.75	3.15

Rectifying antennas (rectennas) are the most essential parts in RF energy harvesting systems. A rectenna fundamentally consists of a receiving antenna and a rectifier that converts the collected RF energy into DC power. The peak ambient power level and power density of the most occupied RF generators in a semi-urban environment is summarized in Table 2-1 [79], where the frequency bands with the highest power density outdoor are GSM900 and 3G. Till now, most of the existing rectennas have been focusing on collecting GSM (850-900MHz, 1710MHz-1930MHz) and ISM (2.45GHz and 5.8 GHz) signals. Some of the recenna designs

operate in single narrow band, such as the work reported in [80]-[82]. However, the available power to be harvested for a single band rectenna is rather limited. For the purpose of increasing the output power level, dual-band, multi-band and broadband rectennas have been developed in [83]-[85], where it is presented that the output power level of such rectennas are considerably higher than single band ones.

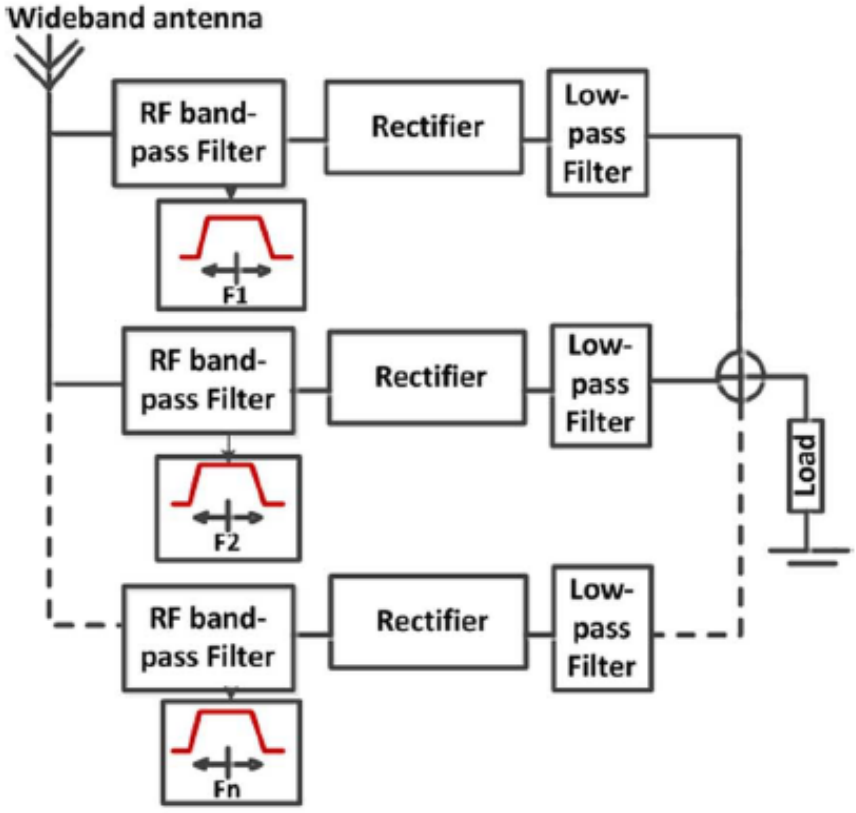

Fig. 2-14. Rectenna structure with multiple rectifying circuits [86].

Since rectifiers possess strong nonlinearity, their impedance usually varies with the frequency over a large bandwidth, which can easily induce impedance mismatch and makes the design of multiband or broadband rectennas particularly challenging. In [86], a rectenna architecture has been proposed to solve this problem. As presented in Fig. 2-14, an RF bandpass filter is applied in each chosen frequency band of a single wide band antenna so that the rectifier impedance can be matched individually at the dedicated frequencies. Therefore, the availability of RF spectrum becomes less sensitive, and the RF-to-DC conversion efficiency is dramatically increased. At the end of each brunch, a low-pass filter is applied to block any additional RF signals and the DC outputs are summed up at the load. [87] has also illustrated a similar concept where an array of antennas with multiple working frequencies are

separately matched to rectifiers and the DC outputs of which are combined together to sum the harvested power, i.e. a DC combiner as it shows in Fig. 2-15.

Another challenge exists in RF energy harvester designing is that the efficiency of the rectifier tends to get low at a low input power level while the ambient RF power is mostly below -15 dBm. In order to solve this problem, the Schottky diodes selected for the rectifier should possess a low barrier i.e. high saturation current, which performs more efficiently at low input power levels than externally biased detector diodes [88] [89]. Another suitable approach is to apply complementary metal–oxide–semiconductor (CMOS) technology in the rectifier design and reducing the threshold in standard CMOS circuits. As reported in [90] and [91], the CMOS rectifiers achieve conversion efficiency of 23% at -20 dBm and 42.8 % at -16 dBm, respectively.

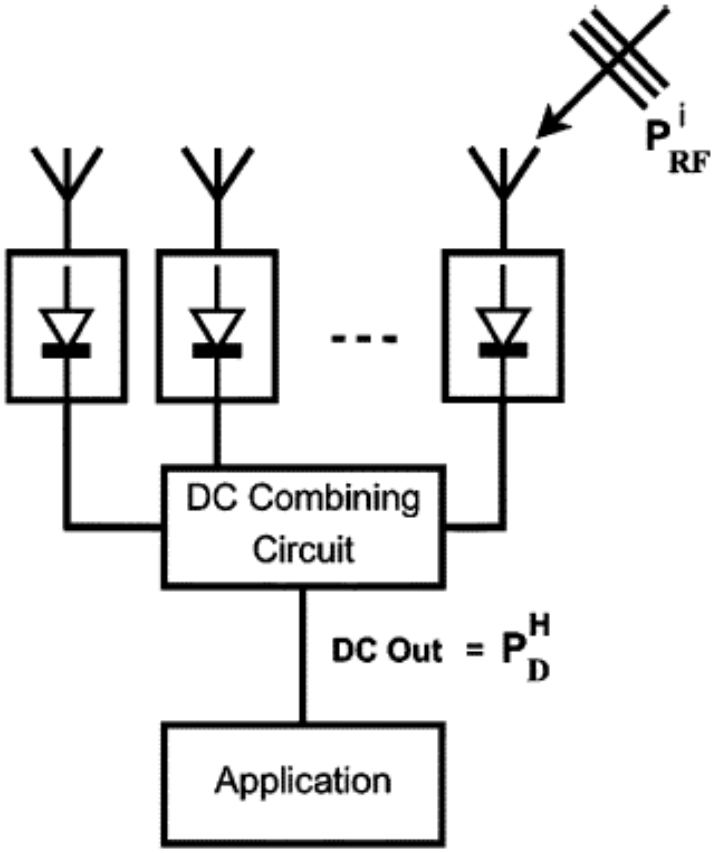

Fig. 2-15. A DC combining structure for energy harvesting [87].

For the purpose of personalized environmental friendly power supply for wearable electronic devices such as medical body sensors, RF energy harvesting devices designed to be integrated with daily wearables have been developed in recent years. In [92], a wearable UHF

patch rectenna made with non-woven conductive fabric and jean and pile substrate has been proposed, which works in frequency band of 860-918MHz with maximum efficiency of 50%. The rectenna model proposed in [93] and [94] operates in multi-frequency bands, including GSM900, GSM1800 and WIFI sources. In most recent works, the fully textile integrated rectenna reported in [95] is able to achieve power conversion efficiency of 41.8% at 820 MHz at -20dBm. Textile rectenna designs for signals of super high frequencies are presented in [96] and [97]. Among the research reported so far, wearable rectennas fabricated with conductive thread embroidery have hardly been discussed. In Chapter 7, the development an e-textile integrated RF energy harvesting system based on e-textile embroidered antenna array will be presented in detail.

2.6. Summary

In this chapter, some historic milestones, background theory and state-of-art development of RFID technology (UHF and NFC), wearable sensing, e-textile antennas and RF energy harvesting have been reviewed. It has been shown that wearable electronics based on e-textile applications has become significant to the field of modern communication, health care and even energy development. During the study of e-textile integrated antennas, it has been found that very few of the existing researches have been focused on NFC antennas and further applications based on wearable NFC antennas. Furthermore, the idea of developing e-textile integrated antennas as a part of advanced wearable systems, such as body sensing systems and RF harvesting systems, is still at an early stage with tremendous possibilities and potentials for further developments. The information presented in this chapter is essential for a better understanding of the existing achievements in wearable applications based on e-textile antennas and body sensors and identifying the key research challenges to focus on in this work.

2.7. References

[1] "The History Of RFID Technology | RFID JOURNAL". Rfidjournal.Com, 2020, https://www.rfidjournal.com/the-history-of-rfid-technology.

[2] R. Want, "An introduction to RFID technology," in IEEE Pervasive Computing, vol. 5, no. 1, pp. 25-33, Jan.-March 2006, doi: 10.1109/MPRV.2006.2.

[3] Zhu, Xiaowei et al. "A Review of RFID Technology and Its Managerial Applications In Different Industries". Journal of Engineering and Technology Management, vol 29, no. 1, 2012, pp. 152-167. Elsevier BV, doi:10.1016/j.jengtecman.2011.09.011.

[4] Haddara, Moutaz, and Anna Staaby. "RFID Applications And Adoptions In Healthcare: A Review On Patient Safety". Procedia Computer Science, vol 138, 2018, pp. 80-88. Elsevier BV, doi:10.1016/j.procs.2018.10.012.

[5] R. Nair, E. Perret, S. Tedjini and T. Barron, "A humidity sensor for passive chipless RFID applications," 2012 IEEE International Conference on RFID-Technologies and Applications (RFID-TA), Nice, 2012, pp. 29-33, doi: 10.1109/RFID-TA.2012.6404534.

[6] D. Lee, S. Kim, H. Kim and N. Park, "Mobile Platform for Networked RFID Applications," 2010 Seventh International Conference on Information Technology: New Generations, Las Vegas, NV, 2010, pp. 625-630, doi: 10.1109/ITNG.2010.188.

[7] X. Jia, Q. Feng, T. Fan and Q. Lei, "RFID technology and its applications in Internet of Things (IoT)," 2012 2nd International Conference on Consumer Electronics, Communications and Networks (CECNet), Yichang, 2012, pp. 1282-1285, doi: 10.1109/CECNet.2012.6201508.

[8] Smiley, Suzanne. "The Difference Between Active RFID & Passive RFID - Fundifix Solutions". Fundifix Solutions, 2020, https://fundifix.com/difference-active-rfid-passive-rfid/.

[9] "Uhf Rfid Tags". Indiamart.Com, 2020, https://www.indiamart.com/proddetail/uhf-rfid-tags-19983456133.html.

[10] G. Marrocco, "The art of UHF RFID antenna design: impedance-matching and size-reduction techniques," in IEEE Antennas and Propagation Magazine, vol. 50, no. 1, pp. 66-79, Feb. 2008, doi: 10.1109/MAP.2008.4494504.

[11] J. Landt, "The history of RFID," in IEEE Potentials, vol. 24, no. 4, pp. 8-11, Oct.-Nov. 2005, doi: 10.1109/MP.2005.1549751.

[12] P. V. Nikitin, K. V. S. Rao and S. Lazar, "An Overview of Near Field UHF RFID," 2007 IEEE International Conference on RFID, Grapevine, TX, 2007, pp. 167-174, doi: 10.1109/RFID.2007.346165.

[13] E. Moradi, T. Björninen, L. Ukkonen and Y. Rahmat-Samii, "Characterization of embroidered dipole-type RFID tag antennas," 2012 IEEE International Conference on RFID-Technologies and Applications (RFID-TA), Nice, 2012, pp. 248-253, doi: 10.1109/RFID-TA.2012.6404522.

[14] K. Koski, L. Sydänheimo, Y. Rahmat-Samii and L. Ukkonen, "Fundamental Characteristics of Electro-Textiles in Wearable UHF RFID Patch Antennas for Body-Centric Sensing Systems," in IEEE Transactions on Antennas and Propagation, vol. 62, no. 12, pp. 6454-6462, Dec. 2014, doi: 10.1109/TAP.2014.2364071.

[15] S. Ma, L. Ukkonen, L. Sydänheimo and T. Björninen, "Wearable E-textile split ring passive UHF RFID tag: Body-worn performance evaluation," 2017 IEEE Asia Pacific Microwave Conference (APMC), Kuala Lumpar, 2017, pp. 166-168, doi: 10.1109/APMC.2017.8251404.

[16] X. Chen, L. Ukkonen and T. Björninen, "Passive E-Textile UHF RFID-Based Wireless Strain Sensors With Integrated References," in IEEE Sensors Journal, vol. 16, no. 22, pp. 7835-7836, Nov.15, 2016, doi: 10.1109/JSEN.2016.2608659.

[17] X. Chen, H. He, Z. Khan, L. Sydänheimo, L. Ukkonen and J. Virkki, "Textile-Based Batteryless Moisture Sensor," in IEEE Antennas and Wireless Propagation Letters, vol. 19, no. 1, pp. 198-202, Jan. 2020, doi: 10.1109/LAWP.2019.2957879.

[18] X. Chen et al., "Electro-textile glove-tags for wearable RFID applications," 2017 International Symposium on Antennas and Propagation (ISAP), Phuket, 2017, pp. 1-2, doi: 10.1109/ISANP.2017.8228764.

[19] K. Koski, E. S. Lohan, L. Sydänheimo, L. Ukkonen and Y. Rahmat-Samii, "Electro-textile UHF RFID patch antennas for positioning and localization applications," 2014 IEEE RFID Technology and Applications Conference (RFID-TA), Tampere, 2014, pp. 246-250, doi: 10.1109/RFID-TA.2014.6934237.

[20] K. V. S. Rao, P. V. Nikitin and S. F. Lam, "Antenna design for UHF RFID tags: a review and a practical application," in IEEE Transactions on Antennas and Propagation, vol. 53, no. 12, pp. 3870-3876, Dec. 2005, doi: 10.1109/TAP.2005.859919.

[21] Coskun, Vedat et al. *Near Field Communication*. John Wiley & Sons Ltd, 2012.

[22] "Minitrack NFC | Avery Dennison | RFID". Smartrac-Group.Com, 2020, https://www.smartrac-group.com/minitrack-nfc.html.

[23] Rfid-Ready.Com, 2020, http://www.rfid-ready.com/201311228484/nxp-launches-esd-protection-diodes-for-nfc-antennas.html.

[24] "History Of Near Field Communication - Nearfieldcommunication.Org". Nearfieldcommunication.Org, 2020, http://nearfieldcommunication.org/history-nfc.html.

[25] K. Curran, A. Millar, and C. Mc Garvey, "Near Field Communication," International Journal of Electrical and Computer Engineering (IJECE), vol. 2, no. 3, 2012

[26] L. Roselli. *Green RFID systems*. 1st ed. Cambridge, United Kingdom: Cambridge University Press, 2012, p.8.

[27] Y. Lee. *Antenna Circuit Design for RFID Applications*. Microchip Technology Inc, 2003, pp.1-49.

[28] Choi, Eun Kuk et al. "Fabrication Of Electrodes And Near-Field Communication Tags Based On Screen Printing Of Silver Seed Patterns And Copper Electroless Plating". International Journal of Precision Engineering And Manufacturing, vol. 16, no. 10, 2015, pp. 2199-2204. Springer Science And Business Media LLC, doi:10.1007/s12541-015-0283-y.

[29] Wang, T.-W.; Lin, S.-F. Wearable Piezoelectric-Based System for Continuous Beat-to-Beat Blood Pressure Measurement. Sensors 2020, 20, 851.

[30] C. Mariotti, V. Lakafosis, M. M. Tentzeris and L. Roselli, "An IPv6-enabled wireless shoe-mounted platform for health-monitoring," 2013 IEEE Topical Conference on Wireless Sensors and Sensor Networks (WiSNet), Austin, TX, 2013, pp. 46-48, doi: 10.1109/WiSNet.2013.6488629.

[31] Khalid Hasan, Kamanashis Biswas, Khandakar Ahmed, Nazmus S. Nafi, Md Saiful Islam, "A comprehensive review of wireless body area network", Journal of Network and Computer Applications, Vol. 143, 2019, pp. 178-198, doi: 10.1016/j.jnca.2019.06.016.

[32] Ahmed Abdelgawad, Kumar Yelamarthi, "Internet of Things (IoT) Platform for Structure Health Monitoring", Wireless Communications and Mobile Computing, 2017, https://doi.org/10.1155/2017/6560797

[33] Nicola Bui and Michele Zorzi, “Health care applications: a solution based on the internet of things”, In Proceedings of the 4th International Symposium on Applied Sciences in Biomedical and Communication Technologies (ISABEL '11). Association for Computing Machinery, New York, USA, vol. 131, 2011, pp.1–5. https://doi.org/10.1145/2093698.2093829

[34] Montón, E. et al. "Body Area Network For Wireless Patient Monitoring". IET Communications, vol 2, no. 2, 2008, p. 215. Institution Of Engineering And Technology (IET), doi:10.1049/iet-com:20070046.

[35] Falck, Thomas et al. "Plug ‘N Play Simplicity For Wireless Medical Body Sensors". Mobile Networks And Applications, vol 12, no. 2-3, 2007, pp. 143-153. Springer Science And Business Media LLC, doi:10.1007/s11036-007-0016-2.

[36] Khan, Jamil Yusuf et al. "Wireless Body Area Network (WBAN) Design Techniques And Performance Evaluation". Journal Of Medical Systems, vol 36, no. 3, 2010, pp. 1441-1457. Springer Science And Business Media LLC, doi:10.1007/s10916-010-9605-x.

[37] Z. H. Jiang, D. E. Brocker, P. E. Sieber and D. H. Werner, "A Compact, Low-Profile Metasurface-Enabled Antenna for Wearable Medical Body-Area Network Devices," in IEEE Transactions on Antennas and Propagation, vol. 62, no. 8, pp. 4021-4030, Aug. 2014, doi: 10.1109/TAP.2014.2327650.

[38] H. Yoo, "Your Heart on Your Sleeve: Advances in Textile-Based Electronics Are Weaving Computers Right into the Clothes We Wear," in IEEE Solid-State Circuits Magazine, vol. 5, no. 1, pp. 59-70, winter 2013, doi: 10.1109/MSSC.2012.2232781.

[39] Seulki Lee, Binhee Kim, Taehwan Roh, Sunjoo Hong and Hoi-Jun Yoo, "Arm-band type textile-MP3 player with multi-layer Planar Fashionable Circuit Board (P-FCB) techniques," International Symposium on Wearable Computers (ISWC) 2010, Seoul, 2010, pp. 1-7, doi: 10.1109/ISWC.2010.5665879.

[40] Parrilla, Marc et al. "A Textile-Based Stretchable Multi-Ion Potentiometric Sensor". Advanced Healthcare Materials, vol 5, no. 9, 2016, pp. 996-1001. Wiley, doi:10.1002/adhm.201600092.

[41] J. Meyer, B. Arnrich, J. Schumm and G. Troster, "Design and Modeling of a Textile Pressure Sensor for Sitting Posture Classification," in IEEE Sensors Journal, vol. 10, no. 8, pp. 1391-1398, Aug. 2010, doi: 10.1109/JSEN.2009.2037330.

[42] W. Xu, M. Huang, N. Amini, L. He and M. Sarrafzadeh, "eCushion: A Textile Pressure Sensor Array Design and Calibration for Sitting Posture Analysis," in IEEE Sensors Journal, vol. 13, no. 10, pp. 3926-3934, Oct. 2013, doi: 10.1109/JSEN.2013.2259589.

[43] X. Yang et al., "Textile Fiber Optic Microbend Sensor Used for Heartbeat and Respiration Monitoring," in IEEE Sensors Journal, vol. 15, no. 2, pp. 757-761, Feb. 2015, doi: 10.1109/JSEN.2014.2353640.

[44] G. Medrano, L. Beckmann, N. Zimmermann, T. Grundmann, T. Gries, S. Leonhardt, “Bioimpedance Spectroscopy with textile Electrodes for a continuous Monitoring Application”, 4th International Workshop on Wearable and Implantable Body Sensor Networks, IFMBE Proceedings, vol. 13, 2007, Springer, Berlin, Heidelberg, https://doi.org/10.1007/978-3-540-70994-7_4

[45] T. Linz, L. Gourmelon, and G. Langereis, “Contactless EMG sensors embroidered onto textile”, 4th International Workshop on Wearable and Implantable Body Sensor Networks, IFMBE Proceedings, vol. 13, 2007, Springer, Berlin, Heidelberg, https://doi.org/10.1007/978-3-540-70994-7_5

[46] E. Strommer, J. Kaartinen, J. Parkka, A. Ylisaukko-oja and I. Korhonen, "Application of Near Field Communication for Health Monitoring in Daily Life," 2006 International Conference of the IEEE Engineering in Medicine and Biology Society, New York, NY, 2006, pp. 3246-3249, doi: 10.1109/IEMBS.2006.260021.

[47] J. Morak, H. Kumpusch, D. Hayn, R. Modre-Osprian and G. Schreier, "Design and Evaluation of a Telemonitoring Concept Based on NFC-Enabled Mobile Phones and Sensor Devices," in IEEE Transactions on Information Technology in Biomedicine, vol. 16, no. 1, pp. 17-23, Jan. 2012, doi: 10.1109/TITB.2011.2176498.

[48] T. Kinkeldei, C. Zysset, K. H. Cherenack and G. Tröster, "A textile integrated sensor system for monitoring humidity and temperature," 2011 16th International Solid-State Sensors, Actuators and Microsystems Conference, Beijing, 2011, pp. 1156-1159, doi: 10.1109/TRANSDUCERS.2011.5969238.

[49] Dimie Ogoina, “Fever, fever patterns and diseases called ‘fever’ – A review”, Journal of Infection and Public Health, Vol. 4, no. 3, 2011, pp. 108-124, doi:10.1016/j.jiph.2011.05.002.

[50] McCann, Jane, and David Bryson. *Smart Clothes and Wearable Technology*. Woodhead Publishing, 2009, pp. 3-5.

[51] Cherenack, Kunigunde, and Liesbeth van Pieterson. "Smart Textiles: Challenges And Opportunities". Journal Of Applied Physics, vol 112, no. 9, 2012, p. 091301. AIP Publishing, doi:10.1063/1.4742728.

[52] Shi, Jidong et al. "Smart Textile-Integrated Microelectronic Systems For Wearable Applications". Advanced Materials, vol 32, no. 5, 2019, p. 1901958. Wiley, doi:10.1002/adma.201901958.

[53] Salvado, Rita et al. "Textile Materials For The Design Of Wearable Antennas: A Survey". Sensors, vol 12, no. 11, 2012, pp. 15841-15857. MDPI AG, doi:10.3390/s121115841.

[54] P. J. Massey, "GSM fabric antenna for mobile phones integrated within clothing," IEEE Antennas and Propagation Society International Symposium. 2001 Digest. Held in conjunction with: USNC/URSI National Radio Science Meeting (Cat. No.01CH37229), Boston, MA, USA, 2001, pp. 452-455 vol.3, doi: 10.1109/APS.2001.960132.

[55] M. Klemm and G. Troester, "Textile UWB Antennas for Wireless Body Area Networks," in IEEE Transactions on Antennas and Propagation, vol. 54, no. 11, pp. 3192-3197, Nov. 2006, doi: 10.1109/TAP.2006.883978.

[56] C. Hertleer, H. Rogier, L. Vallozzi and L. Van Langenhove, "A Textile Antenna for Off-Body Communication Integrated Into Protective Clothing for Firefighters," in IEEE Transactions on Antennas and Propagation, vol. 57, no. 4, pp. 919-925, April 2009, doi: 10.1109/TAP.2009.2014574.

[57] Z. Wang, L. Z. Lee, D. Psychoudakis and J. L. Volakis, "Embroidered Multiband Body-Worn Antenna for GSM/PCS/WLAN Communications," in IEEE Transactions on Antennas and Propagation, vol. 62, no. 6, pp. 3321-3329, June 2014, doi: 10.1109/TAP.2014.2314311.

[58] S. J. Chen, T. Kaufmann, D. C. Ranasinghe and C. Fumeaux, "A Modular Textile Antenna Design Using Snap-on Buttons for Wearable Applications," in IEEE Transactions

on Antennas and Propagation, vol. 64, no. 3, pp. 894-903, March 2016, doi: 10.1109/TAP.2016.2517673.

[59] Y. Bayram et al., "E-Textile Conductors and Polymer Composites for Conformal Lightweight Antennas," in IEEE Transactions on Antennas and Propagation, vol. 58, no. 8, pp. 2732-2736, Aug. 2010, doi: 10.1109/TAP.2010.2050439.

[60] T. F. Kennedy, P. W. Fink, A. W. Chu, N. J. Champagne, G. Y. Lin and M. A. Khayat, "Body-Worn E-Textile Antennas: The Good, the Low-Mass, and the Conformal," in IEEE Transactions on Antennas and Propagation, vol. 57, no. 4, pp. 910-918, April 2009, doi: 10.1109/TAP.2009.2014602.

[61] Y. Vardaxoglou, R. D. Seager, N. Riauka, A. Chauraya and P. deMaagt, "Metamaterial based antennas with super- and substrates," 2009 3rd European Conference on Antennas and Propagation, Berlin, 2009, pp. 2862-2866.

[62] W. M. Mongan, I. Rasheed, K. Ved, A. Levitt, E. Anday, K. Dandekar, G. Dion, T. Kurzweg, and A. Fontecchio, "Real-time detection of apnea via signal processing of time-series properties of RFID-based smart garments," in 2016 IEEE Signal Processing in Medicine and Biology Symposium (SPMB), 2016, pp. 1-6.

[63] Virkki, Johanna et al. "Wearable Passive E-Textile UHF RFID Tag Based On A Slotted Patch Antenna With Sewn Ground And Microchip Interconnections". International Journal Of Antennas And Propagation, vol 2017, 2017, pp. 1-8. Hindawi Limited, doi:10.1155/2017/3476017.

[64] G. Ginestet et al., "Embroidered Antenna-Microchip Interconnections and Contour Antennas in Passive UHF RFID Textile Tags," in IEEE Antennas and Wireless Propagation Letters, vol. 16, pp. 1205-1208, 2017, doi: 10.1109/LAWP.2016.2628086.

[65] Wang, Shiqi et al. "Towards Washable Electrotextile UHF RFID Tags: Reliability Study Of Epoxy-Coated Copper Fabric Antennas". International Journal Of Antennas And Propagation, vol 2015, 2015, pp. 1-8. Hindawi Limited, doi:10.1155/2015/424150.

[66] Baker-Jarvis, James et al. "High-Frequency Dielectric Measurements". IEEE Instrumentation & Measurement Magazine, vol 13, no. 2, 2010, pp. 24-31. Institute Of Electrical And Electronics Engineers (IEEE), doi:10.1109/mim.2010.5438334.

[67] Morton, William E, and John W. S Hearle. *Physical Properties Of Textile Fibres*. Textile Inst., 2012.

[68] P. Salonen and Y. Rahimat-Samii, "Textile antennas: effects of antenna bending on input matching and impedance bandwidth," in IEEE Aerospace and Electronic Systems Magazine, vol. 22, no. 3, pp. 10-14, March 2007, doi: 10.1109/MAES.2007.340501.

[69] S. Zhu and R. Langley, "Dual-Band Wearable Textile Antenna on an EBG Substrate," in IEEE Transactions on Antennas and Propagation, vol. 57, no. 4, pp. 926-935, April 2009, doi: 10.1109/TAP.2009.2014527.

[70] Oh, Kyung Wha et al. "Electrically Conductive Textiles Byin Situ Polymerization Of Aniline". Journal Of Applied Polymer Science, vol 74, no. 8, 1999, pp. 2094-2101. Wiley, doi:10.1002/(sici)1097-4628(19991121)74:8<2094::aid-app26>3.0.co;2-9.

[71] Atwa, Yahya et al. "Silver Nanowire Coated Threads For Electrically Conductive Textiles". Journal Of Materials Chemistry C, vol 3, no. 16, 2015, pp. 3908-3912. Royal Society Of Chemistry (RSC), doi:10.1039/c5tc00380f.

[72] Knittel, Dierk, and Eckhard Schollmeyer. "Electrically High-Conductive Textiles". Synthetic Metals, vol 159, no. 14, 2009, pp. 1433-1437. Elsevier BV, doi:10.1016/j.synthmet.2009.03.021.

[73] Zhang, Rui et al. "Carbon Nanotube Polymer Coatings For Textile Yarns With Good Strain Sensing Capability". Sensors And Actuators A: Physical, vol 179, 2012, pp. 83-91. Elsevier BV, doi:10.1016/j.sna.2012.03.029.

[74] Dong, By Hong, and Juan P. Hinestroza. "Metal Nanoparticles On Natural Cellulose Fibers: Electrostatic Assembly And In Situ Synthesis". ACS Applied Materials & Interfaces, vol 1, no. 4, 2009, pp. 797-803. American Chemical Society (ACS), doi:10.1021/am800225j.

[75] Stoppa, Matteo, and Alessandro Chiolerio. "Wearable Electronics And Smart Textiles: A Critical Review". Sensors, vol 14, no. 7, 2014, pp. 11957-11992. MDPI AG, doi:10.3390/s140711957.

[76] I. Locher, M. Klemm, T. Kirstein and G. Troster, "Design and Characterization of Purely Textile Patch Antennas," in IEEE Transactions on Advanced Packaging, vol. 29, no. 4, pp. 777-788, Nov. 2006, doi: 10.1109/TADVP.2006.884780.

[77] Xu, Bin. "A Short Review Of Textile Applications In Antenna Design". Trends In Textile Engineering & Fashion Technology, vol 1, no. 5, 2018. Crimson Publishers, doi:10.31031/tteft.2018.01.000522.

[78] Donchev, Evgeniy et al. "The Rectenna Device: From Theory To Practice (A Review)". MRS Energy & Sustainability, vol 1, 2014. Cambridge University Press (CUP), doi:10.1557/mre.2014.6.

[79] Khalid, Fatima et al. "Quad-Band 3D Rectenna Array For Ambient RF Energy Harvesting". International Journal Of Antennas And Propagation, vol 2020, 2020, pp. 1-23. Hindawi Limited, doi:10.1155/2020/7169846.

[80] Riviere, Samuel et al. "A COMPACT RECTENNA DEVICE AT LOW POWER LEVEL". Progress In Electromagnetics Research C, vol 16, 2010, pp. 137-146. EMW Publishing, doi:10.2528/pierc10071604.

[81] H. Sun, Y. Guo, M. He and Z. Zhong, "Design of a High-Efficiency 2.45-GHz Rectenna for Low-Input-Power Energy Harvesting," in IEEE Antennas and Wireless Propagation Letters, vol. 11, pp. 929-932, 2012, doi: 10.1109/LAWP.2012.2212232.

[82] M. Zeng, A. S. Andrenko, X. Liu, Z. Li and H. Tan, "A Compact Fractal Loop Rectenna for RF Energy Harvesting," in IEEE Antennas and Wireless Propagation Letters, vol. 16, pp. 2424-2427, 2017, doi: 10.1109/LAWP.2017.2722460.

[83] K. Niotaki, S. Kim, S. Jeong, A. Collado, A. Georgiadis and M. M. Tentzeris, "A Compact Dual-Band Rectenna Using Slot-Loaded Dual Band Folded Dipole Antenna," in IEEE Antennas and Wireless Propagation Letters, vol. 12, pp. 1634-1637, 2013, doi: 10.1109/LAWP.2013.2294200.

[84] S. Chandravanshi, S. S. Sarma and M. J. Akhtar, "Design of Triple Band Differential Rectenna for RF Energy Harvesting," in IEEE Transactions on Antennas and Propagation, vol. 66, no. 6, pp. 2716-2726, June 2018, doi: 10.1109/TAP.2018.2819699.

[85] C. Song, Y. Huang, J. Zhou, J. Zhang, S. Yuan and P. Carter, "A High-Efficiency Broadband Rectenna for Ambient Wireless Energy Harvesting," in IEEE Transactions on Antennas and Propagation, vol. 63, no. 8, pp. 3486-3495, Aug. 2015, doi: 10.1109/TAP.2015.2431719.

[86] V. Kuhn, C. Lahuec, F. Seguin and C. Person, "A Multi-Band Stacked RF Energy Harvester With RF-to-DC Efficiency Up to 84%," in IEEE Transactions on Microwave Theory and Techniques, vol. 63, no. 5, pp. 1768-1778, May 2015, doi: 10.1109/TMTT.2015.2416233.

[87] U. Olgun, C. Chen and J. L. Volakis, "Investigation of Rectenna Array Configurations for Enhanced RF Power Harvesting," in IEEE Antennas and Wireless Propagation Letters, vol. 10, pp. 262-265, 2011, doi: 10.1109/LAWP.2011.2136371.

[88] B. R. Franciscatto, V. Freitas, J. Duchamp, C. Defay and T. P. Vuong, "High-efficiency rectifier circuit at 2.45 GHz for low-input-power RF energy harvesting," 2013 European Microwave Conference, Nuremberg, 2013, pp. 507-510, doi: 10.23919/EuMC.2013.6686703.

[89] I. Chaour, S. Bdiri, A. Fakhfakh and O. Kanoun, "Modified rectifier circuit for high efficiency and low power RF energy harvester," 2016 13th International Multi-Conference on Systems, Signals & Devices (SSD), Leipzig, 2016, pp. 619-623, doi: 10.1109/SSD.2016.7473714.

[90] T. Le, K. Mayaram and T. Fiez, "Efficient Far-Field Radio Frequency Energy Harvesting for Passively Powered Sensor Networks," in IEEE Journal of Solid-State Circuits, vol. 43, no. 5, pp. 1287-1302, May 2008, doi: 10.1109/JSSC.2008.920318.

[91] S. M. Noghabaei, R. L. Radin, Y. Savaria and M. Sawan, "A High-Efficiency Ultra-Low-Power CMOS Rectifier for RF Energy Harvesting Applications," 2018 IEEE International Symposium on Circuits and Systems (ISCAS), Florence, 2018, pp. 1-4, doi: 10.1109/ISCAS.2018.8351149.

[92] G. Monti, L. Corchia and L. Tarricone, "UHF Wearable Rectenna on Textile Materials," in IEEE Transactions on Antennas and Propagation, vol. 61, no. 7, pp. 3869-3873, July 2013, doi: 10.1109/TAP.2013.2254693.

[93] M. Dini et al., "A fully-autonomous integrated rf energy harvesting system for wearable applications," 2013 European Microwave Conference, Nuremberg, 2013, pp. 987-990, doi: 10.23919/EuMC.2013.6686825.

[94] D. Masotti, A. Costanzo and S. Adami, "Design and realization of a wearable multi-frequency RF energy harvesting system," Proceedings of the 5th European Conference on Antennas and Propagation (EUCAP), Rome, 2011, pp. 517-520.

[95] M. Wagih, A. S. Weddell and S. Beeby, "Omnidirectional Dual-Polarized Low-Profile Textile Rectenna with over 50% Efficiency for Sub-μW/cm2 Wearable Power Harvesting," in IEEE Transactions on Antennas and Propagation, doi: 10.1109/TAP.2020.3030992.

[96] B. Naresh, V.K. Singh, V. Bhargavi, A. Garg, A.K. Bhoi, “Dual-Band Wearable Rectenna for Low-Power RF Energy Harvesting,” in Advances in Power Systems and Energy Management. Lecture Notes in Electrical Engineering, vol 436. Springer, Singapore, 2018, doi: 10.1007/978-981-10-4394-9_2

[97] B. Naresh, V.K. Singh, V. Bhargavi, “Low Power Circularly Polarized Wearable Rectenna for RF Energy Harvesting,” in Advances in Power Systems and Energy Management. Lecture Notes in Electrical Engineering, vol 436. Springer, Singapore, 2018, doi: 10.1007/978-981-10-4394-9_13

Chapter 3 Methodology

This chapter explains the experiments discussed in subsequent chapters of this thesis, covers the contents that are not fully described in the papers and presents results and findings in a broader perspective. The design procedures of NFC antennas and UHF RFID antennas are presented. Detailed experiments of NFC performance under pressure, modification of the Dickson charge pump implanted in the NFC sensing device and rectifier development for the wearable RF energy harvesting system are also included.

3.1. e-Textile embroidered wearable NFC antennas

3.1.1. NFC antenna design

Fig. 3-1 presents equivalent circuit models for an NFC tag. In Fig. 3-1(a), it specifies three parts of the circuit: the antenna part (mainly inductive), the chip part (mainly capacitive) and the matching circuit (connection between the first two parts). For most designs in reality, the matching network is absorbed by the antenna, i.e. the antenna is designed to conjugate match the microchip as it shows in Fig. 3-1(b). The resonance frequency of the circuit can be calculated by (3-1)

$$f_r = \frac{1}{2\pi\sqrt{C_{chip}L_{ant}}} \tag{3-1}$$

where $\boldsymbol{C_{chip}}$ stands for the chip capacitance and $\boldsymbol{L_{ant}}$ stands for the antenna coil inductance which can be derived from (3-1) as (3-2)

$$L_{ant} = \frac{1}{(2\pi f_r)^2 C_{chip}} \tag{3-2}$$

The quality factor of the circuit can be obtained by (3-3)

$$Q = \frac{2\pi f L_{ant}}{R_{eq}} \tag{3-3}$$

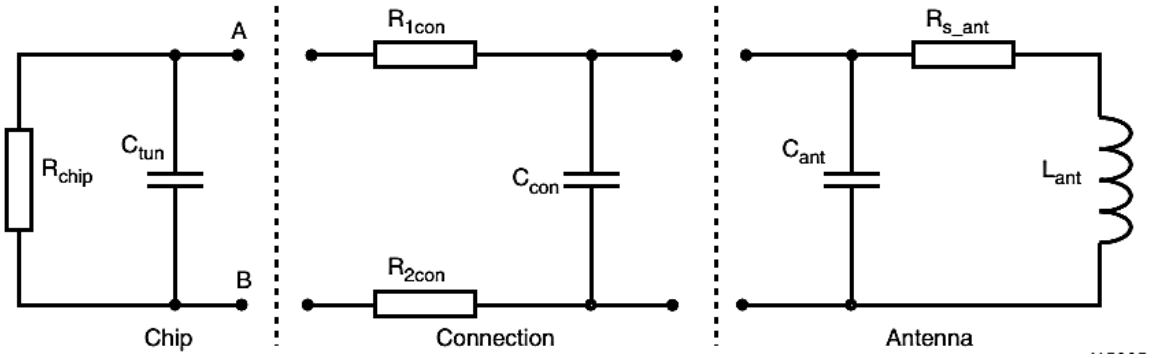

(a)

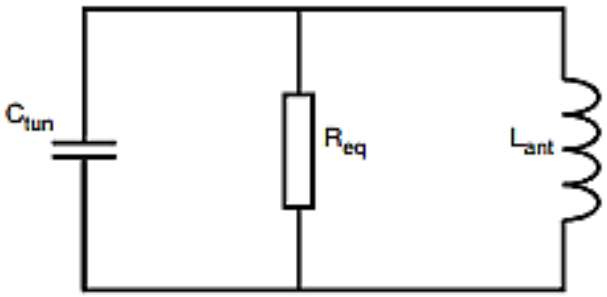

(b)

Fig. 3-1. Equivalent circuit of an NFC RFID tag: (a) chip, matching antenna and connections between them (b) simplified equivalent circuit [1]

The quality factor (Q) is affected by equivalent resistance value and antenna inductance. An ideal Q factor for NFC circuits is typically around 30-40 [2]. A high Q factor indicates high energy efficiency and low damping output but narrow bandwidth. The drawback of narrow bandwidth for a textile NFC circuit is that the tag becomes very sensitive to the geometrical change of the tag such as bending and stretching as well as the choice of substrate materials.

The most common structures of NFC tag coils are spiral coils and square coils as it presents respectively in Fig. 3-2. The relationship between the coil inductance and its dimensions for spiral coils can be calculated by (3-4).

$$L_{ant} = 31.33\mu_0 N^2 \frac{a^2}{8a+11c} \tag{3-4}$$

Where $\boldsymbol{a} = (\boldsymbol{r_{in}} + \boldsymbol{r_{out}})/2$ which is the mean coil radius in meter; $\boldsymbol{c} = \boldsymbol{r_{out}} - \boldsymbol{r_{in}}$ in meter; $\boldsymbol{N}$ is the number of turns and $\boldsymbol{\mu_0}$ is the free space permeability ($4\pi \times 10^{-7}$H/m).

As for square coils, the coil inductance can be obtained by (3-5).

$$L_{ant} = K_1 \mu_0 N^2 \frac{d}{1+K_2 p} \tag{3-5}$$

where $\boldsymbol{d}$ is the coil diameter which is the mean value of the outer and inner diameters of the coil (d_{out} and d_{in}); $\boldsymbol{N}$ is the number of turns; $\boldsymbol{K_1}$ and $\boldsymbol{K_2}$ are parameters that depend on the layout, which in this case are respectively 2.34 and 2.75 for a squire coli; $\boldsymbol{\mu_0}$ is the free space permeability which is $4\pi \times 10^{-7}$H/m and $\boldsymbol{p}$=($\boldsymbol{d_{out}} - \boldsymbol{d_{in}}$)/($\boldsymbol{d_{out}} + \boldsymbol{d_{in}}$).

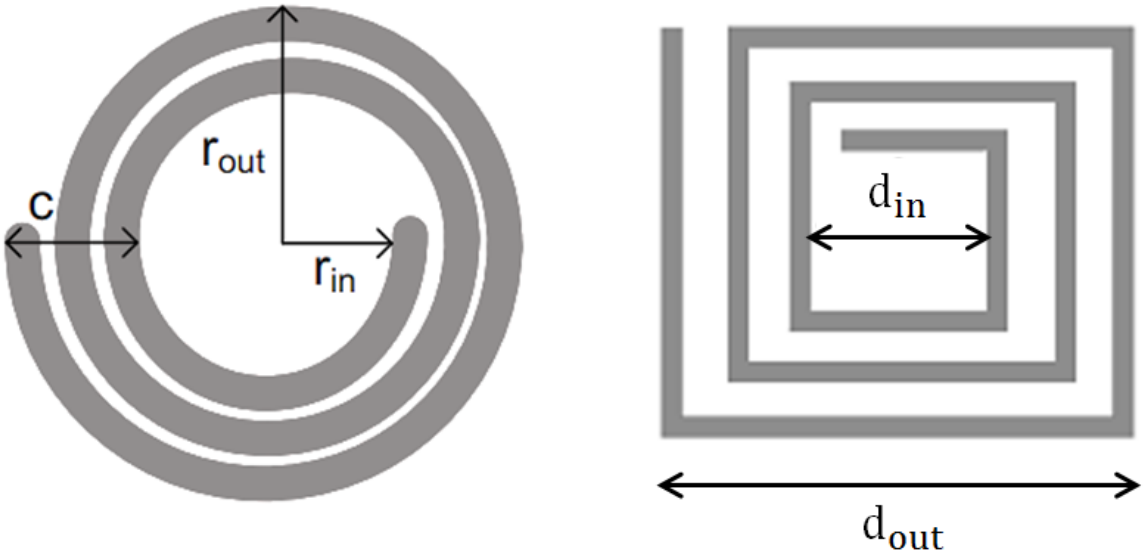

(a) (b)

Fig. 3-2. (a) spiral coil (b) square coil [1]

For textile material selection, as it is shown in Fig. 3-3, 30 textile NFC antennas woven with different conductive materials, including silver, aluminium, stainless steel, copper and assorted alloys are produced on cotton substrate, and the approximate resistance value of the antennas are measured with a Multimeter. As presented in Fig. 3-3, the resistance range of these NFC circuits is between 11.6 Ω and 410 Ω.

According to (3-3), a larger equivalent resistance leads to significant reduction of Q factor and affects the operational efficiency of an NFC circuit. Therefore, In order to minimize the loss in the antenna circuit, the type of conductive threads with the lowest DC resistance is selected for further testing, which is silver coated nylon threads with resistance of 17.2 Ω/m.

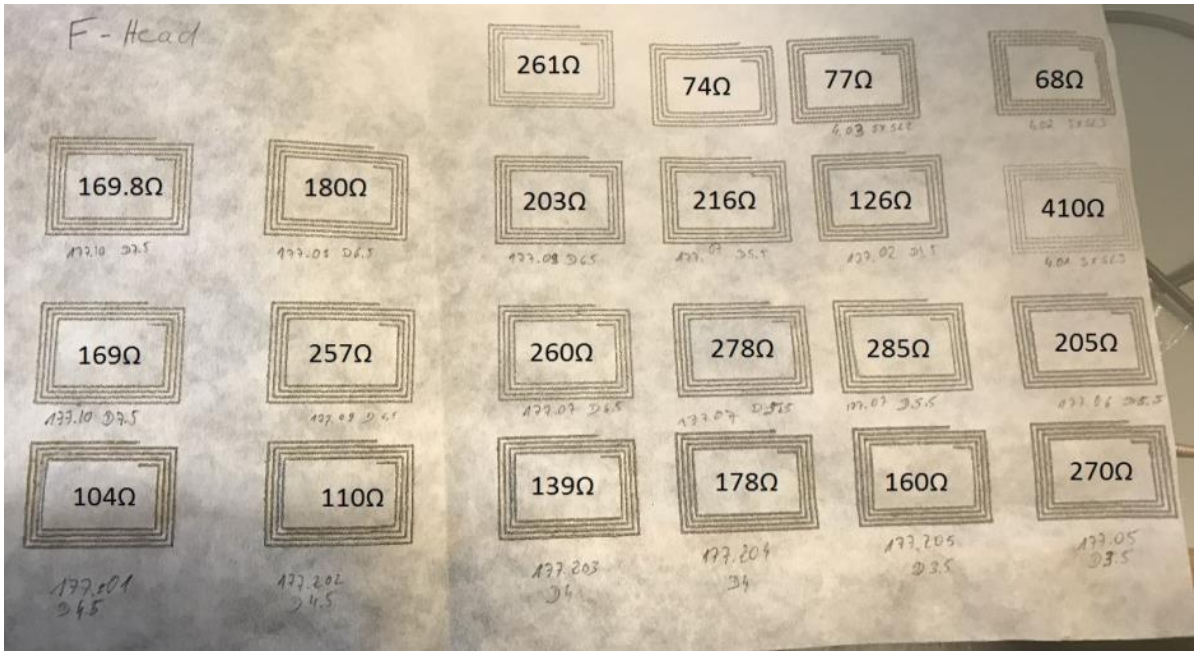

(a)

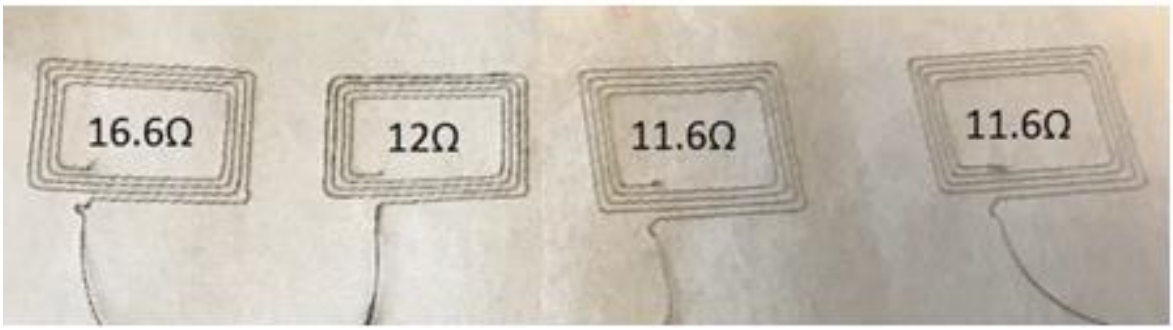

(b)

Fig. 3-3. NFC antennas weaved with conductive threads made in different types of metals (a) multiple cord threads (b) single cord threads

3.1.2. Pressure test of NFC antennas

In order to observe the S-parameter performance of an NFC circuit under increasing pressure applying upon its surface, weights in a range from 10 g to 3.2 kg are orderly placed onto a matched NFC tag as it demonstrates in Fig. 3-4. The circuit is tested between two pieces of low loss poly-foam plate which are used for blocking the EM influence from the metal weights.

Fig. 3-4. 1600g weights applied on the textile NFC tag measured by a VNA.

As it presents in Fig. 3-5, in general, the NFC resonant frequency shifts from 13.75 MHz to 14.3 MHz as the weight increases from 0 to 3.2 Kg. The most rapid frequency shift lies in the weight range from 0 to 20 g, and the resonant frequency basically stays stable as the weight reaches 1.6 Kg.

Referring to (3-1), an increment in the circuit working frequency indicates reduction of antenna inductance. Since the conductive threads are constructed with hundreds of micro-thin fibres, this might be due to short circuit induced between threads as the circuit is getting increasingly compressed. Furthermore, recalling (3-5), the pressure might slightly decrease the antenna diameter which leads to a reduction in the coil inductance.

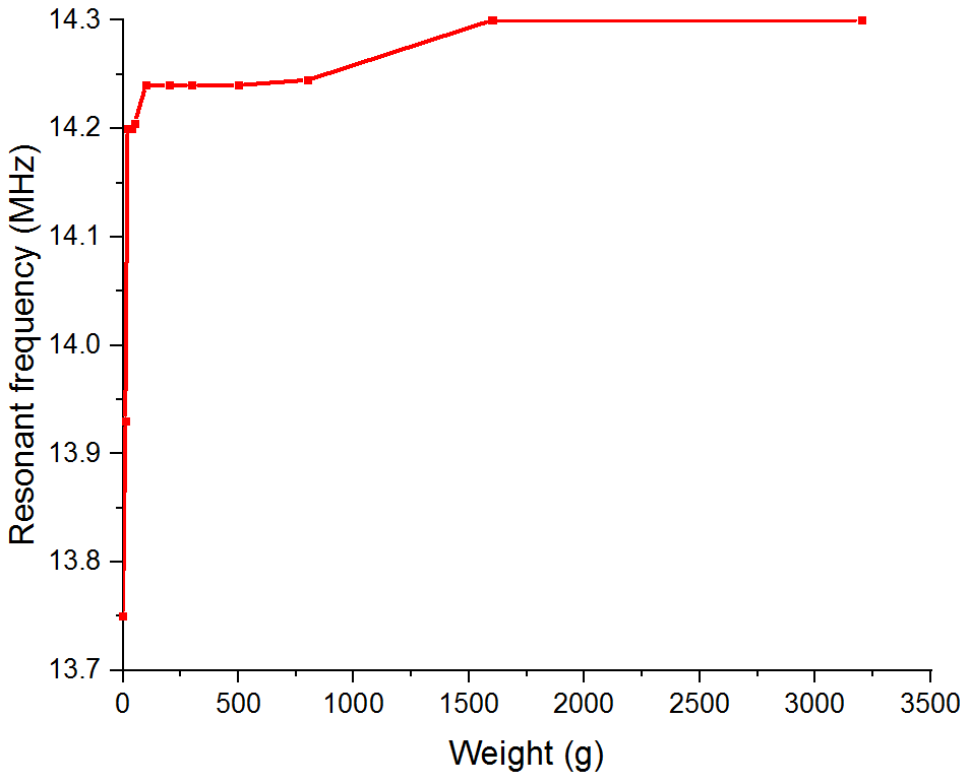

(a)

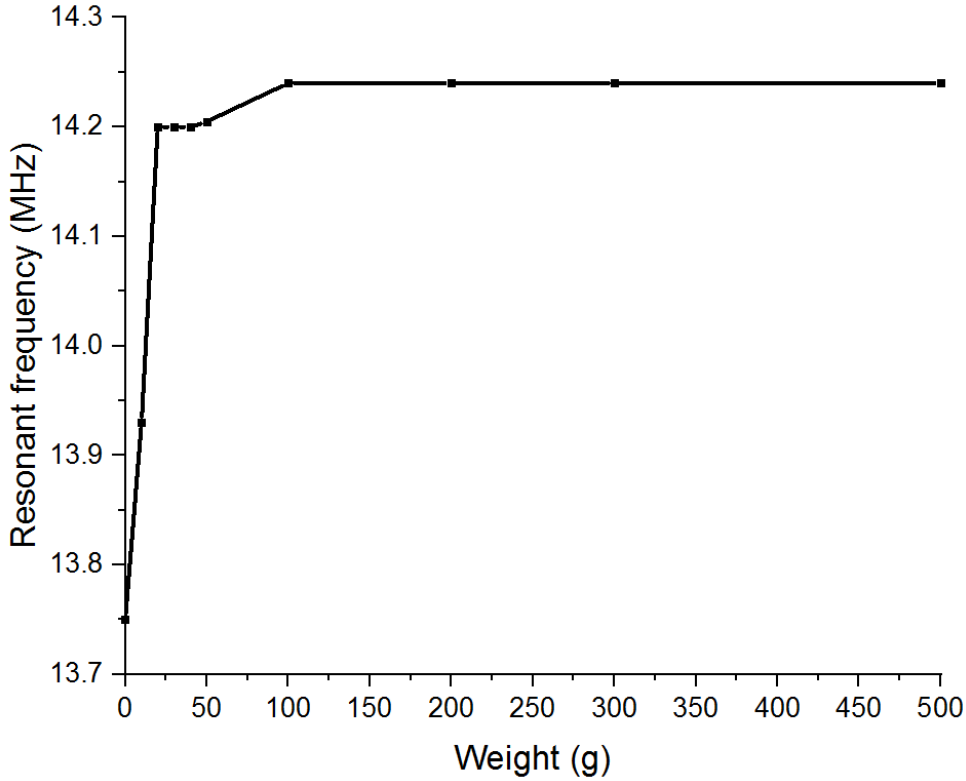

(b)

Fig. 3-5. Resonant frequency of the NFC tag against applied weight: (a) 0 - 3.2 Kg, (b) 0 - 500 g.

3.2. Dickson charge pump modification

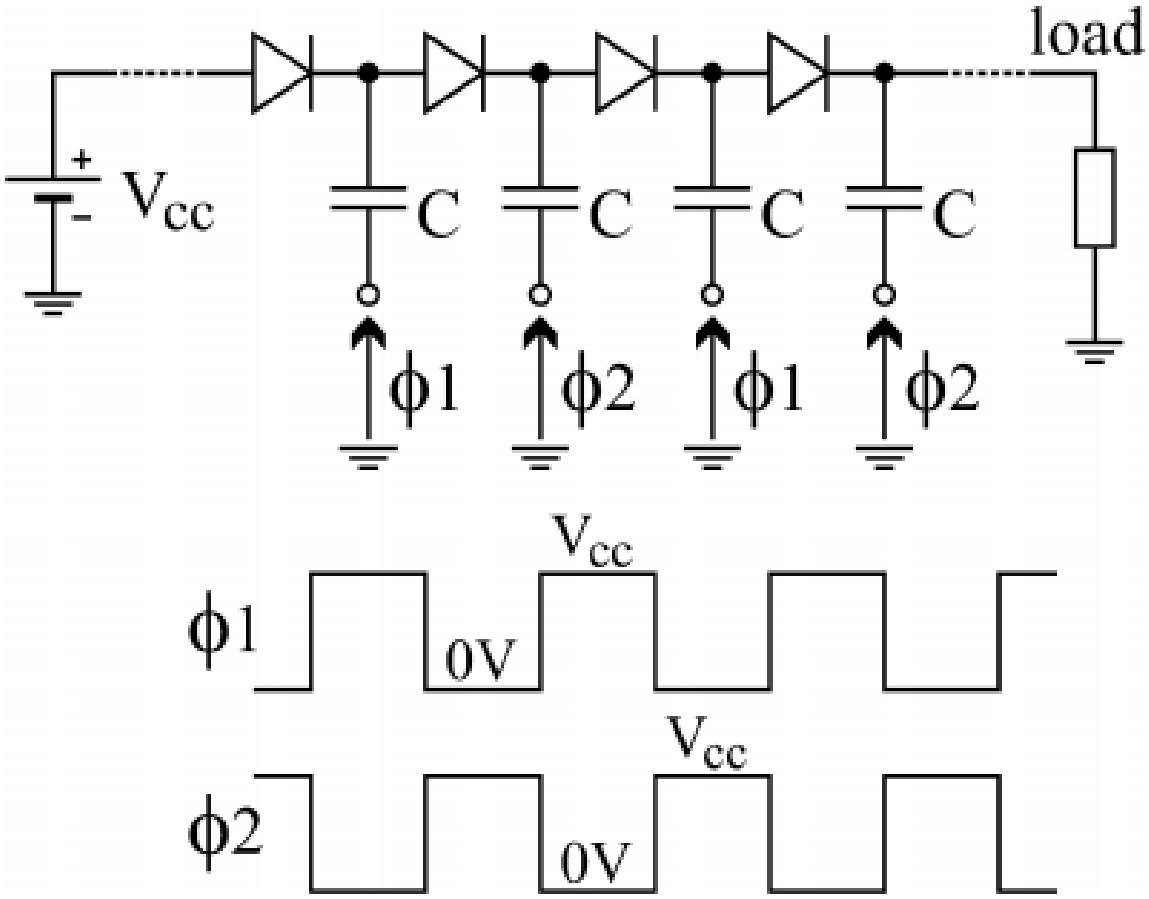

Fig. 3-6. Dickson Charge Pump diagram [3].

Dickson charge pump is a high efficiency voltage multiplier that was first introduced in 1976 [4]. The basic layout of a Dickson charge pump is shown in Fig. 3-6. The charge pump circuit is composed of a number of identical stages (N), each containing a diode and a capacitor, where the bottom plates of the capacitors in consecutive stages are driven by 2 clock signals in anti-phase. Charge is transferred from one capacitor to the next during each half a clock cycle, resulting in an output voltage that can be ideally N+1 times higher than the input voltage. This structure is also called N-stage voltage multiplier [4].

The purpose of implanting a voltage multiplier in this work is to boost up the voltage of an NFC tag in order to power a humidity sensor that operates at a higher voltage level. As it presents in Fig. 3-7, a modified layout of a Dickson Charge Pump is proposed to meet this requirement. Since the output voltage of an NFC is an AC voltage at a single frequency (13.56 MHz), by connecting adjacent capacitors to the voltage input and ground separately,

the two complementary clock cycles are automatically generated by the circuit. The output voltage of such circuits can be calculated as (3-6) [3],

$$V_{out} = (N+1) \cdot (V_{cc} - V_T) - \frac{N \cdot I_{out}}{f \cdot C} \tag{3-6}$$

where $\boldsymbol{V_{cc}}$ represents the input voltage, $\boldsymbol{V_T}$ is the forward voltage of each diode, $\boldsymbol{N}$ is the number of stages, $\boldsymbol{I_{out}}$ is the charge pump output current, $\boldsymbol{f}$ is the signal frequency and $\boldsymbol{C}$ is the capacitance applied at each node.

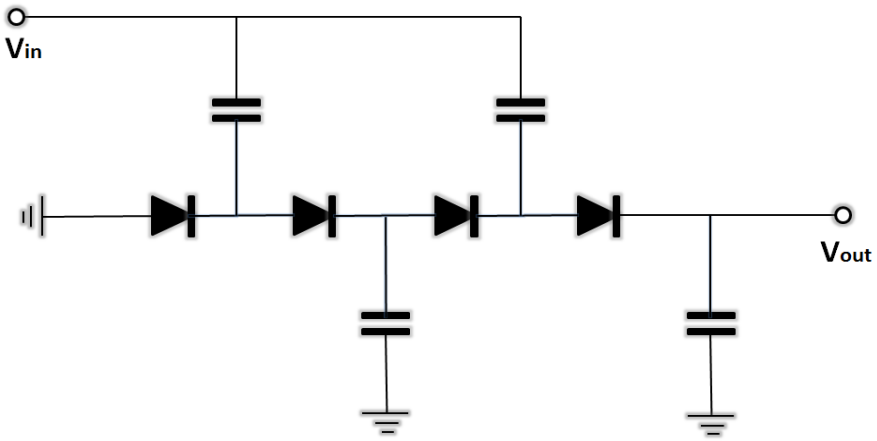

Fig. 3-7. Modified Dickson Charge Pump.

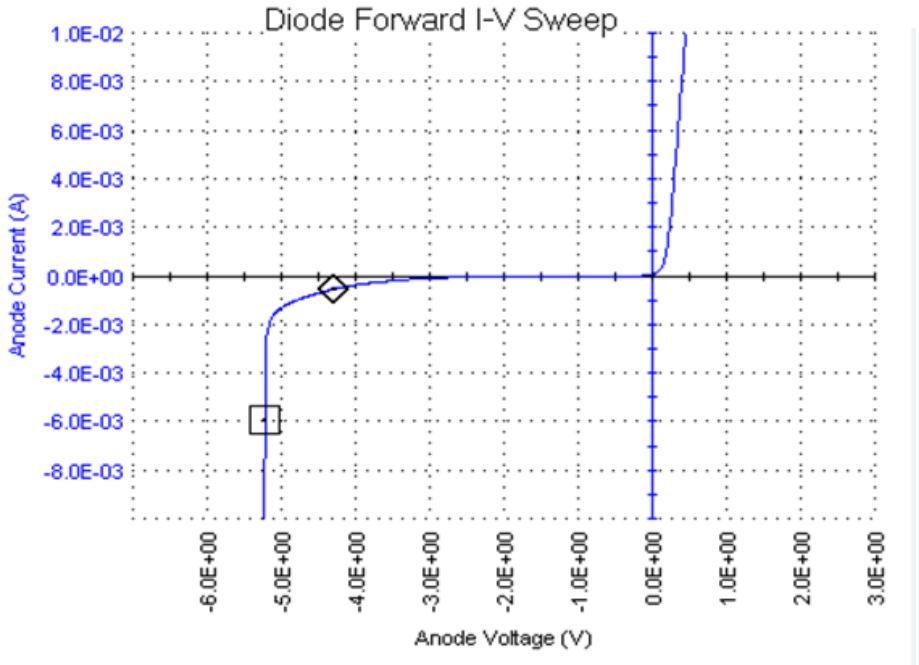

Fig. 3-8. I-V characteristic of Schottky diode SMS7630.

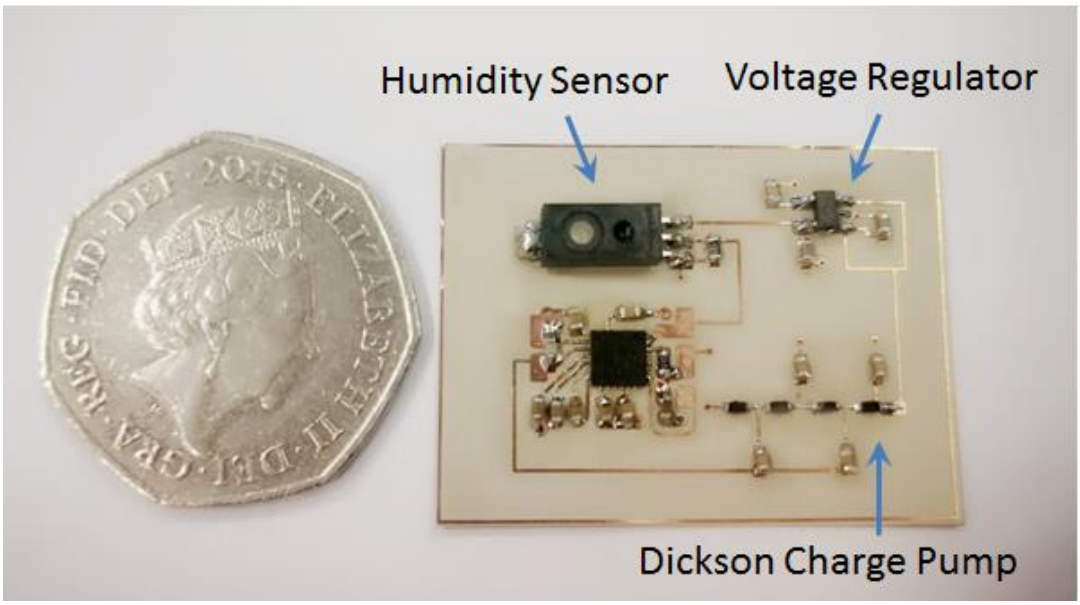

Fig. 3-9. Sensing circuit.

The maximum output voltage delivered by the charge pump is limited by the break out voltage of the diodes. Fig. 3-8 shows the measured I-V characteristic of the selected diode model in this circuit (SMS7630), where the reverse current starts to flow as the reverse voltage reaches around -4 V. Therefore, the output voltage cannot exceed 16 V.

The fabricated Dickson Charge Pump implanted in the sensing circuit is presented in Fig. 3-9. As a result, the circuit delivers DC voltage from 5V to 14.5 V corresponding to the NFC read distance from 6cm to 1cm.

3.3. e-Textile embroidered UHF RFID antenna design

The proposed RFID antenna layout with detailed dimensions is presented in Fig. 3-10, where the 2 mm gap in the middle is designed for the connection of a RFID IC chip (Monza R6) with capacitance of 1.45 pF. The antenna structure is a bowtie integrated with an inductive matching loop. The size of the antenna is designed in typical dimensions of RFID tags, and the slots highlighted in Fig. 3-10 are optimised using CST for better impedance matching. The total power collected by the tag (P_{tag}) and received by the chip (P_{chip}) is expressed in (3-7), where τ is the power transmission coefficient that can be expressed in terms of the antenna and chip impedance (Z_A and Z_C) as it derives in (3-8) and (3-9) [5].

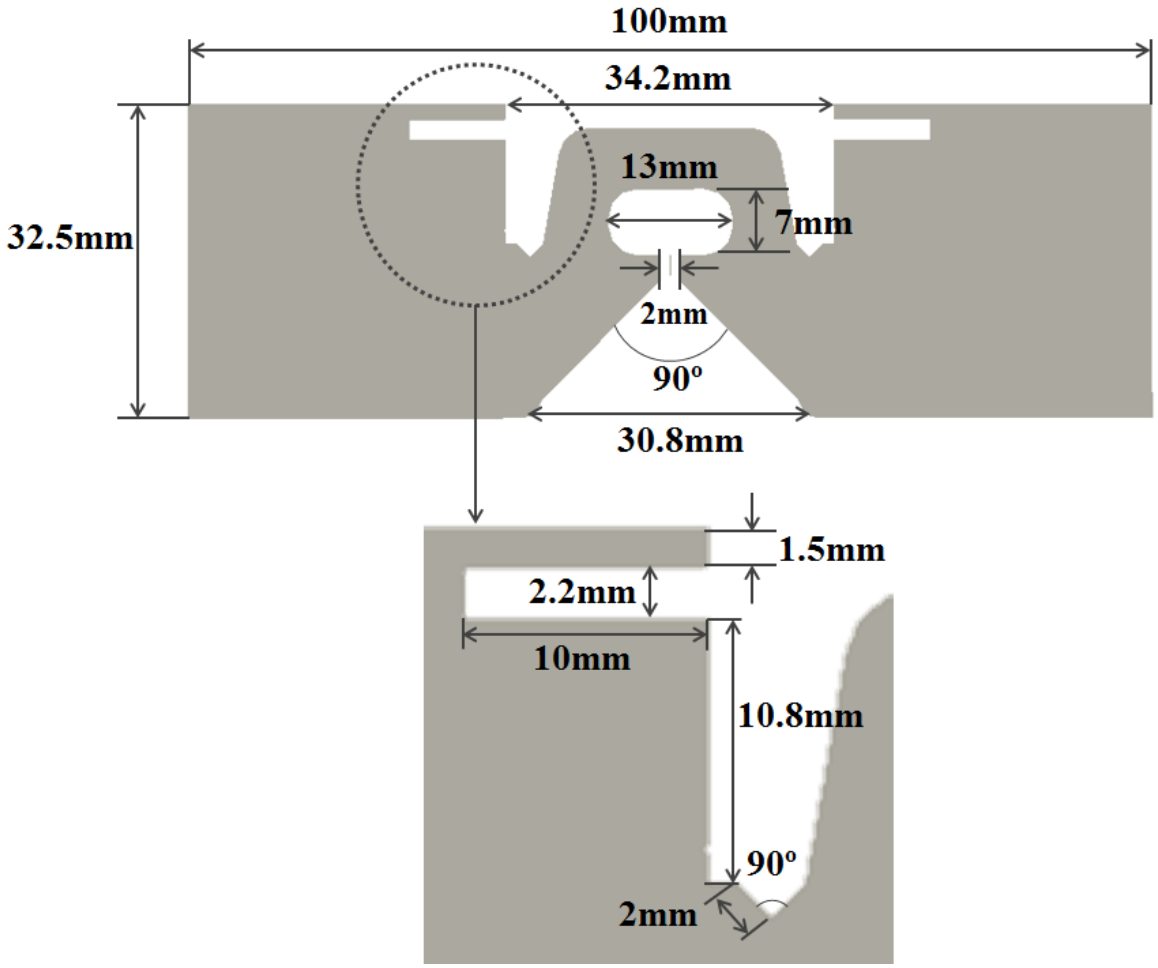

Fig. 3-10. Proposed RFID antenna layout.

$$P_{chip} = \tau P_{tag} \tag{3-7}$$

$$\tau = 1 - |\Gamma_{tag}|^2 \tag{3-8}$$

$$\Gamma_{tag} = \frac{Z_C - Z_A^*}{Z_C + Z_A} \tag{3-9}$$

In order to increase the value of τ, the reflection coefficient of the tag (Γ_{tag}) should be minimized by conjugate matching the antenna and chip impedance. Fig. 3-11 presents the simulated resistance (R) and reactance (X) of the optimized antenna and chip in the frequency range from 100 MHz to 2500 MHz. The results indicate the antenna and chip reactance is completely cancelled out at 870 and 952 MHz, which matched the desired frequency band for UHF RFID (860-960 MHz).

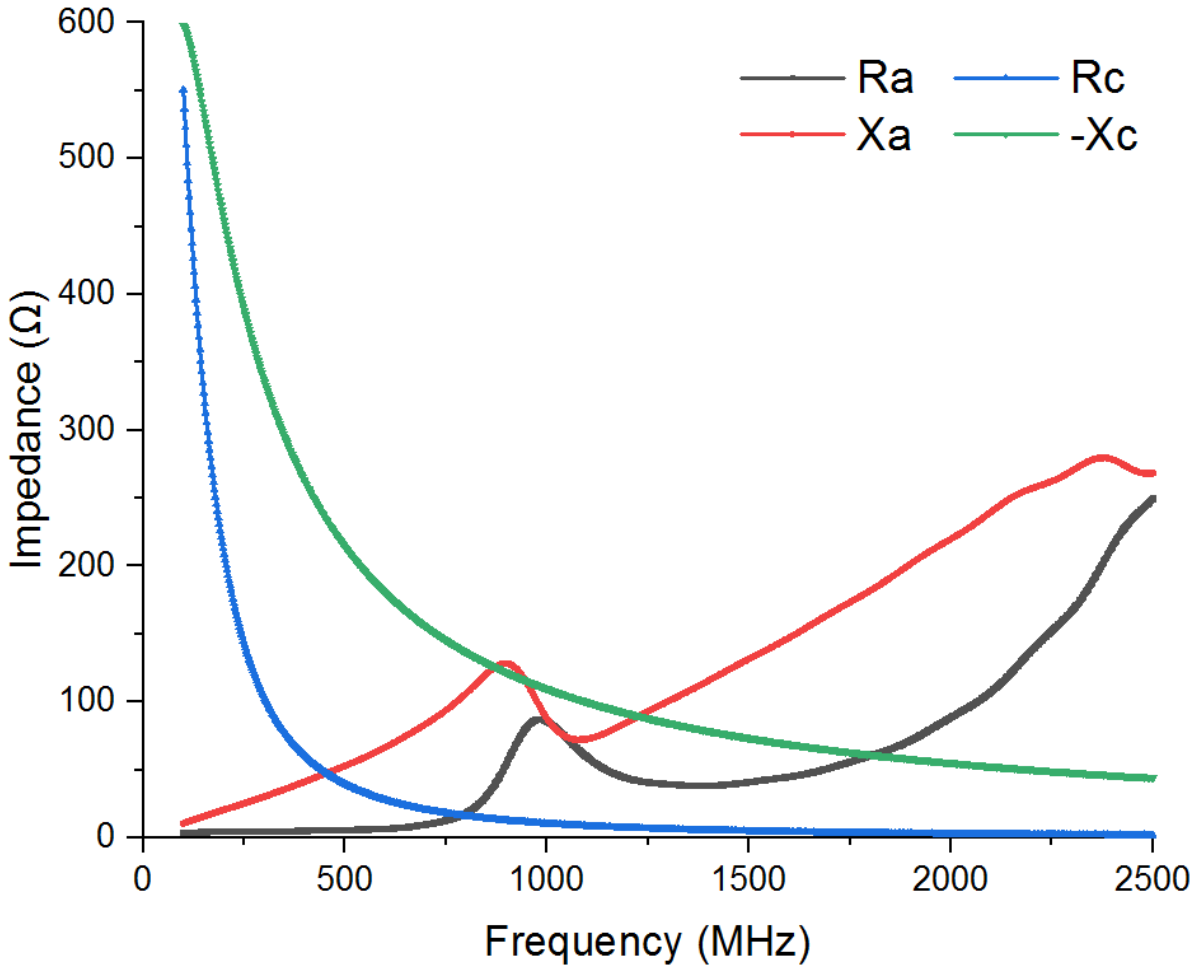

Fig. 3-11. Antenna and chip impedance.

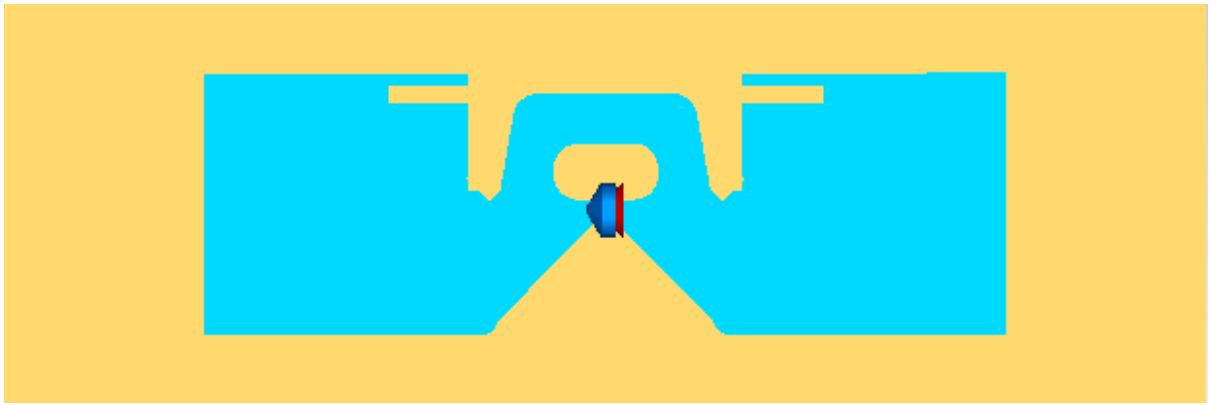

Fig. 3-12. CST Antenna simulation model

The antenna simulation model in CST is presented in Fig. 3-12, where the antenna is set up as an ohmic sheet with sheet resistance of 0.4 Ω/sq, corresponding to the conductive yarn resistance. A 0.5 mm thick cotton sheet (ε_r = 1.4) with the size of 150 mm×50 mm is placed

below the antenna as substrate. Fig. 3-13 shows the simulated antenna S-parameter before and after it is matched with the chip capacitor and with and without the cotton sheet. The self-resonant frequency of the antenna before matching is around 1058 MHz within the given range. After matching, the -10 dB operating bandwidth of the antenna is 503 MHz (from 840 MHz to 1343 MHz). The results also indicate that the integration of cotton substrate barely affects the antenna operation bandwidth.

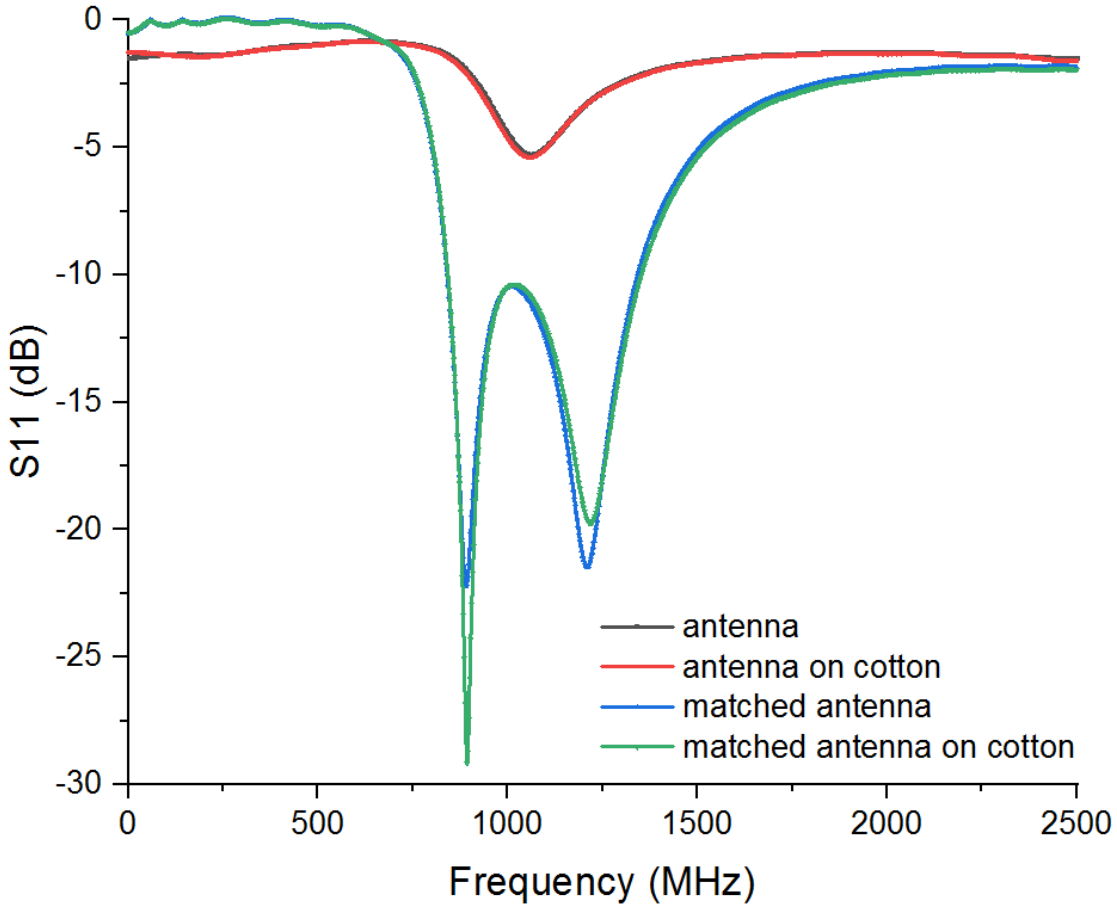

Fig. 3-13. Simulated antenna S-parameters.

The simulated antenna gain over frequency is presented in Fig. 3-14. Maximum gain is defined as the antenna gain disregarding any loss due to impedance mismatch [6]. The maximum and realized gain of the antenna increases from -1.28 dB to 1.63 dB and from -3.22 dB to 0.96 dB, respectively. Furthermore, the realized gain achieves maximum gain between 880 MHz and 910 MHz, which indicates the losses due to the mismatch are minimized in this frequency range.

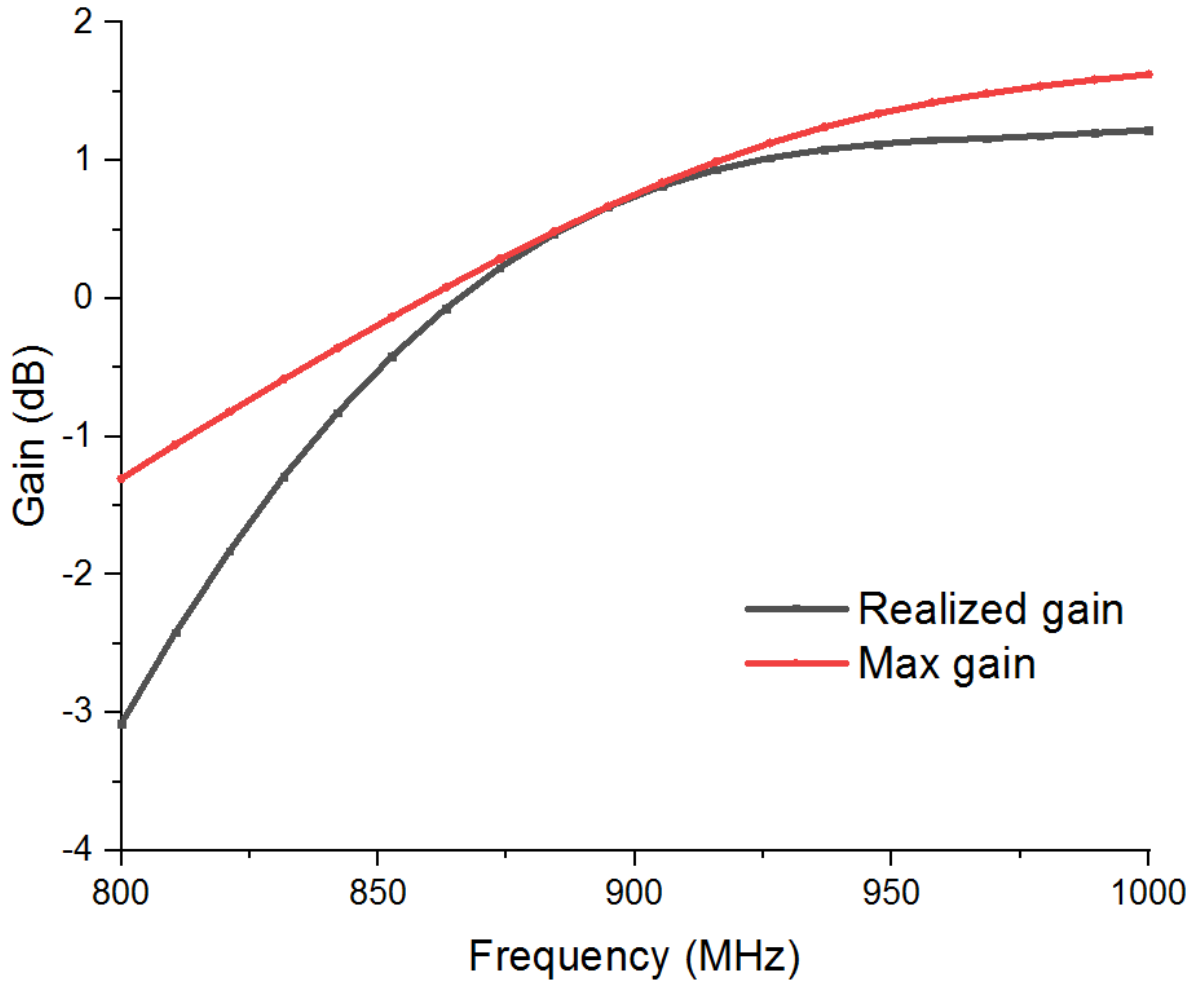

Fig. 3-14. Simulated gain over frequency.

3.4. Six band Rectifier development

In order to harvest maximum possible RF energy from the available frequency bands, the rectennas proposed in this thesis are structured with a broadband receiving antenna and a mutiband rectifier. Firstly, a mutiband rectifier structure is developed according to the topology proposed in [7] and [8].

As it presents in Fig. 3-15, the rectifier is constructed with three branches connected in parallel, each branch contains an RF filter (bandpass filter) and a diode rectifier. The purpose of the filters is to match the rectifers to different operating frequency bands, and then the rectifiers pass on the DC power to the load resistor.

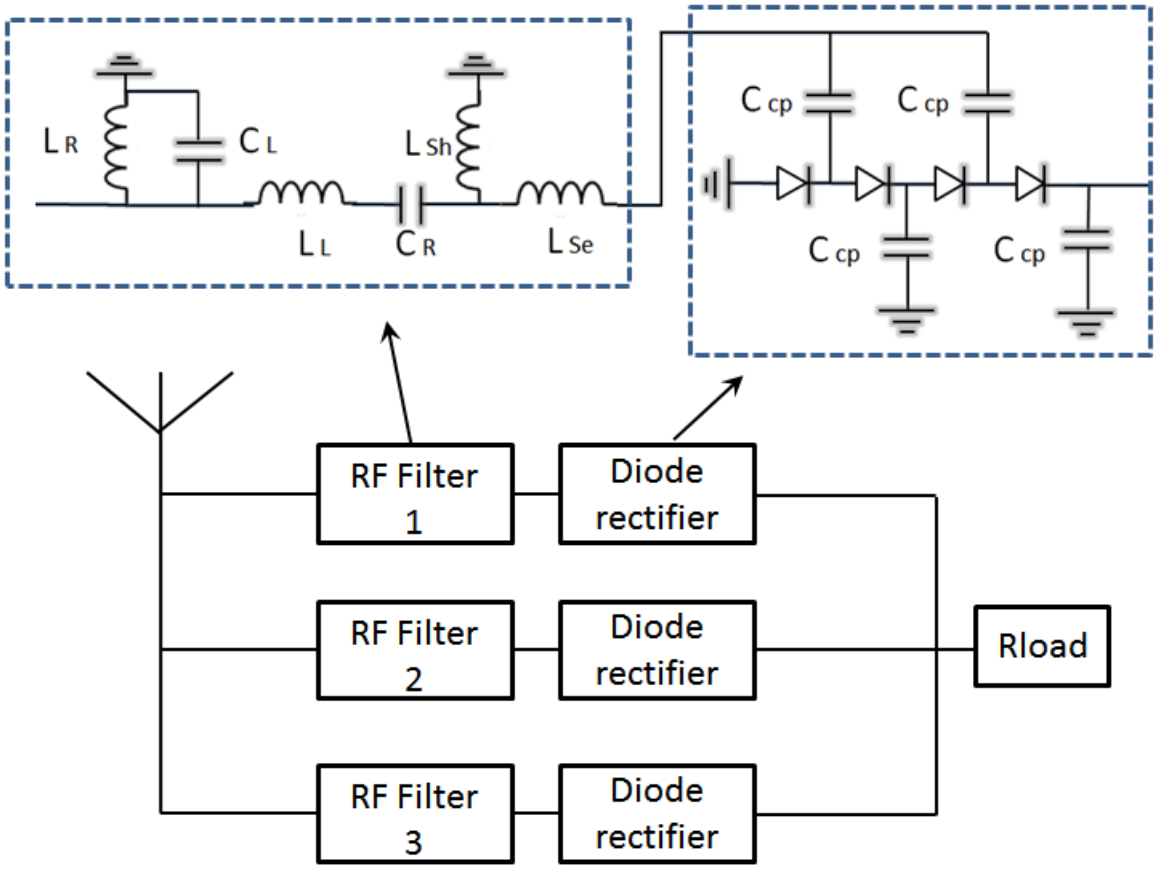

Fig. 3-15. Multiband RF rectifier layout

Table 3-1. Simulated Lump component parameters of the bandpass filters.

	Branch 1	Branch 2	Branch 3
L_R (nH)	44.3	19.2	12.9
C_L (pF)	2.9	2.7	0.5
L_L (nH)	0.2	4.4	0.1
C_R (pF)	6.6	2.9	0.2
L_{sh} (nH)	12	15.2	18.6
L_{se} (nH)	24.6	2.3	25.5

The simulation model of the rectifier is developed using ADS. Schottky diodes (SMS7630, Skyworks) are selected due to its low barrier and low forward voltage, and the capacitance of the coupling capacitors is 100 nF. The load resistance is set at 6.2 kΩ as a tested value for the highest conversion efficiency.

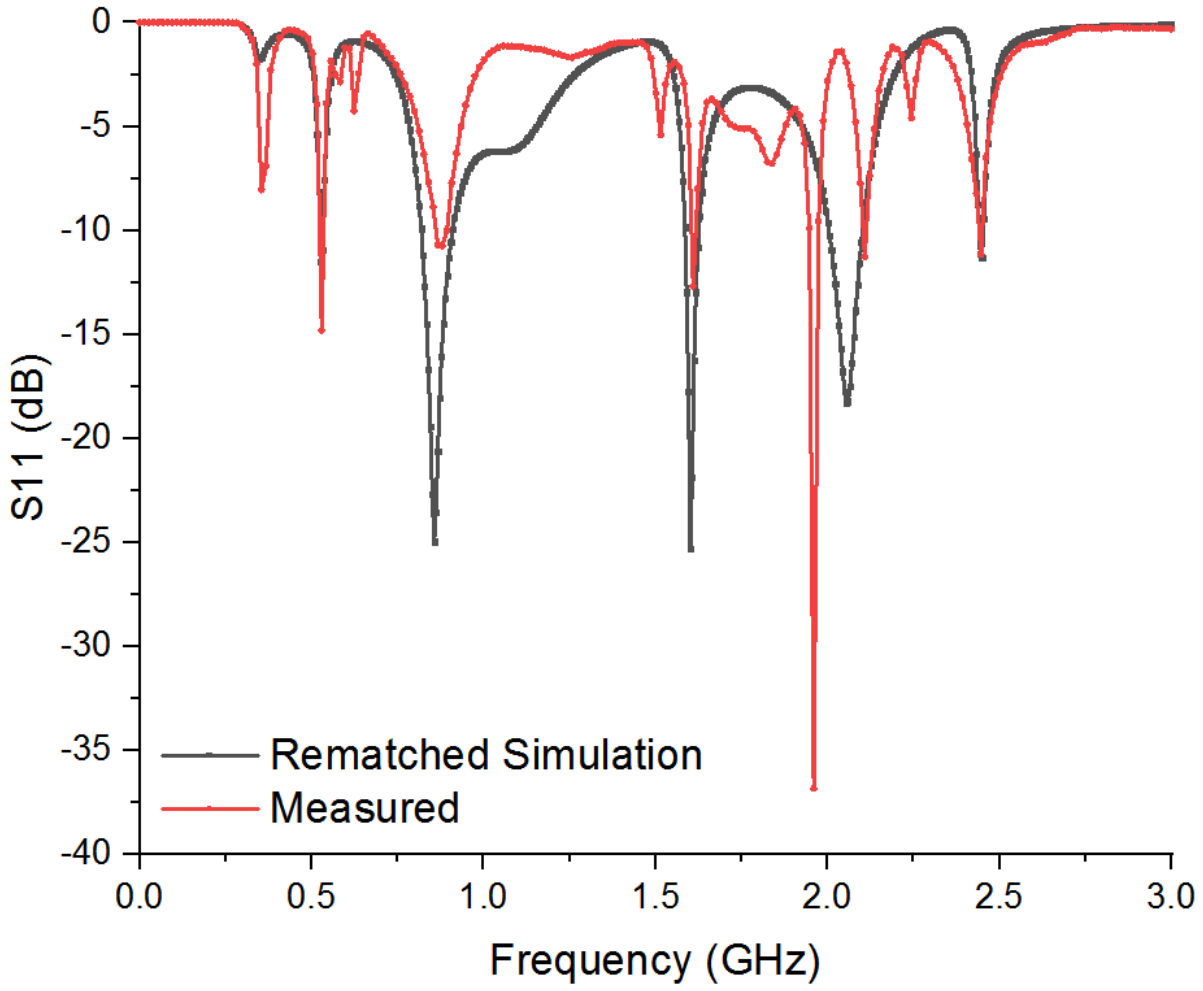

Fig. 3-16. Rematched simulation and measured S11 results for the six-band rectifier

The RF to DC conversion efficiency can be calculated with (3-10)

$$\eta = \frac{P_{DC}}{P_{in}} \tag{3-10}$$

where P_{DC} is the output DC power, and P_{in} is the input power.

For a multiband RF rectifier, there are three main factors that could induce mismatch between simulation and measured results. Firstly, the SPICE parameters for the simulation models of Schottky diodes are measured in a short range of frequencies, which could induce serious inconsistency between the simulated and measured S11 over a wide frequency range. Secondly, the metal track connections in the circuit can act as microstrip transmission lines that possess various impedances at different input frequencies. Furthermore, mismatch can also be caused by the unknown behavior of the lump components at various frequencies. To solve this problem, the matching networks for the rectifier are calculated using the measured

input impedance of the diode circuits. Afterwards, the simulated matching networks are adjusted to match up with the measured S11, and transmission lines with width of 10 mils (track line width) are added to each matching branch. As presented in Fig. 3-16, the S11 of the adjusted simulation circuit covers all resonant frequencies of the measurements under -10 dB, which ensures a better correspondence of conversion efficiency between simulation and measurements. The lump component parameters for the simulated matching networks are presented in Table 3-1.

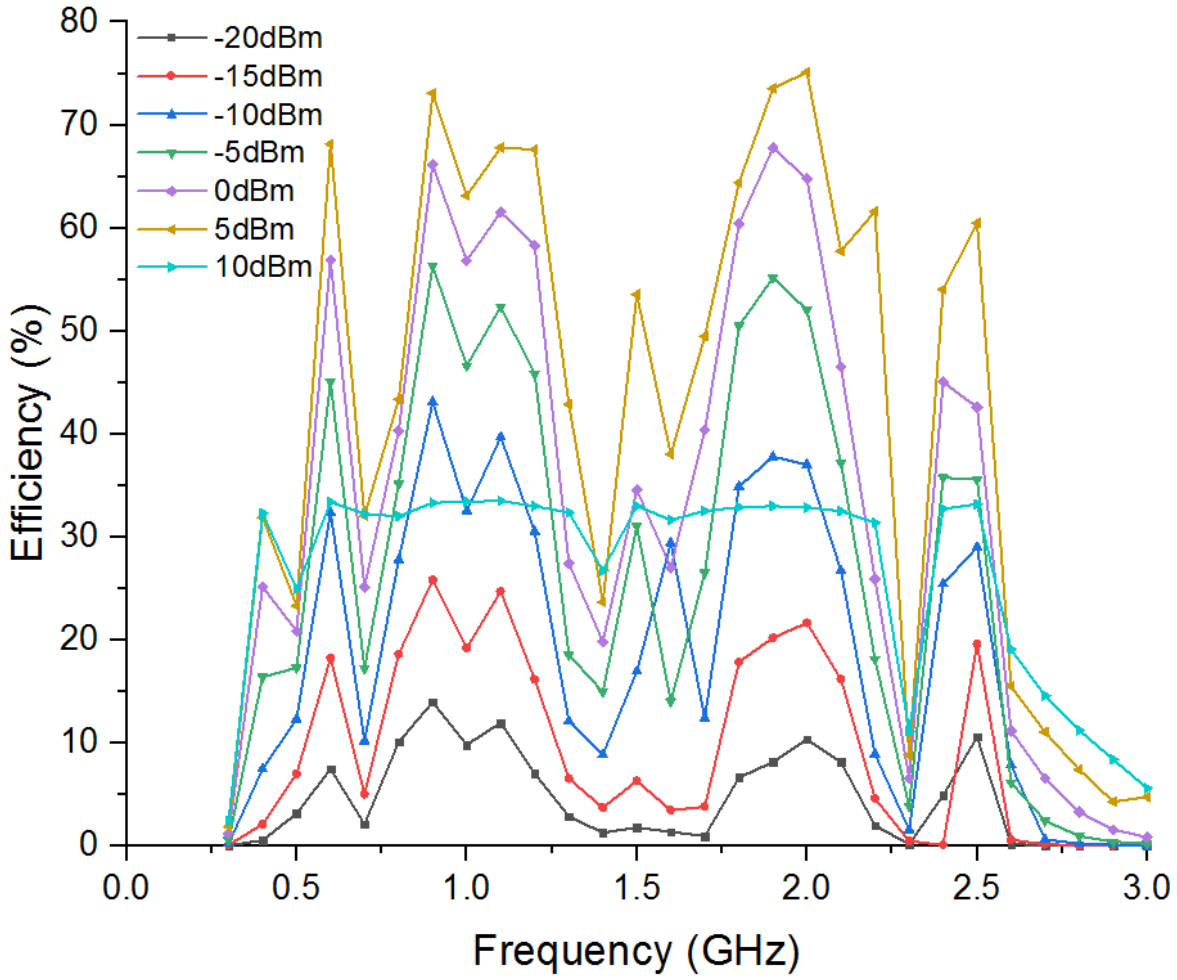

Fig. 3-17. Simulated conversion efficiency over frequency

The simulated conversion efficiency of the rectifier with input power level from -20dBm to 10 dBm is presented in Fig. 3-17. Within the frequency range between 0.3 to 3 GHz, the higher efficiencies mostly exist in the frequency bands corresponding to the S11 pattern. From -20 to 5 dBm, the average efficiency increases as the input power goes up. The efficiency achieves peak value at 0.9 and 2 GHz with input power level of 5 dBm. As the input power further increases to 10 dBm, the output voltage of the rectifier is limited by the

reverse breakdown voltage of the diodes, which results in a rapid decrement of the conversion efficiency.

The development of the six-band rectifier as a part of body worn energy harvesting system will be presented in detail in Chapter 7.

3.5. References

[1] How to design a 13.56 MHz customized tag antenna. AN2866 Application note, 2009. Available at: http://www.st.com/content/ccc/resource/technical/document/application_note/d9/29/ad/cc/04/7c/4c/1e/CD00221490.pdf/files/CD00221490.pdf/jcr:content/translations/en.CD00221490.pdf [Accessed 10 Mar. 2020].

[2] M. Gebhart, R. Neubauer and M. Stark, "Design of 13.56 MHz Smartcard Stickers with Ferrite for Payment and Authentication". *Third International Workshop on Near Field Communication*, 978-0-7695-4327-7/11, 2011. pp.59-64.

[3] D. Jan, "Fully Integrated High-Voltage Generators with Optimized Power Efficiency," Journal of Computer and Communications, vol. 2, no. 13, pp.1-8, Aug. 2014.

[4] J. Dickson, "On-chip high-voltage generation in MNOS integrated circuits using an improved voltage multiplier technique," IEEE Journal of Solid-State Circuits, vol. 11, no. 3, pp.374-378, Jun. 1976.

[5] E. Perret, S. Tedjini and R. S. Nair, "Design of Antennas for UHF RFID Tags," in Proceedings of the IEEE, vol. 100, no. 7, pp. 2330-2340, July 2012, doi: 10.1109/JPROC.2012.2186950.

[6] Hill J E. Gain of directional antennas. Watkins-Johnson Company Tech-notes, 1976

[7] V. Kuhn, C. Lahuec, F. Seguin and C. Person, "A Multi-Band Stacked RF Energy Harvester With RF-to-DC Efficiency Up to 84%," in IEEE Transactions on Microwave Theory and Techniques, vol. 63, no. 5, pp. 1768-1778, May 2015, doi: 10.1109/TMTT.2015.2416233.

[8] C. Song et al., "A Novel Six-Band Dual CP Rectenna Using Improved Impedance Matching Technique for Ambient RF Energy Harvesting," in IEEE Transactions on Antennas and Propagation, vol. 64, no. 7, pp. 3160-3171, July 2016, doi: 10.1109/TAP.2016.2565697.

e-Textile Embroidered Wearable Near-Field Communication RFID Antennas

IET Microwaves, Antennas & Propagation, vol. 13, no. 1, 2018, pp. 99-104

My contributions:

I have designed and fabricated the proposed devices, performed all of the measurements and data analyzation, and prepared all the graphs.

Chapter 4 e-Textile Embroidered Wearable Near-Field Communication RFID Antennas

Yutong Jiang [1], Lulu Xu [2], Kewen Pan [1], Ting Leng[1], Yi Li[2], Laith Danoon[1] and Zhirun Hu[1]

[1] School of Electrical and Electronic Engineering, the University of Manchester, Oxford Road, Manchester, United Kingdom.

[2]School of Materials the University of Manchester, Oxford Road, Manchester, United Kingdom

Abstract

Wearable e-textile Near Field Communication (NFC) RFID antennas fully integrated with garments using embroidery techniques, which enables everyday clothing to become connective to wireless communication systems, is presented. The e-textile wearable antennas have been designed through full electromagnetic wave simulation based on the electrical properties of conductive treads and textile substrates at the High Frequency (HF) band, allocated for NFC wireless communications. The e-textile wearable NFC antenna performance under mechanical bending as well as human body effects have been experimentally studied and evaluated; the antennas can operate under significantly bending angle and body effects attributed to its broad operating bandwidth. This is highly desirable and distinguished to conventional NFC antennas; the proposed e-textile wearable NFC antennas can be placed almost any place on clothes and still capable to communicate at desired operating frequency of 13.56 MHz. The maximum read range of the e-textile wearable NFC tags are measured to be around 5.6 cm, being compatible to typical commercially available metallic NFC tags. The e-textile wearable NFC tags can lead to numerous potential applications such as information exchange, personal security, health monitoring and IoTs.

4.1. Introduction

In recent years, Near Field Communication (NFC) has become increasingly popular in commodity market and believed to be one of the technologies that would realize the ubiquitous connectivity between the virtual internet world and the physical world for internet of things (IoTs) applications. The main function of an NFC system is contactless communication between NFC tag and reader without the requirement of any external battery. The first development of NFC tags can be traced back to 1970 when it was called "Short-Range Radio-Telemetry for Electronic Identification Using Modulated Backscatter" [1]. Till this day, NFC technology has been applied in numerous fields such as, ID cards, debit/credit cards, itemized commodities and hotel room keys [2].

The operating frequency of an NFC antenna is typically set at 13.56 MHz. A passive NFC tag operates by the transmitted power from the reader [3]. Magnetic induction coupling is applied between the tag antenna and the reader antenna within a short distance to draw its necessary operating power for the IC chip on the tag from the reader's electromagnetic field. NFC antennas possess a working distance that is typically around a couple of cm to a few tens of cm and a data transfer rate around 424 kbits/s for which the maximum value is up to 848 kbits/s [4].

The application of NFC tags for wearable wireless communications has been challenging since existing antenna fabrication methods, including chemical etching and screen printing, are not particularly suitable for close-fitting wearables [5]. Recently, researchers have developed various types of textile antennas that realize off-body communications, such as patch antennas applied in protective clothing for firefighters and basic attachments for normal garments [6], [7]. Wearable UHF RFID antennas have also been developed and implemented on smart textiles for various applications, such as body centric sensing and apnea detection and the maximum read range is up to 16 meters for patch UHF RFID antenna circuits with microchip connections [8]-[11]. Very different from UHF RFIDs, NFC RFIDs have limited read range usually within a few centimetres, which are preferred in more personal applications that require high security levels. Moreover, NFC RFIDs can be read by NFC-enabled smartphones while the reading of UHF RFIDs requires specific receiving antenna with relatively large sizes [12].

Among existing NFC tag antenna research, [13] has analysed metal NFC circuit performance regarding to varies resonant frequencies and return loss presented with simulation results only, and [14] has mainly discussed how textile based NFC circuits measurements respond to different types of substrate material. In this paper, NFC RFID antennas integrated with garment using embroidery technology are proposed, designed, fabricated, measured and characterized. Different from previous research, our work focuses on design and performance of purely textile based NFC tags regarding to specific requirements for daily wearables, for instance, when an NFC tag is bent from body movements, the resonant frequency shifts away from 13.56 MHz, which could easily result in communication failure. To prevent this, the NFC structure in this work is designed to achieve an operating bandwidth that is considerably wider than commercial ones. In fabrication, conductive treads with fairly low resistivity are integrated seamlessly with skin-friendly textile material, such as cotton, which possesses the flexibility to be easily applied on everyday garments. Microchips are bonded on the NFC antennas, which contain the information to be accessed by an NFC reader wirelessly. The novel e-textile wearable NFC tags are expected to lead to numerous potential applications within the fields such as information exchange, personal security, health monitoring and IoTs [15]-[16].

This paper is structured as follows. Section II will discuss the design methodology of e-textile wearable NFC antennas, material selections and embroidery technique. In Section III, measurements of the fabricated NFC tags are presented together with their RF performance evaluation (S-parameters) under various degrees of bending. Furthermore, the wireless reading measurements of the NFC tags including the effects of bending and human body contact are provided. Section IV summarizes the key results and findings.

4.2. Design methods and procedures

4.2.1. NFC Design and Simulation

For a passive NFC tag, the read range depends on the minimum transmitted power needed to operate the tag circuitry. Therefore, the main challenges in the design process are (a) to minimize the power dissipated by the antenna and (b) to maximize the conversion efficiency between the electromagnetic power from the reader and the DC power consumed by the tag [3].

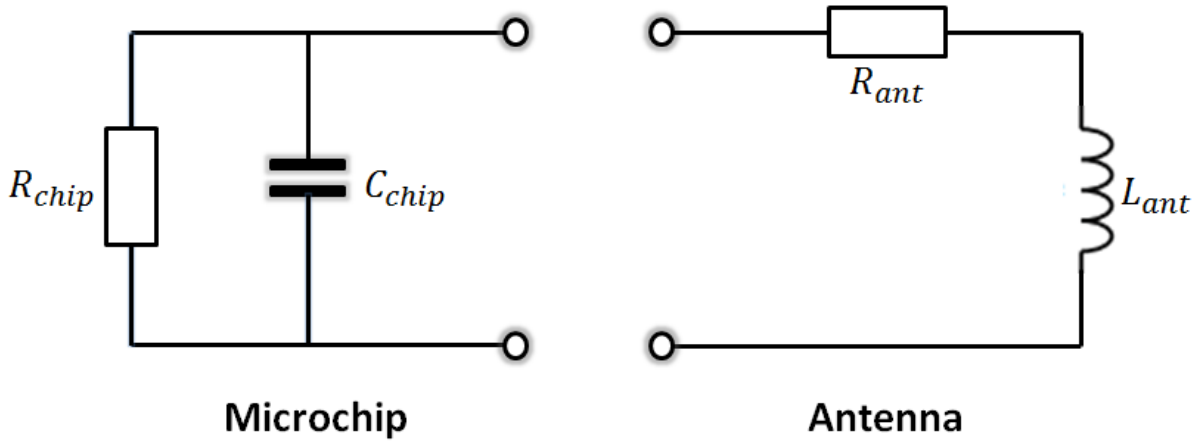

Fig. 4-1. Equivalent circuit model of an NFC-microchip matching network

Fig. 4-1 presents a simplified equivalent circuit for the microchip and antenna, where the antenna is designed to conjugately match the microchip. The antenna inductance $\boldsymbol{L_{ant}}$ which can be derived from (4-1) [17],

$$L_{ant} = \frac{1}{(2\pi f_r)^2 C_{chip}} \tag{4-1}$$

where $\boldsymbol{f_r}$ stands for the circuit resonant frequency and $\boldsymbol{C_{chip}}$ stands for the chip capacitance

Commercially available metallic NFC tags are usually designed with narrow bandwidth and Q factor around 30-40 in order to achieve high transmitting efficiency [18]. However, textile based NFC tags especially require relatively wide operating bandwidth to be able to tolerate clothing shape change and human body effects. The proposed NFC structure is designed and optimized to meet this requirement.

The NFC antennas in this work have been designed in a shape of rectangular spiral coil. The antenna dimensions are optimized with the antenna inductance according to (4-2) [17], based on which the preliminary layout of the NFC antenna is built for full wave simulation.

$$L_{ant} = K_1 \mu_0 N^2 \frac{d}{1+K_2 p} \tag{4-2}$$

where $\boldsymbol{d}$ is the coil diameter which is the mean value of the outer and inner diameters of the coil ($\boldsymbol{d_{out}}$ and $\boldsymbol{d_{in}}$); Note: for a square shaped coil, $\boldsymbol{d_{out}}$ and $\boldsymbol{d_{in}}$ respectively represent the outer and inner lengths of the edges which are highlighted in Fig. 2. $\boldsymbol{N}$ is the number of turns; $\boldsymbol{K_1}$ and $\boldsymbol{K_2}$ are parameters that depend on the layout, which are respectively 2.34 and 2.75 for square line inductors [12]; $\boldsymbol{\mu_0}$ is the free space permeability and $\boldsymbol{p=(\, d_{out} - d_{in}\,)/(\, d_{out} + d_{in})}$.

Fig. 4-2(a) and (b) present the NFC antenna layout created with CST Microwave Studio [19]. The antenna is fed by a discrete port that connects both ends of the NFC coil. The cross section of the thread is assumed to be circle with radius of 0.25mm. The choice of threads and yarns for these NFC RFID antennas is a trade-off between their electrical and mechanical properties. In other words, they are selected to be not only conductive but also structurally stable under possible bending [20]. In order to meet these requirements, threads used to construct NFC antennas are chosen as polyamide threads coated with silver. Although metal wire threads have also been considered in the design process due to their relatively low resistivity, their toughness and electrical stability are rather low and less suitable for textile circuits. The thread used in this work has a resistivity of 17.2 Ω/m, which is an order higher than aluminium used for commercial metallic NFC antennas. Cotton (ε_r = 1.4) has been chosen as substrate material due to its comfort level to human skin. NXP SL2S2102FTB microchip has been chosen in this work. The chip input capacitance is 97 pF at 13.56 MHz.

Fig. 4-2(c) illustrates simulated reflection coefficient (S11) of the optimized NFC antenna in the Smith chart. The NFC antenna model has impedance of 16.71+j120.32 Ω at 13.56 MHz, which indicates an antenna inductance of 1.41 μH. The imaginary part conjugately matches the microchip (SL2S2102FTB) input reactance -j121 Ω, and the chip resistance is large enough to be considered as an open circuit and therefore to be ignored in the connection with tag coil [21].

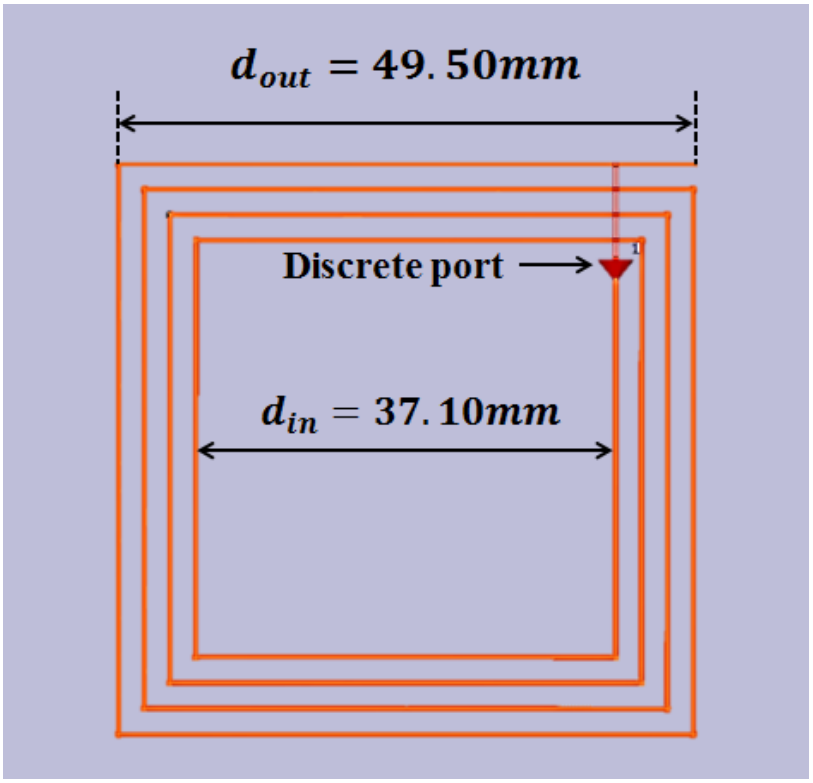

(a)

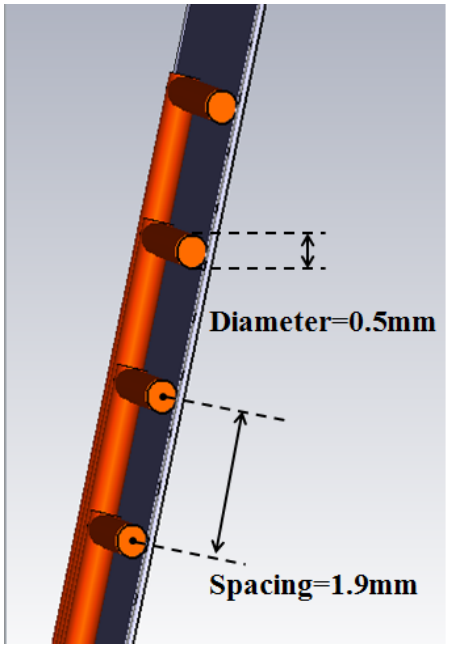

(b)

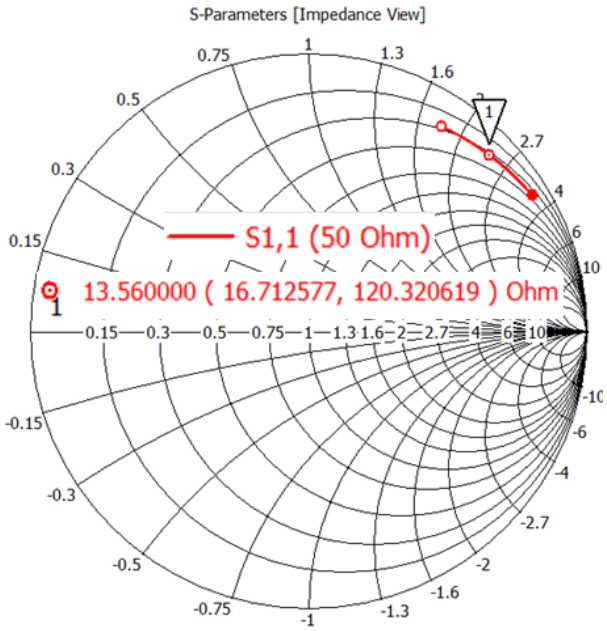

(c)

Fig. 4-2. CST model of designed NFC RFID antenna and simulated results:
(a) Model front view, (b) Cross-section cutting plane, (c) Simulated reflection coefficient (S_{11}) from the CST model

4.2.2. Fabrication

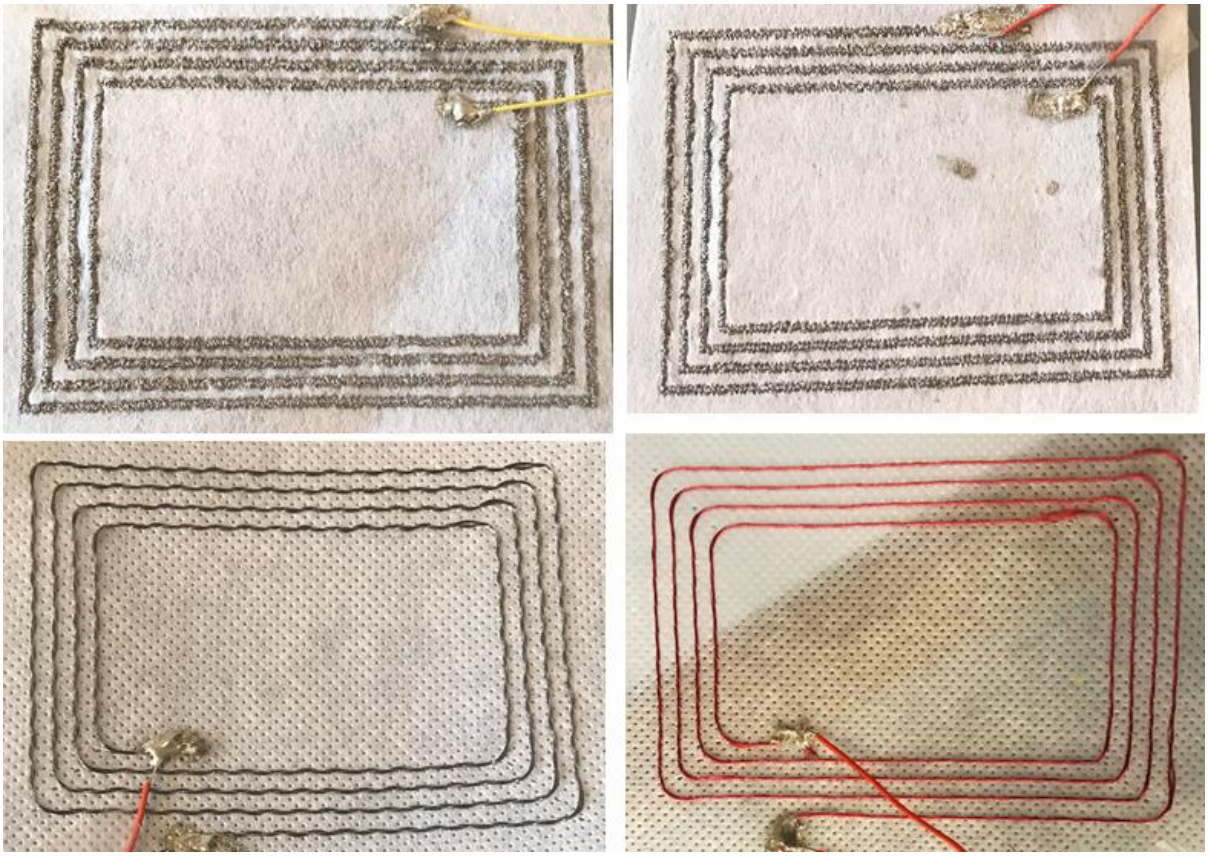

Fig. 4-3. Selected NFC antenna samples

Thirty NFC antenna prototypes embroidered on cotton substrate, made with conductive yarns coated with several types of metals, including silver, stainless steel and aluminium, have been designed and fabricated on cotton. Four samples of these circuits are shown in Fig. 4-3. Among all the coating materials, silver and stainless steel are believed to be the best choices for such conductive yarns to apply on wearables [22], [23]. Because of the high inertness of these two types of metal, they would not be much affected by sweat or moisture from the user. Moreover, silver and stainless steel have a high resistance against water and low concentrated acid so that the textile circuit would be applicable to dry cleaning and even mild water cleaning.

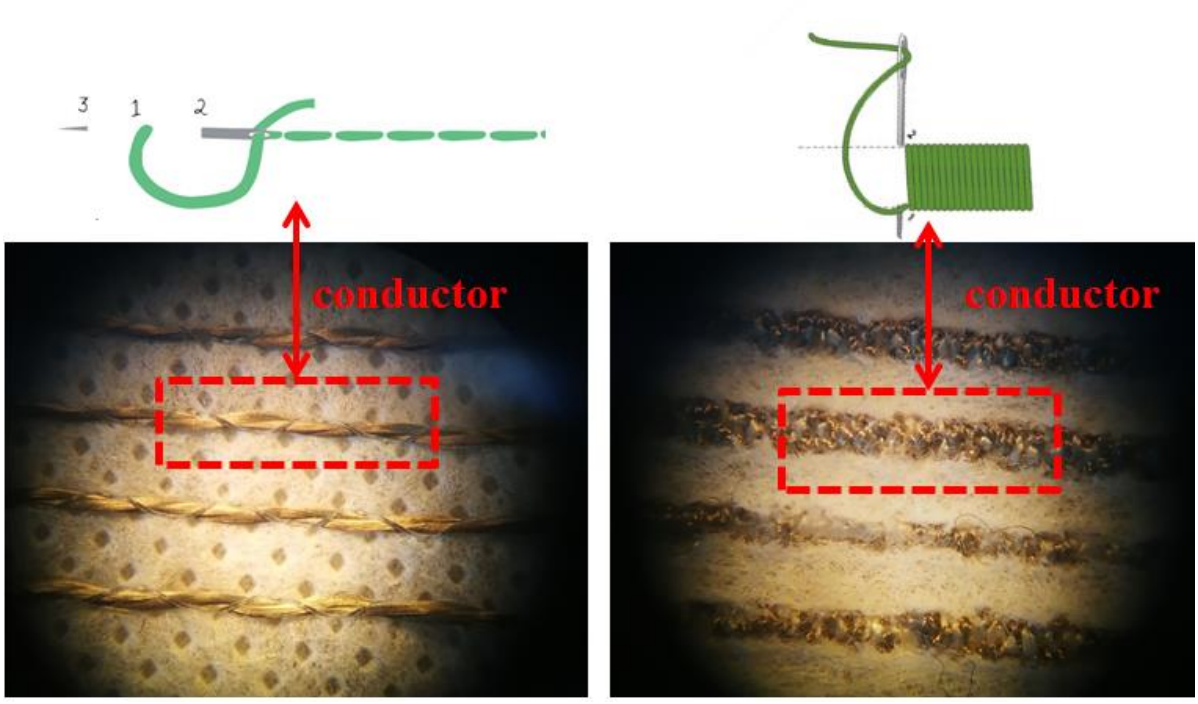

(a) (b)

Fig. 4-4. Stainless steel coated NFC antennas observed under a microscope corresponding to two different fabrication techniques: (a) Back stitch technique, (b) Satin stitch technique

Fig. 4-4 illustrates two embroidery techniques, back stitch and satin stitch, in fabricating NFC antennas respectively. Both antennas were constructed using stainless steel coated nylon threads. From the perspective of the stability of the structure, satin stitch is better than back stitch since it is more difficult to be snapped or ripped off. However, due to the fact that the satin stitch requires much longer threads for the same antenna size, the DC resistance of the antenna in Fig. 4-4(b) is measured as 70 Ω, which is much higher than the one in Fig. 4-4(a) that is 11.6Ω. For this very reason, back stitch is used in this work.

4.3. Results and discussion

4.3.1. DC characteristics

In Fig. 4-5, three NFC RFID antennas with the same structure are presented, where Fig. 4-5(a) is the proposed circuit and Fig. 4-5(b) and (c) are fabricated for the purpose of performance comparison. The antenna dimensions are listed in Table 4-1. Fig. 4-5(a) and (b) show antenna coils made with silver coated nylon conductive threads with 0.5mm thickness (Arduino Flux Workshop) and stainless steel coated conductive threads with 0.3mm thickness (BEKAERT)

by back stitch embroidery technique. The DC resistance of the antenna is measured as 9.9 Ω and 21.6 Ω respectively. A copper NFC tag with on FR4 substrate (ε_r=4.7) with a line width of 0.5mm and a thickness of 17.5 mm is presented in Fig. 4-5(c) as copper is one of the most common material in commercial NFC manufacture, the DC resistance of which is only 2.2 Ω.

(a)

(b)

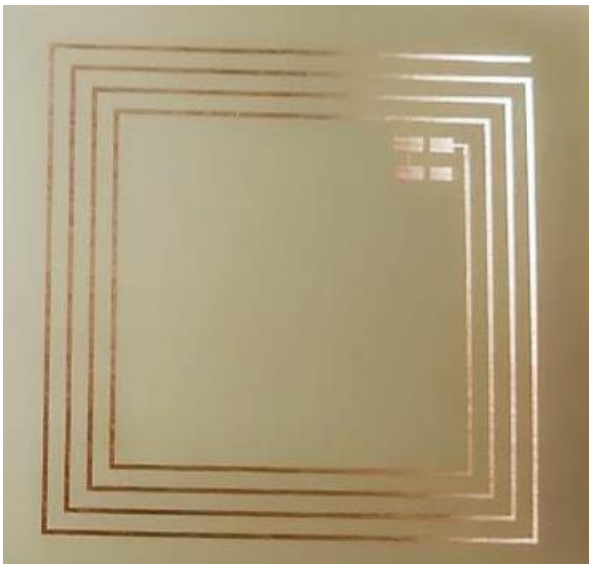

(c)

Fig. 4-5. NFC antenna prototypes:
(a) Silver coated conductive threads embroidered with cotton, (b) Stainless steel coated conductive threads embroidered with cotton, (c) Copper on PCB

The antenna is designed to be matched up with an NXP microchip SL2S2102FTB which can be regarded as purely capacitive. Referring to Fig. 4-1, only the imaginary parts between the microchip and antenna can be matched conjugately as the coil antenna can't be lossless. To realize the best power transmitting efficiency the microchip series resistance (approximately zero) and antenna resistance need to be as close as possible [24]. Therefore, silver coated conductive threads are preferred rather than those with stainless steel coatings due to a lower resistivity.

Table 4-1. NFC antenna parameters

Length (mm)	Width (mm)	Spacing between turns (mm)	Number of turns
49.5	49.5	1.9	4

4.3.2. Bandwidth

In order to verify the resonant frequency and bandwidth of the NFC tag antennas, S-parameters of the antenna were measured using Keysight Fieldfox VNA N9918A. Fig. 4-6(a) shows the S11 of the silver coated textile antenna coil in the Smith chart, the antenna has measured impedance of 13.5+j119.5 Ω at 13.56 MHz, which is fairly close to the designed value (16.7+j120.3 Ω). The coil inductance calculated from this measurement is 1.4 μH.

The quality factor of the antenna can be calculated from the measured resistance and inductance using (4-3) [25],

$$Q = \frac{2\pi f_r L_{ant}}{R} \tag{4-3}$$

where $\boldsymbol{f_r}$ is the antenna resonant frequency and $\boldsymbol{L_{ant}}$ and $\boldsymbol{R}$ are the coil inductance and resistance respectively. The Q factor of the proposed textile NFC tag is 8.85.

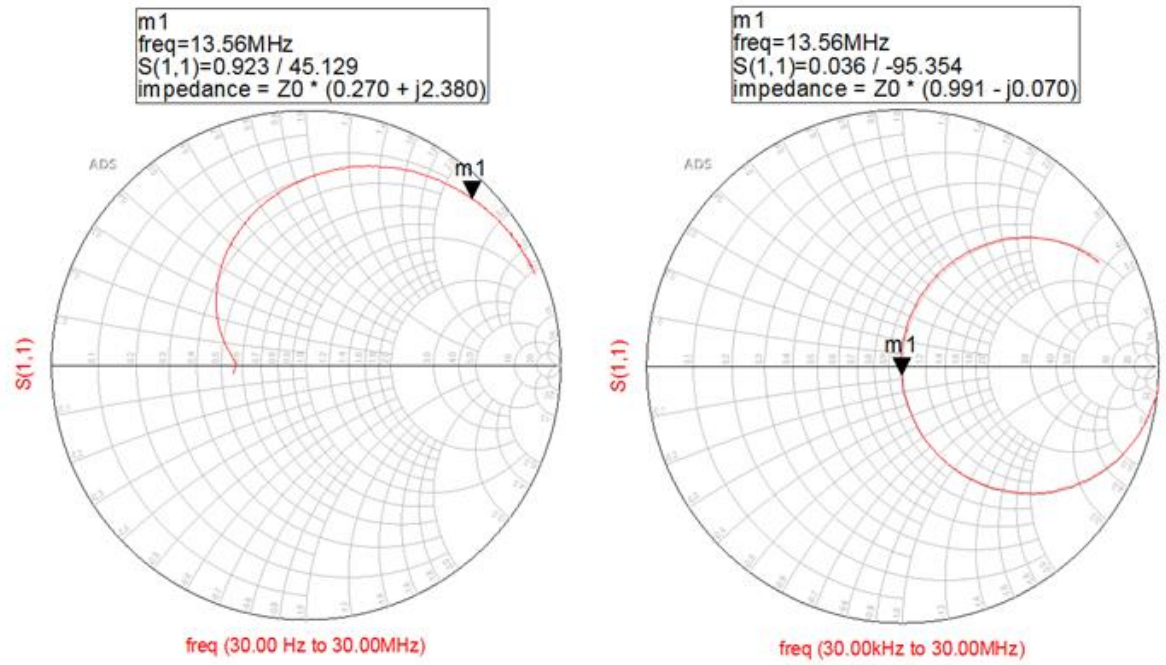

(a) (b)

Fig. 4-6. Measured reflection coefficient S_{11} in Smith Chart format:
(a) Antenna coil measurements, (b) Antenna connected with matching circuit

In order to test the tag performance at the operating frequency, a matching circuit consisted with a resistor (36 Ω) and a capacitor (97 pF) is connected in series with the antenna coil. The capacitor value is chosen as the input capacitance of the microchip so that the imaginary part is matched to zero, and the purpose of the series resistor is to match the circuit impedance with the VNA input impedance (50 Ω) in order to minimize reflected power at the resonant point. The circuit impedance after matching is presented in Fig. 4-6(b), where the admittance is almost entirely cancelled out and the resistance is matched to approximated 50 Ω.

Fig. 4-7 depicts the measured S_{11} magnitude of the three NFC antennas shown in Fig. 4-5. The detailed comparison results are listed in Table 4-2. All three antennas resonate around 13.56 MHz as designed with return loss of -32.52 dB, -32.03 dB and -38.09 dB, respectively. The 10 dB bandwidth results of the textile antennas coated with silver (3.787 MHz) and stainless steel (3.794MHz) are slightly wider than the one of copper antenna (3.61 MHz), which is also considerably wider than that of commercial NFC tag antennas [26]. The wide bandwidth is a critical parameter for wearable applications as the resonant frequency of the

antenna shifts when the garment bends. For a narrow band antenna, the shift of the resonance frequency will cause the tag unreadable by NFC readers.

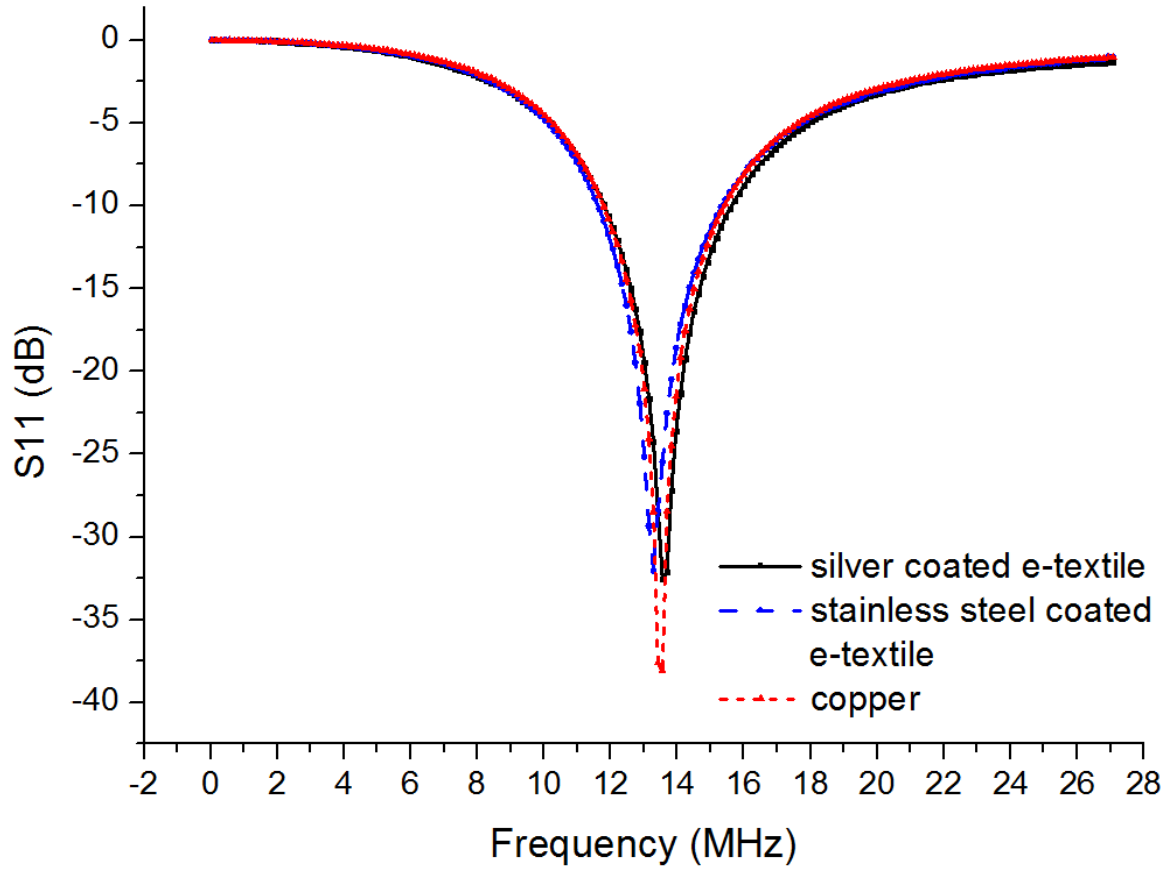

Fig. 4-7. S_{11} results of NFC circuits made of e-textile and copper in magnitude (dB) against frequency

In Table 4-2, the Q factor of copper NFC circuit is considerably higher than the ones made with metal coated conductive threads since the power transmitting efficiency is directly related to the antenna resistance. Considering a trade-off between the working efficiency and operating bandwidth required for textile integrated circuits, the proposed silver coated e-textile based NFC antenna is fairly applicable.

Table 4-2. Experimental result comparison between NFC tags manufactured with e-textile and copper

Material	Silver coated	Stainless steel coated	Copper
DC resistance (Ω)	9.9	21.6	2.2
Network impedance at 13.56MHz (Ω)	13.5+ j119.5	26.2+ j124.5	2.5+ j119.2
Q factor	8.85	4.75	47.7
S11 (dB)	-32.52	-32.03	-38.09
10dB bandwidth (MHz)	3.787	3.794	3.610

4.3.3. Bending tests

To integrate e-textile NFC RFID antennas into close-fitting garments, it is essential to ensure it has stable electrical properties, such as operating efficiency and read range, when the antenna is under natural human body movements. Since the antenna is applied to a cotton substrate which can be easily bent out of shape, natural bending seems to be the factor that would most likely affect the antenna operation. Therefore, it is necessary to determine how the antenna performance would change with different bending.

Fig. 4-8 illustrates bending tests of the NFC antenna using U bend method [27] where four plastic cylinders with different diameters are applied for the NFC antenna to be bent around. The measured S11 magnitude and impedance with and without bending are shown in Fig. 4-9 and Table 4-3, respectively.

As presented in Fig. 4-9, the resonance frequency and operational bandwidth of the NFC antenna change slightly as the bending increases. However, due to the broad bandwidth of the

antenna, the shift of resonant frequency would not affect the RFID reading as long as 13.56 MHz still falls within the 10 dB bandwidth.

(a) (b) (c) (d)

Fig. 4-8. Antenna bent around four cylinders with decreasing diameters of:
(a) 35 mm, (b) 28 mm, (c) 23 mm, (d) 17 mm

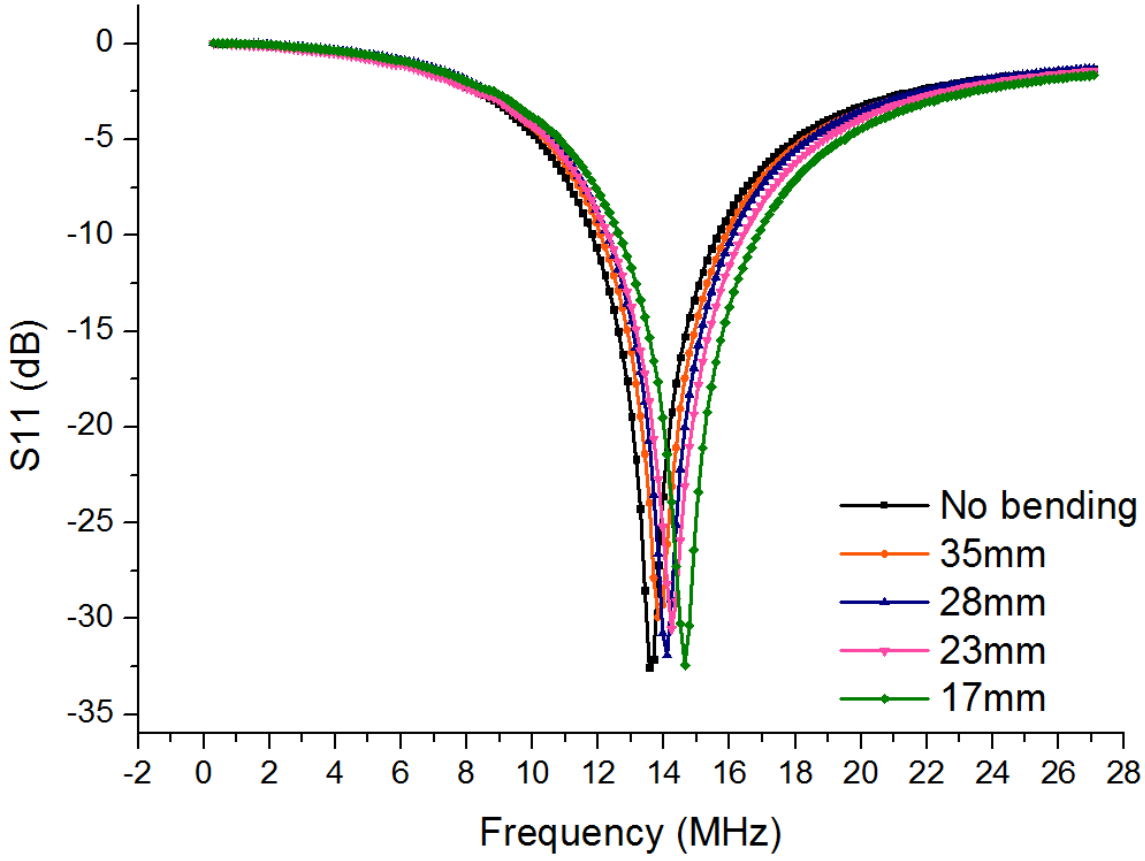

Fig. 4-9. Measured S_{11} magnitudes for 4 different bending cases shown in Fig. 4-8 and without bending

Table 4-3. Results for bending tests

Bending diameter /mm	N/A	35	28	23	17
f_c /MHZ	13.56	13.82	14.10	14.23	14.64
S(1,1)/dB	-32.52	-29.91	-31.1	-30.54	-32.42
$Z(f_c)/\Omega$	49.6-j3.5	51.9-j8.9	50.5-j11.8	50.9-j14.6	50.4-j20.2

In Table 4-3, $\boldsymbol{Z(f_c)}$ represents the matched antenna impedance at each central frequency for different bending. The imaginary part of the antenna impedance decreases as the bending increases, which indicates gradual decrements of the antenna inductance. This is due to the fact that when the antenna is no longer planar but bent around the cylinder, the current flowing in the opposing sides of the antenna is drawn closer to each other, thus the electromagnetic field exists on both sides of the circuit tend to introduce extra electrical coupling that cancels out the inductance of the antenna. Consequently, the NFC resonance frequency goes up as the antenna inductance decreases.

4.3.4. Power transmission and Wireless reading

After the NFC antenna is connected with a microchip, the contactless antenna verification method described in [17] is performed to determine the NFC antenna power transmission pattern during wireless measurements as presented in Fig. 4-10(a).

From the measurements shown in Fig. 4-10(b), the detected voltage levels with an oscilloscope are higher than the source voltage (0.25 V), which means the magnetic field produced by the generator coil induces a current flow in the NFC tag, and the magnetic field generated from this current is captured by the oscilloscope coil. At tag resonant frequency, the current flowing into the tag antenna is maximized. As a result, the proposed NFC antenna is able to achieve the maximum transmitted power at 13.6 MHz, showing the antenna is well tuned.

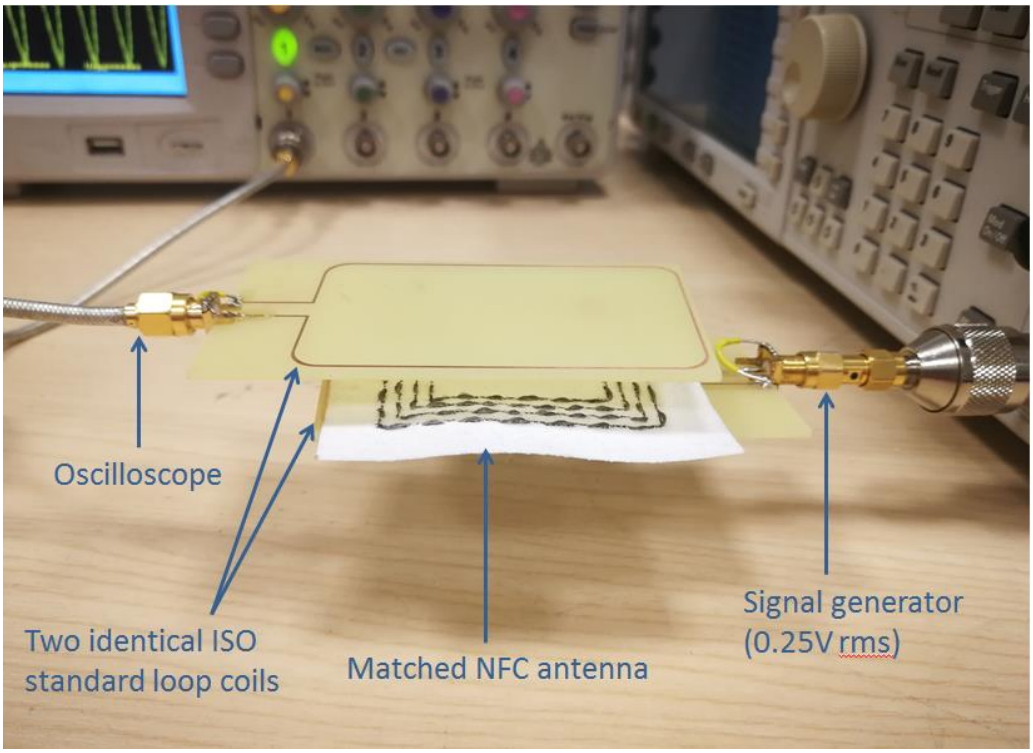

(a)

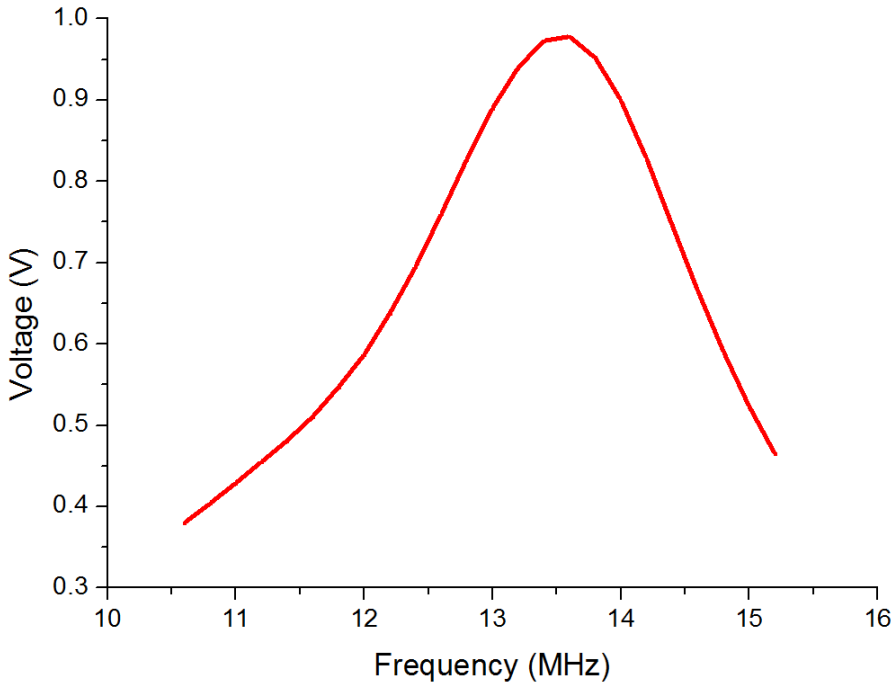

(b)

Fig. 4-10. Contactless antenna verification:

(a) Measurement set up, (b) Detected voltage level vs frequency

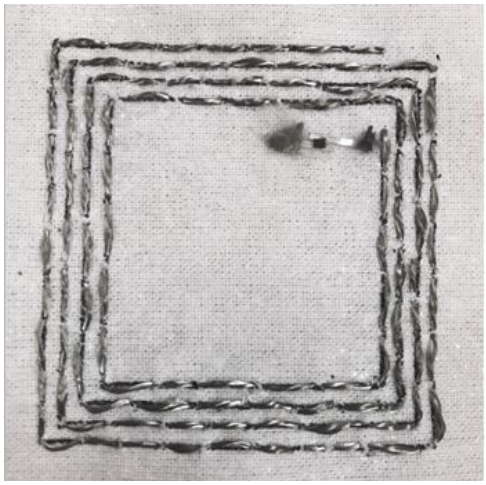

(a)

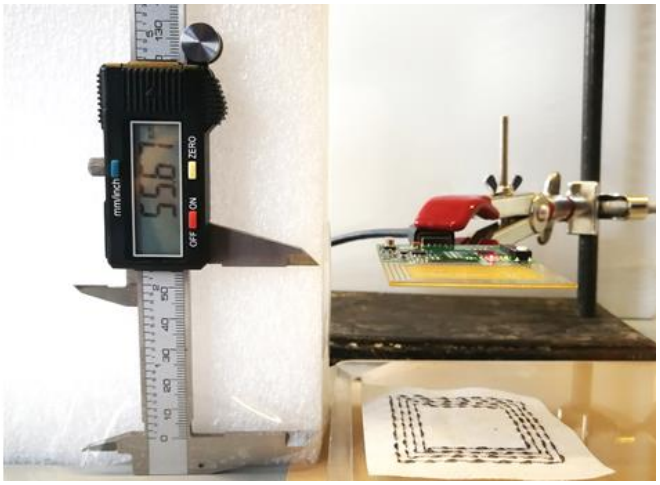

(b)

(c)

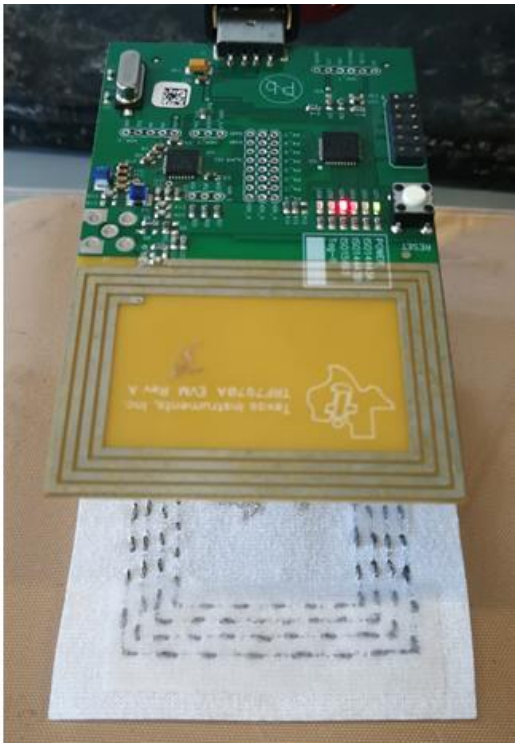

(d)

Fig. 4-11. Read distance measurements:

(a) Fabricated e-textile wearable NFC RFID tag, (b) Tag reading experimental set up, (c) NFC tag detected by the RFID reader (facing forward), (d) NFC tag detected by the RFID reader (facing backward)

(a)

(b)

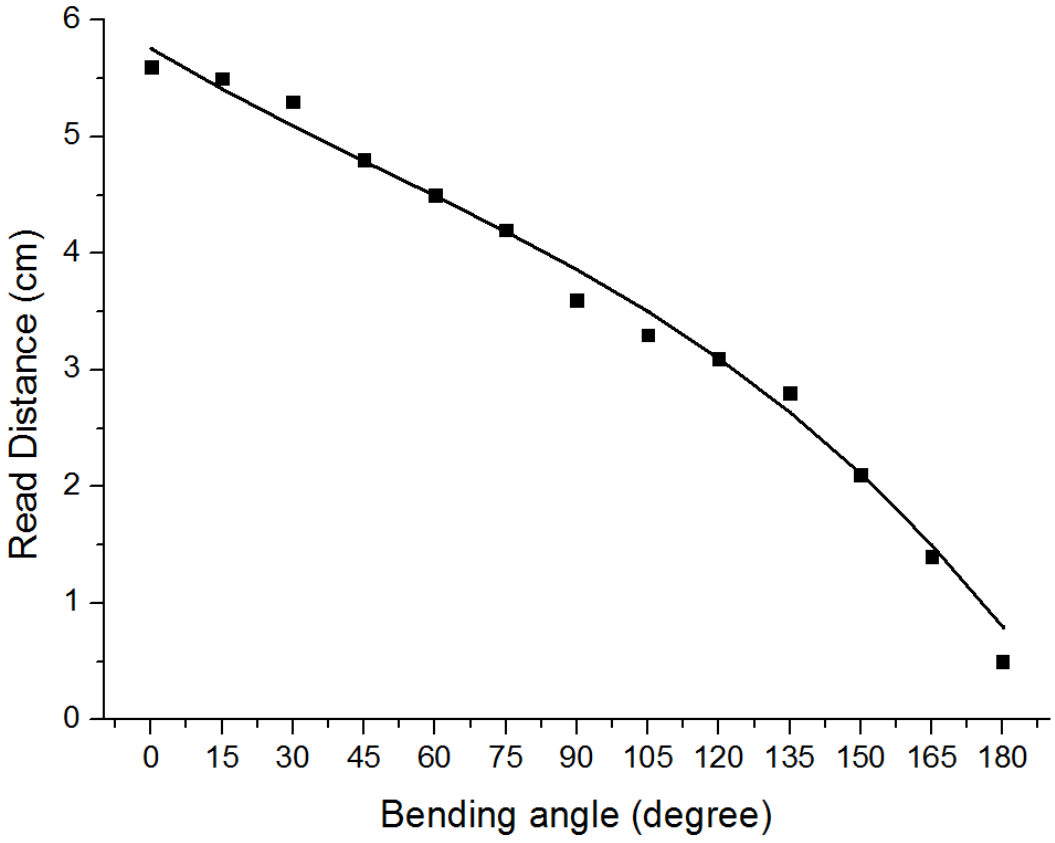

(c)

Fig. 4-12. Wirless bending test:

(a) 120 degree V-bend set up, (b) Tag read with 120 degree bend angle, (c) NFC tag read range decreases with increasing degree of bending

In order to measure the NFC tag read range, a microchip (NXP SL2S2102FTB) has been connected to the NFC antenna as shown in Fig. 4-11(a). A USB-connected Texas Instruments reader, (TRF7970A) is used for the read range measurement. The experimental set up for tag reading is presented in Fig. 4-11(b), where the reader is held horizontally above the tag with a laboratory stand and the distance between is measured with an electrical vernier caliper. It is crucial that no metal surface is near the tag or the reader, otherwise the read distance would be affected. Once an NFC tag is held within a certain range of the reader, the red LED on the reader goes on as shown in Fig. 4-11(c) and (d), meaning the RFID data has been received by the reader.

Both forward and backward facing directions were tested in the measurements, between which hardly any difference has been observed. The best read range of the NFC RFID tag is 5.57 cm. Comparing to the read distance of a commercial aluminium NFC tag (ST25TA64K) tested with the same reader which is 8.17 cm; such results are satisfying for an NFC tag that aims for short range reading.

A simple bending test has also been applied in order to observe the read range limits of the tag, where a V-bend method has been carried out [27] as shown in Fig. 4-12(a) and (b). The bending angles are set up with an electrical angle meter and maintained with scotch tapes and plastic tweezers during measurements. The results are presented in Fig. 4-12(c), showing how the read range is affected by increasing degree of bending.

As the antenna working frequency shifts further from its original point with increasing degrees of bending, the reflected power from the NFC tag gradually decreases. Consequently, the read range of the tag is shortened since there is less magnetic flux going through the antenna coil. Nonetheless, due to the wide bandwidth of the antenna, the NFC tag is able to be read within 0.5cm even though the tag is almost completely folded (180° bending angle).

4.3.5. Effect of Human Body

In order to ensure the e-textile wearable NFC RFID tag is fully functional in daily use, it is necessary to take measurements with human skin contact. In existing research, [28] has presented that how vicinity of skin affects the performance of wearable patch antennas. Since the NFC coil in this paper is seamlessly integrated with very light substrate, direct skin contact can easily occur.

Among all conditions listed in Table 4-4, the tag is mostly reduced by direct skin contact. This is due to the fact that transmitted EM energy is partially absorbed by body tissue layers, which leads to a slight reduction in the tag current [29].

Table 4-4. NFC read range with different levels of skin contact

Condition	Read range (cm)
Direct skin contact	5.3
Vicinity of skin without touching (1mm)	5.5
A thin cotton layer (0.5mm thickness) between skin and tag	5.5
Without skin contact	5.6

4.4. Conclusion

This paper has presented the design and fabrication process of novel e-textile wearable NFC antennas which are fully integrated with garment, enabling truly ubiquitous wireless connectivity to everyday clothing. The NFC tags perform well under bending and human body effects. The 10 dB bandwidth of the fabricated NFC antenna is 3.787 MHz and the quality factor is 8.85. The broad operation bandwidth of the e-textile NFC RFID tags proposed in this work is highly desirable for smart textile due to its flexibility towards bending and can potentially lead to numerous applications, such as personal security, health and wellbeing monitoring, big data and IoTs.

4.5. References

[1] Landt, J. (2005). The history of RFID. IEEE Potentials, 24(4), pp.8-11.

[2] Coskun, V., Ok, K. and Ozdenizci, B. (2011). Near Field Communication (NFC). 1st ed. Somerset: Wiley.

[3] Roselli, L. (2014). Green RFID systems. 1st ed. Cambridge, United Kingdom: Cambridge University Press, p.8.

[4] Curran, K., Millar, A. and Mc Garvey, C. (2012). Near Field Communication. International Journal of Electrical and Computer Engineering (IJECE), 2(3).

[5] Choi, E., Park, J., Kim, B. and Lee, D. (2015). Fabrication of electrodes and near-field communication tags based on screen printing of silver seed patterns and copper electroless plating. International Journal of Precision Engineering and Manufacturing, 16(10), pp.2199-2204.

[6] Hertleer, C., Rogier, H., Vallozzi, L. and Van Langenhove, L. (2009). A Textile Antenna for Off-Body Communication Integrated Into Protective Clothing for Firefighters. IEEE Transactions on Antennas and Propagation, 57(4), pp.919-925.

[7] Chen, S., Kaufmann, T., Ranasinghe, D. and Fumeaux, C. (2016). A Modular Textile Antenna Design Using Snap-on Buttons for Wearable Applications. IEEE Transactions on Antennas and Propagation, 64(3), pp.894-903.

[8] K. Koski, L. Sydänheimo, Y. Rahmat-Samii and L. Ukkonen, "Fundamental Characteristics of Electro-Textiles in Wearable UHF RFID Patch Antennas for Body-Centric Sensing Systems," in IEEE Transactions on Antennas and Propagation, vol. 62, no. 12, pp. 6454-6462, Dec. 2014.

[9] W. M. Mongan, I. Rasheed, K. Ved, A. Levitt, E. Anday, K. Dandekar, G. Dion, T. Kurzweg, and A. Fontecchio, "Real-time detection of apnea via signal processing of time-series properties of RFID-based smart garments," in 2016 IEEE Signal Processing in Medicine and Biology Symposium (SPMB), 2016, pp. 1-6.

[10] Virkki, J., Wei, Z., Liu, A., Ukkonen, L. and Björninen, T. (2017). Wearable Passive E-Textile UHF RFID Tag Based on a Slotted Patch Antenna with Sewn Ground and Microchip Interconnections. International Journal of Antennas and Propagation, 2017, pp.1-8.

[11] Ginestet, G., Brechet, N., Torres, J., Moradi, E., Ukkonen, L., Bjorninen, T. and Virkki, J. (2017). Embroidered Antenna-Microchip Interconnections and Contour Antennas in Passive UHF RFID Textile Tags. IEEE Antennas and Wireless Propagation Letters, 16, pp.1205-1208.

[12] Nikitin, P. and Rao, K. (2006). Theory and measurement of backscattering from RFID tags. IEEE Antennas and Propagation Magazine, 48(6), pp.212-218.

[13] Iqbal, R. and Saeed, M. (2014). Wearable Near Field Communication Ring Antenna for Mobile Communication. International Conference on Open Source Systems and Technologies.

[14] Del-Rio-Ruiz, R. and Lopez-Garde, J. (2017). Design and Performance Analysis of a Purely Textile Spiral Antenna for On-Body NFC Applications. IEEE MTT-S International Microwave Workshop Series on Advanced Materials and Processes.

[15]Shaikh, F., Zeadally, S. and Exposito, E. (2017). Enabling Technologies for Green Internet of Things. IEEE Systems Journal, 11(2), pp.983-994.

[16] Atzori, L., Iera, A. and Morabito, G. (2010). The Internet of Things: A survey. Computer Networks, 54(15), pp.2787-2805.

[17] How to design a 13.56 MHz customized tag antenna. (2009). AN2866 Application note. [online] Available at: http://www.ebvnews.ru/doc/AN15284.pdf [Accessed 10 Mar. 2017].

[18] RF430CL330H Practical Antenna Design Guide. (2014). TEXAS INSTRUMRNTS, (SLOA197).

[19] Cst.com. (2017). CST MICROWAVE STUDIO® - 3D EM Simulation Software. [online] Available at: https://www.cst.com/products/cstmws [Accessed 26 Nov. 2017].

[20] Post, E., Orth, M., Russo, P. and Gershenfeld, N. (2000). E-broidery: Design and fabrication of textile-based computing. IBM Systems Journal, 39(3.4), pp.840-860.

[21] Farnell.com. (2017). [online] Available at: http://www.farnell.com/datasheets/1683422.pdf?_ga=2.61107945.41218670.1493817437-1811059628.1491485357 [Accessed 26 Nov. 2017].

[22] Atwa, Y., Maheshwari, N. and Goldthorpe, I. (2015). Silver nanowire coated threads for electrically conductive textiles. J. Mater. Chem. C, 3(16), pp.3908-3912.

[23] JOSEPH, S., MCCLURE, J., CHIANELLI, R., PICH, P. and SEBASTIAN, P. (2005). Conducting polymer-coated stainless steel bipolar plates for proton exchange membrane fuel cells (PEMFC). International Journal of Hydrogen Energy, 30(12), pp.1339-1344.

[24] Rahola, J. (2008). Power Waves and Conjugate Matching. IEEE Transactions on Circuits and Systems II: Express Briefs, 55(1), pp.92-96.

[25] Measurement and tuning of a NFC and Reader IC antenna with a MiniVNA. (2014). AN11535, (291991).

[26] Lee, Y. (1998). RFID coil design. Microchip Technol. Inc. Appl. Note.

[27] ASTM E290-14 Standard Test Methods for Bend Testing of Material for Ductility, ASTM International, West Conshohocken, PA, 2014, https://doi.org/10.1520/E0290-14

[28] P. Salonen, Y. Rahmnat-Sarnii, and M. Kivikoski (2004), "Wearable Antennas in the Vicinity of Human Body," IEEE International Symposium on Antennas and Propagation Digest, 1, June 20-25, 2004, pp. 467-470.

[29] Klemm, M. and Troester, G. (2006). EM ENERGY ABSORPTION IN THE HUMAN BODY TISSUES DUE TO UWB ANTENNAS. Progress In Electromagnetics Research, 62, pp.261-280.

Smart Textile Integrated Wireless Powered Near Field Communication (NFC) Body Temperature and Sweat Sensing System

IEEE Journal of Electromagnetics, RF and Microwaves in Medicine and Biology, vol. 4, no. 3, 2019, pp. 164-170

My contributions:

I have designed and fabricated the proposed devices, participated in the program writing for device measurements, performed all of the measurements and data analyzation, and prepared all the graphs.

Chapter 5 Smart Textile Integrated Wireless Powered Near Field Communication (NFC) Body Temperature and Sweat Sensing System

Yutong Jiang, Kewen Pan, Ting Leng and Zhirun Hu, *Member, IEEE*

Abstract

Near Field Communication (NFC) is a short-range wireless communication technique that has become attractive devices for healthcare and wellbeing monitoring. The work reported here demonstrates the development of a battery free wearable sensing system with temperature and sweat sensors embedded into and powered by a smart textile NFC antenna. The NFC antenna is seamlessly integrated with closed-body garments, and sensor data can be easily acquired by NFC readers and smart phones in order to achieve real time and wireless monitor of health status in a convenient and non-intrusive way. A Dickson charge pump circuit has been designed and implemented in order to pump up the voltage and ensure a steady voltage supply for the sweat sensor. The maximum read range for accessing sensor data is 6 cm. The on-body measurement accuracy of the temperature sensor and sweat sensor are able to achieve ±0.14°C and ±0.2%, respectively. The presented system can provide wearable battery-free ubiquitous wireless connectivity for point-of-care and any time healthcare and wellbeing monitoring.

5.1. Introduction

In recent years, great interest has been raised in integrating electronic devices, such as antennas, electrodes and sensors with daily wearables to form e-textiles [1], [2]. Since clothes are the most elemental and necessary wearables in our daily life, e-textile sensing devices for personal health care have taken part in various medical applications and internet of things (IoT) [3], [4]. The significance of close-body sensors is also highlighted in their contribution to preventive healthcare by constantly raising the users' awareness of their health status [5].

The main advantage of e-textile integrated sensors is that they are easy and comfortable to wear while providing a convenient and spontaneous way for real-time monitoring one's health status without affecting one's daily life [6], [7]. Among current researches of textile based sensors for health care, most applications have been limited to textile properties, such as pressure sensors for posture monitoring [8]-[10], stretching sensors for ionic species loss [11], bending sensors for heartbeat and respiration [12], and wetness sensors for salinized liquids [13]. In [14] and [15], body temperature and humidity sensors fabricated with conductive textile have been reported. However, all of these sensors are powered by batteries, and the sensing data are acquired through wires and analyzed with data centers such as PCs. The extra work in sensor charging and data processing makes it less desirable in daily personalized healthcare. In this work, e-textile NFC antennas have been developed to be integrated with external temperature and humidity sensors in order to enable battery-free wireless sensing. NFC antennas can be considered as small energy harvesting devices that contribute to green electronic technology since they only rely on the RF power emissions from the reader [16]. Over the past decade, NFC has become one of the potential solutions in wireless health and wellbeing monitoring applications for its low cost, low power consumption, easy access and ability of integration with multiple types of smart sensors [17], [18]. In [19], interfacing external sensors (temperature, humidity, light, pressure etc.) with smart phones through NFC was proposed. In wearable developments, NFC enabled skin-mounted sensing device for heart rate and blood flow has been presented in [20]. However, the development of integrating body-worn textile NFC embedded with sensors for real-time healthcare and wellbeing monitoring has yet to be reported. Based on the characteristics and performance of e-textile NFC antennas discussed in [21] and [22], the contribution and novelty in this work are by applying textile NFC as a communication interface as well as a wireless power harvester, battery-free real-time body temperature and sweat monitoring has been realized simultaneously.

In this paper, we propose a battery-free smart textile NFC enabled sensing device for body temperature and sweat loss monitoring. The NFC antenna is fabricated with silver coated conductive threads and cotton substrate, which is enabled by an NFC sensor transponder (RF430FRL152H, Texas Instruments) connected to an external humidity sensor. In order to achieve battery-free operation, a voltage-boosting rectifier has been applied to provide the DC power required by the humidity sensor wirelessly. An App has also been developed on Android system for the sensor data to be accessed by smart phones. This development aims

for real-time monitoring personal body temperature and sweat loss associated with systemic hyperthermia from fever and sweating symptoms which are often caused by various kinds of infection, inflammation and trauma [23]. It can also be applied in monitoring wound healing progress, daily healthcare and wellbeing.

The main challenge faced by the proposed design is that the conformal structure of textile can easily affect sensor performance under body movements such as bending and stretching. As a solution, the material influence is reduced by minimizing the circuit size and selecting a relatively less influential body location to place the device.

This paper is structured as follows. Section II will demonstrate the overall structure of the textile sensing circuit as well as the design, fabrication and testing of each constituent part of the system including textile NFC circuits, voltage boosting rectifiers and sensors. In Section III, the experiments and measurement results of temperature and humidity sensors are presented. In Section IV, potential applications of this device both for daily use and medical employment are proposed. Section V summarizes the key results and overall circuit performance.

5.2. Sensing system architecture

5.2.1. On body circuit design

The sensing system architecture shown in Fig. 5-1 presents the overall operation methodology of the proposed textile sensing device. A transponder microchip with a build-in temperature sensor is connected to the textile NFC antenna with conjugate impedance matching for maximum power efficiency. When an NFC reader detects the antenna within a read range, the antenna wirelessly receives power to supply the sensor transponder. The maximum output power of the reader (TRF7970A, Texas Instruments) is 23 dBm (200 mW), and the operating power of the transponder (RF430FRL152H, Texas Instruments) at 13.56 MHz and the sweat sensor (HIH-5031, Honeywell) are around 2.85 mW and 600 uW, respectively.

Since almost all commercial humidity sensors operate with external DC voltage source, a Dickson charge pump and a voltage regulator is developed as a voltage boosting rectifier connected between the NFC antenna and the sweat sensor. Meanwhile, the output voltage of

the sweat sensor is connected to an ADC input pin of the NFC transponder so that the reader is able to collect data from both sensors (temperature and sweat) simultaneously.

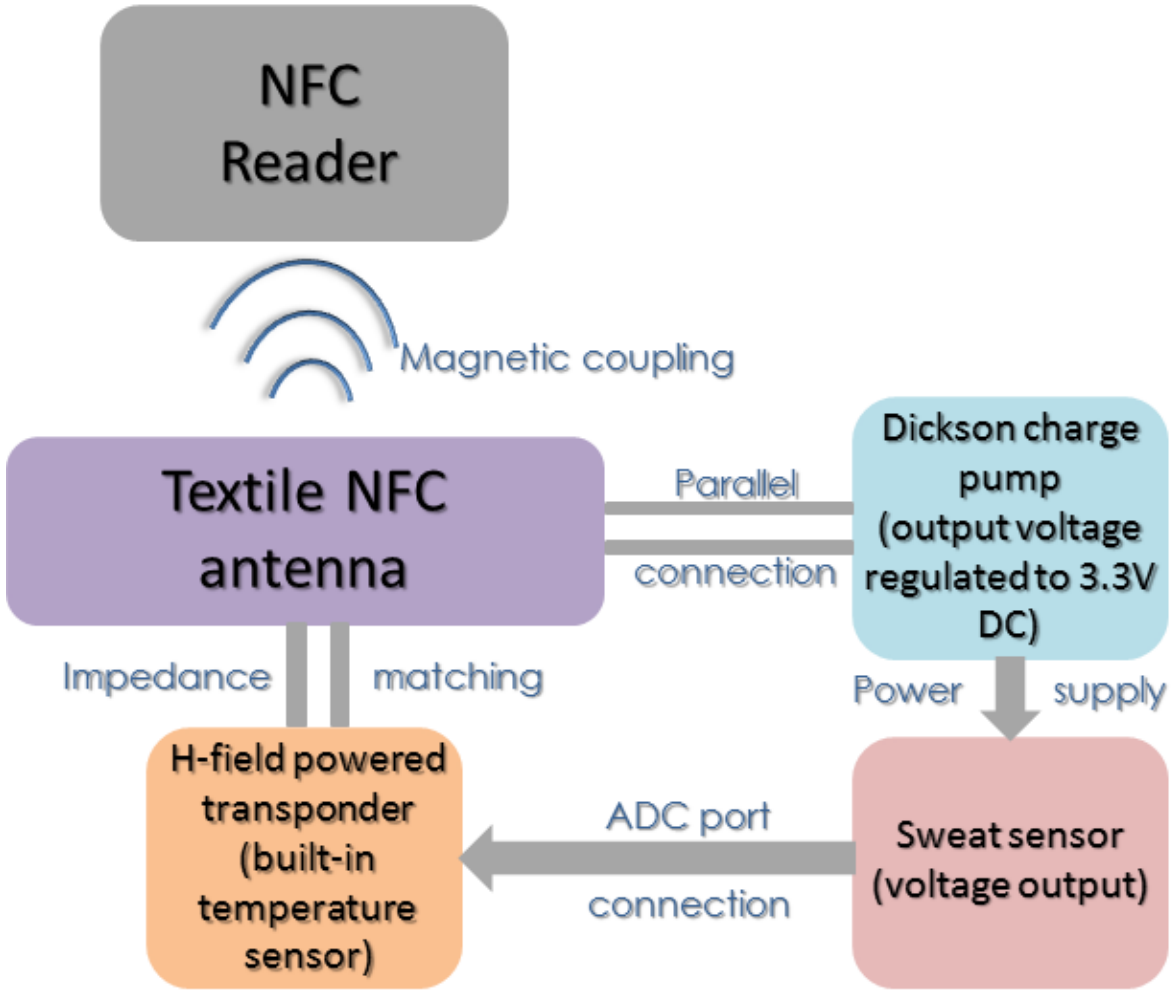

Fig. 5-1. The sensing system architecture.

5.2.2. Smart textile NFC antennas

Smart textile NFC antennas are NFC antennas fabricated by integrating conductive threads with nonconductive textile substrate, which are enabled by conjugate matching with capacitive microchips.

In [21], we have presented the fabrication process and choices of conductive threads, substrate material and embroidery technique of textile NFC antennas. To further investigate the antenna properties and select the best antenna structure for the sensing device, three textile NFC prototypes of different sizes and inductances presented in Fig. 5-2 are studied. The prototypes are fabricated with cotton substrate and silver coated nylon threads (Arduino

Flux Workshop) with resistance of 17.2 Ω/m.

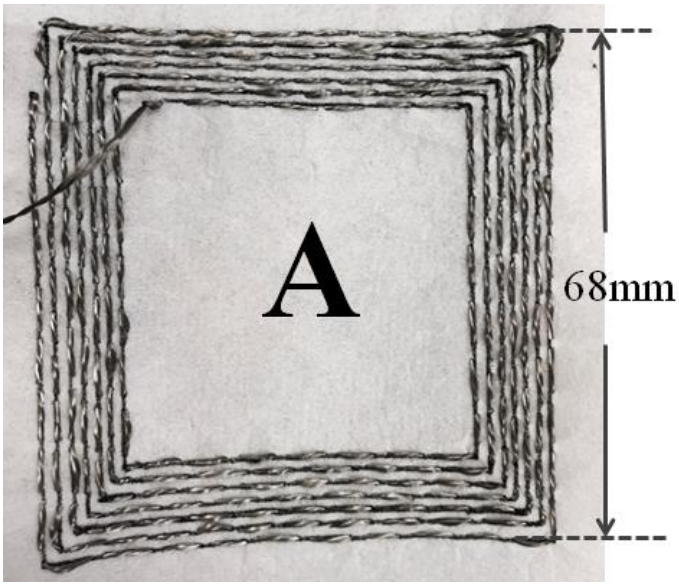

(a)

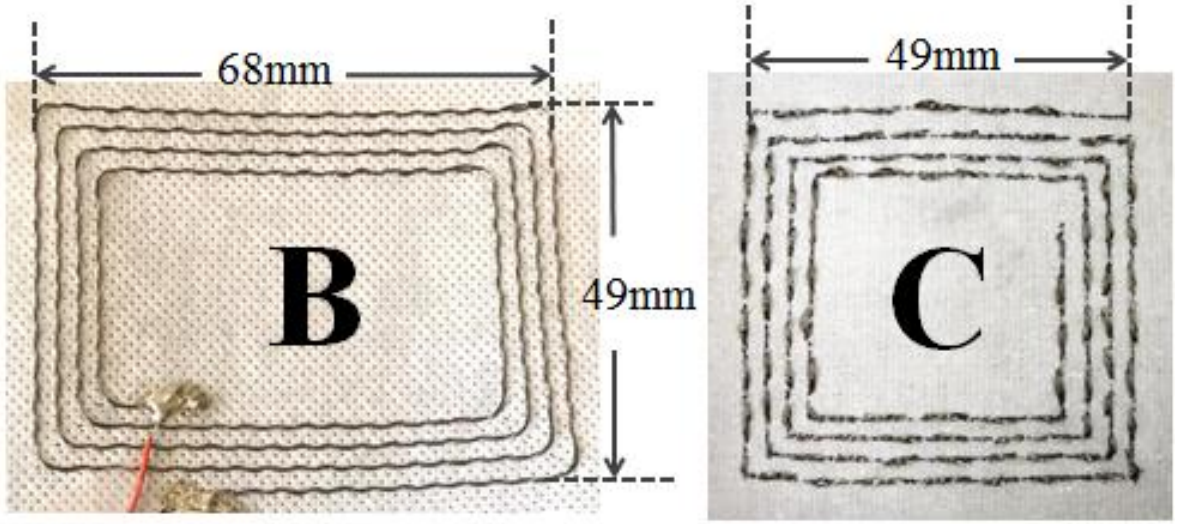

(b) (c)

Fig. 5-2. Textile NFC prototypes with inductance of (a) 5.86 μH (Antenna A), (b) 1.84 μH (Antenna B) and (c) 1.42 μH (Antenna C)

The inductance, resistance at 13.56 MHz and Q factors for the NFC antennas are listed in Table 5-1, where the quality factors of NFC antennas are calculated using (5-1). As the relative difference between antenna inductances is much greater than resistances, antenna A possesses the best transmission efficiency due to its large inductance and receiving surface for magnetic flux. In reality, however, the relatively large sized and densely packed conductive threads might make it less practical.

$$Q = \frac{2\pi f_r \cdot L_{ant}}{R_{eq}} \quad (5\text{-}1)$$

where L_{ant} represents the antenna inductance, f_r represents the operating frequency (13.56 MHz) and R_{eq} represents the antenna resistance at 13.56 MHz.

Table 5-1. NFC antenna parameters

NFC antenna	A	B	C
L_{ant}/μH	5.86	1.84	1.42
R_{eq}/Ω	24.8	15.9	13.5
Q factor	20.13	9.86	8.96

Since the textile based circuits are so flexible that they can be easily bent from body movements of the user, the bending test demonstrated in [21] has been applied to observe how the electrical properties of the antenna A and C (antennas with highest and lowest Q factors) respond to bending. The measurements are taken using Keysight Fieldfox VNA N9918A, and the test results are presented in Fig. 5-3. Fig. 5-3(a) shows how the inductances of the two antennas vary with increasing bending angles. As each antenna is gradually bent from 0° to 180° with its midcourt line being the axis, the inductance of antenna A and C drops from 5.86 μH to 4.73 μH and from 1.42 μH to 1.04 μH, respectively. The decrement is particularly rapid at the bend range between 120° and 180°.

$$f_r = \frac{1}{2\pi\sqrt{C_{chip}L_{ant}}} \quad (5\text{-}2)$$

where C_{chip} stands for the transponder capacitance, L_{ant} for the antenna inductance and f_r the resonant frequency.

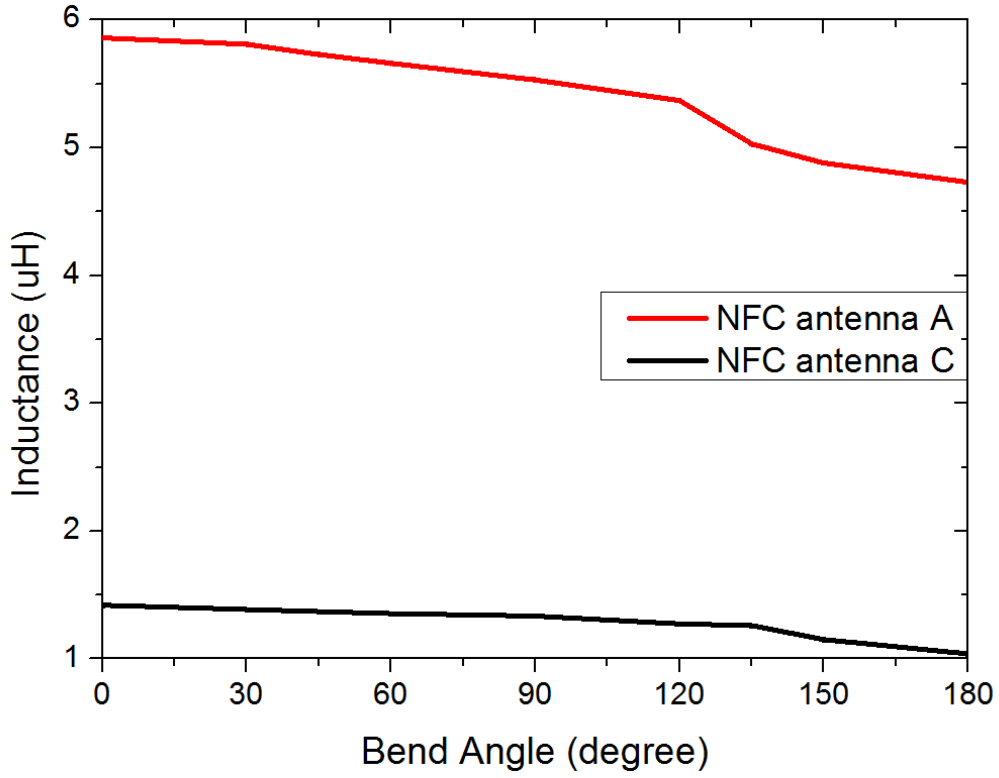

(a)

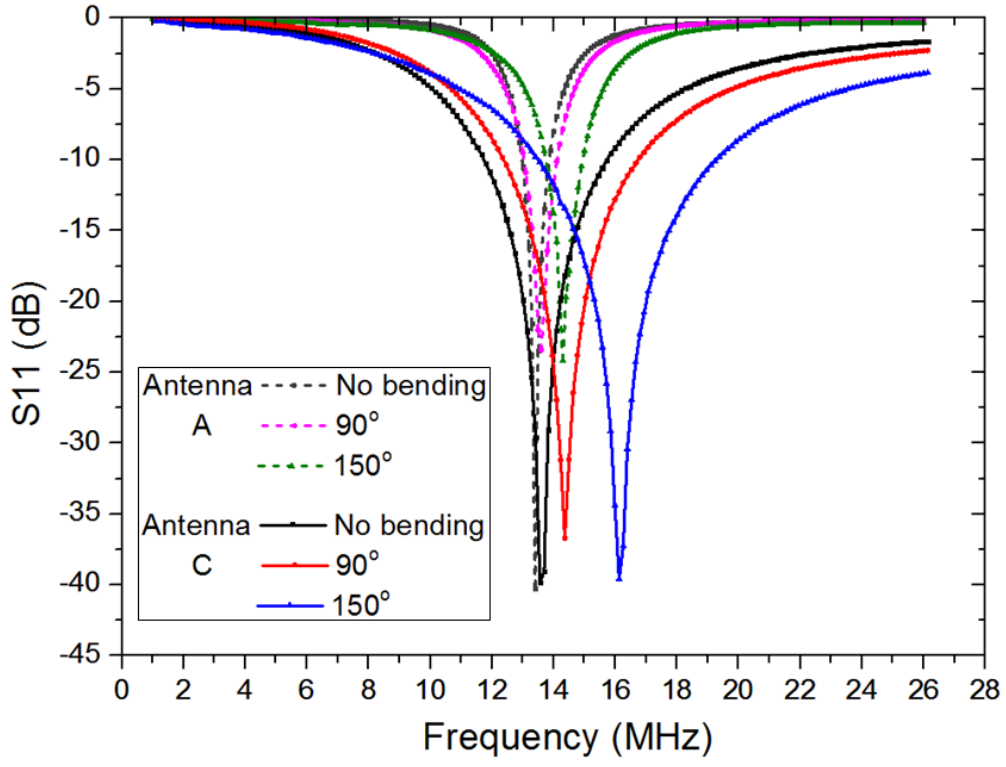

(b)

Fig. 5-3. (a) Inductance variation of NFC antennas at 13.56MHz with bend angle and (b) Measured magnitudes of S_{11} of Antennas A and C in Fig. 5-2, where the textile antennas are bent with angles: 90° and 150°.

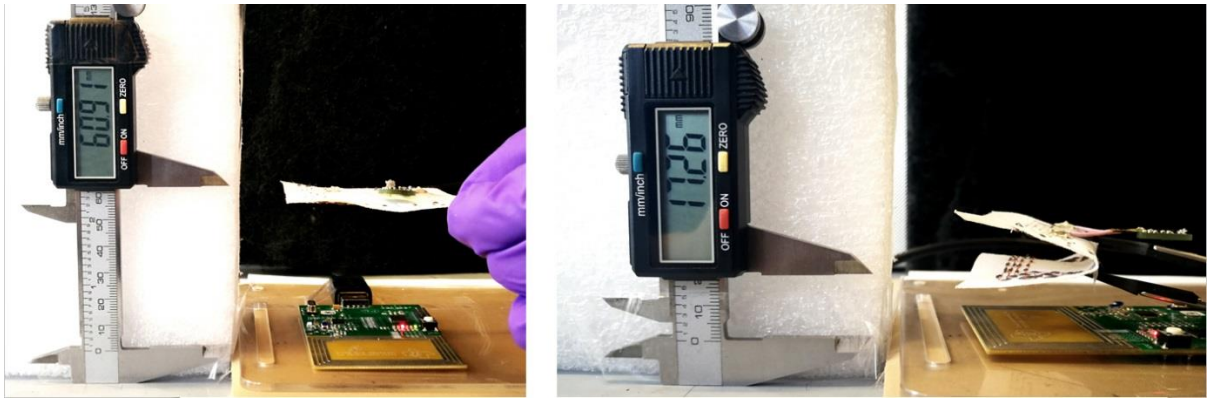

(a) (b)

Fig. 5-4. (a) NFC tag read range measurement set up (b) NFC tag reading with 150 degree bend angle.

It can be deduced from (5-2) that decreasing antenna inductance would lead to small increments in the antenna resonant frequency. In Fig. 5-3(b), where the S_{11} (magnitude) of antenna A and C are measured with increasing bending angles, the measured operating frequency of the antennas indeed increases with the degree of bending. Corresponding to the trend in Fig. 5-3(a), the central frequency shift between the bend angles of 90° and 150° appears as the greatest. Since antenna A possesses a much narrower bandwidth, the 10 dB frequency band of antenna A shifts further away from 13.56 MHz than antenna C under bending, which means it would take more influence in wireless reading performance. Therefore, considering a wearable sensing circuit comes under inevitable bending caused by natural body movements, antenna C has been selected as the NFC interface for its stable performance and relatively small size that is more desirable for on-body placement.

As presented in Fig. 5-4(a), an NFC transponder (RF430FRL152H, Texas Instruments) is connected to antenna C. The read range measured with a TRF7970A (Texas Instruments) reader is 6.09 cm. As it shows in Fig. 5-4(b), the tag is able to be detected under a maximum bent angle of 150°, where the angle is maintained using scotch tape and plastic tweezers. The read distance under this condition is 1.73 cm.

5.2.3. Voltage boosting rectifiers

In this work the selected humidity sensor (HIH-5031, Honeywell) (used as sweat sensor) operates at DC voltage of 3 V and input current of 200 μA. The main challenge for an NFC tag to perform as a wireless power supply for external sensors lies in the low AC voltage it

provides. To overcome this, a voltage multiplier is developed within the circuit in order to raise the supply voltage level for the sensors as well as smooth up the current [24].

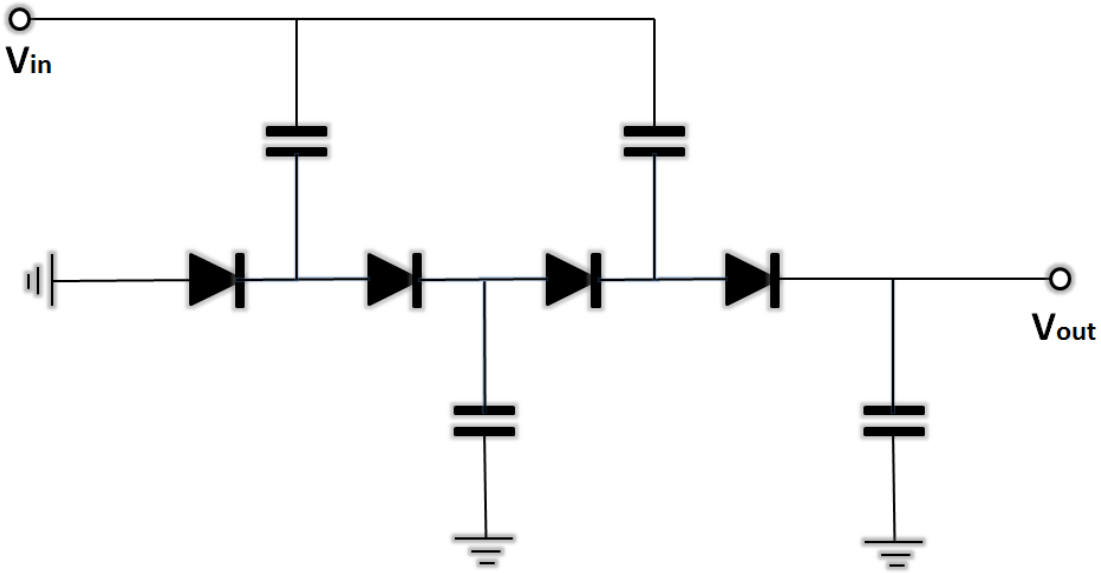

Fig. 5-5. Modified Dickson charge pump circuit layout.

Fig. 5-5 presents a modified structure of a Dickson charge pump, which can be regarded as a half-wave N-stage voltage multiplier [25]. The circuit operates by gaining packets of charge from coupling capacitors charged and discharged at two anti-phased clock cycles, and pushing them along the diode chain [26]. Since each coupling capacitor is approximately charged to the input drive voltage, ideally, the charge pump would generate an output voltage at the end of the chain N+1 times higher than the supply [27] and the output voltage of such circuits can be calculated as (5-3) [28],

$$V_{out} = (N+1) \cdot (V_{cc} - V_T) - \frac{N \cdot I_{out}}{f \cdot C} \tag{5-3}$$

where V_{cc} represents the input voltage, V_T is the forward voltage of each diode, N is the number of stages, I_{out} is the charge pump output current, f is the signal frequency and C is the capacitance applied at each node.

The diodes in this circuit are selected as Schottky diodes (SMS7630, Skyworks), and each coupling capacitor is 15 nF. The minimum voltage to operate the transponder (i.e. charge pump input voltage) is 1.5 V, the maximum diode forward bias current (i.e. charge pump

output current) is 50 mA and the maximum forward voltage of each diode is 0.24 V. At 13.56 MHz, the minimum output voltage of the 4-stage charge pump is calculated at 5.32 V.

5.2.4. Sweat sensor implantation and testing

Fig. 5-6 illustrates the charging circuit for the humidity sensor (HIH-5031, Honeywell), where V1, V2 and V3 represent the input voltage obtained from the NFC antenna, the voltage output of the Dickson charge pump which goes into a voltage regulator (LP2985-N, Texas Instruments) and the regulator output that supplies the sensor, respectively. As the NFC tag is activated by a reader, V2 and V3 are measured with an oscilloscope (Agilent DSO1014A).

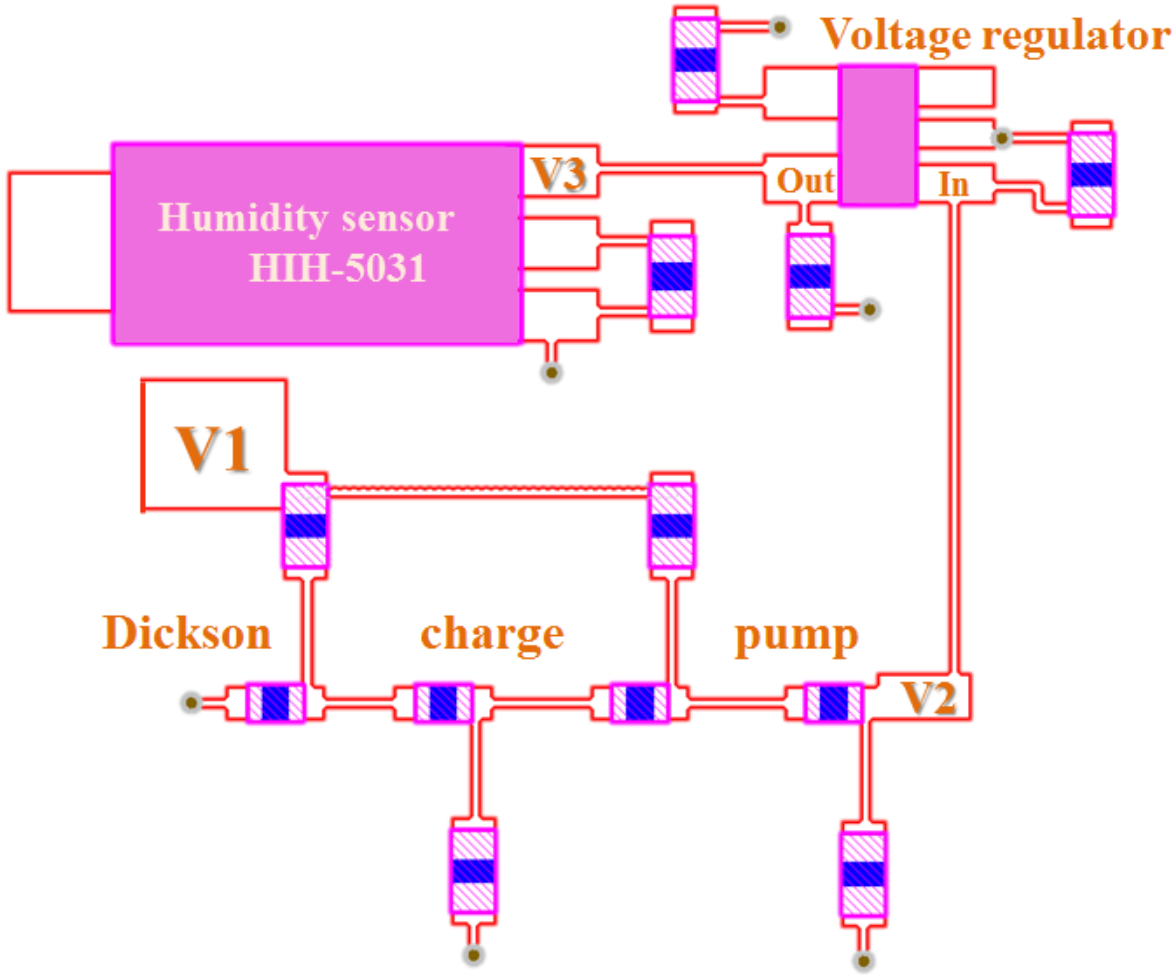

Fig. 5-6. Sweat Sensor circuit layout

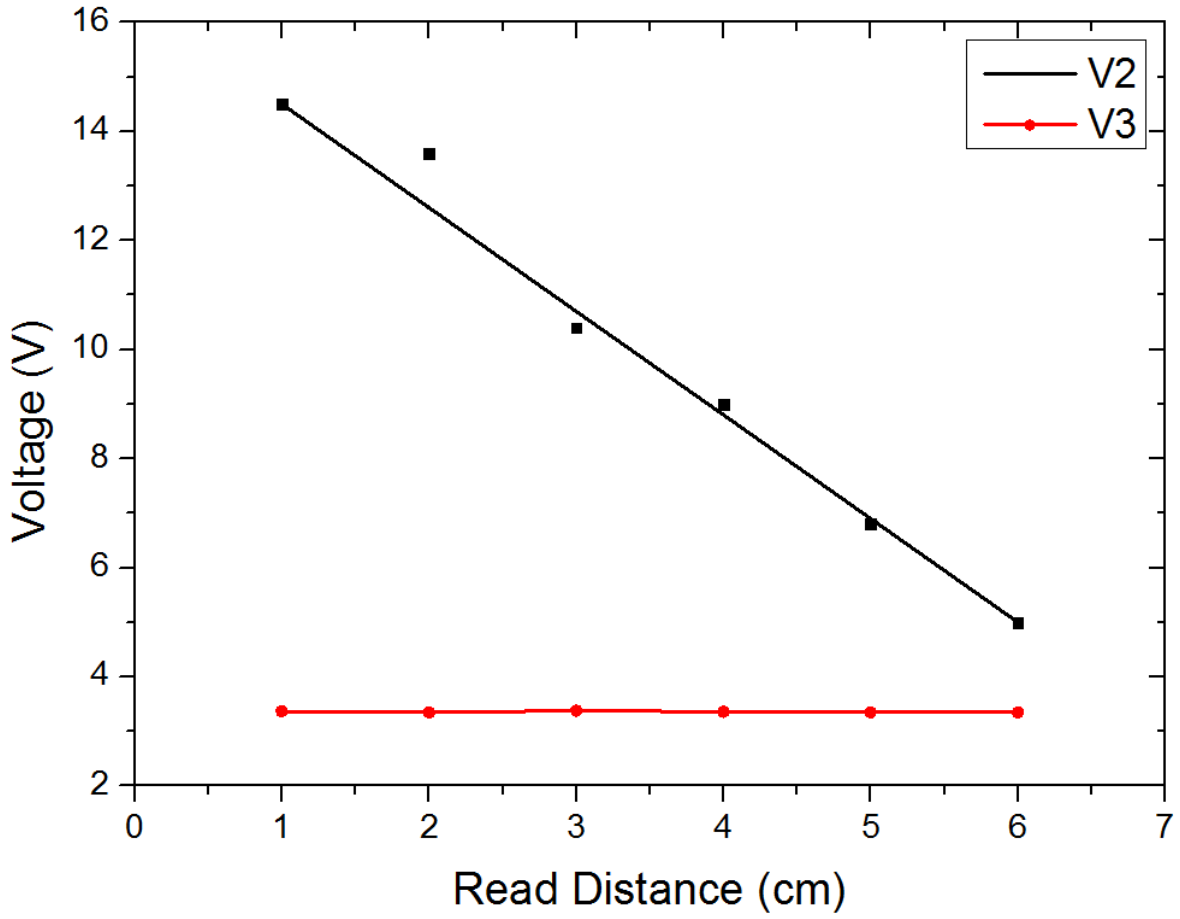

(b)

Fig. 5-7. V2 and V3 (highlighted in Fig. 5-6) vs NFC read distance.

Fig. 5-7 presents how V2 and V3 vary with increasing tag read distance. V2 decreases in direct proportion with the read distance. As the read distance is raised from 1 cm to 6 cm, V2 is reduced from 14.5 V to 5 V which corresponds to the calculated minimum output voltage (5.32 V). Meanwhile, the regulator output voltage (V3) only fluctuates slightly between 3.35 V and 3.38 V, implying that as long as the reader stays within the NFC read range (6cm in our case), the sweat sensor will operate properly.

The complete smart textile NFC enabled temperature and sweat sensing device is presented in Fig. 5-8. The sensing circuit is fabricated on Rogers RO3006 high frequency substrate with thickness of 0.25 mm. The ground plane of the sensing circuit is covered by a thin layer of insulating adhesive to prevent short circuits due to contact between the circuit board and the NFC antenna.

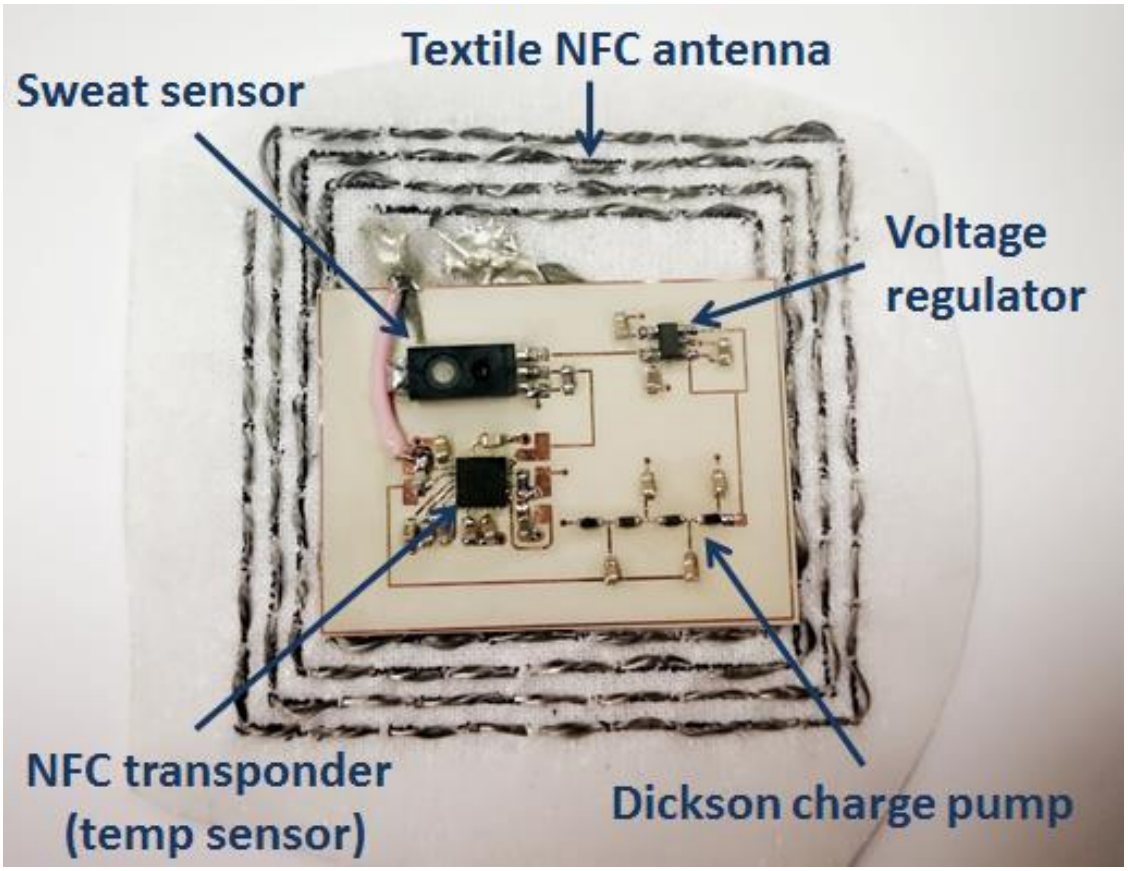

Fig. 5-8. Top view of the complete smart textile NFC enabled sensing system.

5.3. Wireless smart textile NFC enabled temperature and sweat sensing system

5.3.1. Temperature sensor

The transponder (RF430FRL152H, Texas Instruments) has a built-in temperature sensor, and the operating range of which is 0°C -70°C. In this work, the sensor is calibrated with two point calibration method. After calibration, the internal sensor accuracy is able to achieve ±0.14°C, which is better than most medical body thermometers on the market (±0.3°C) [29]. During measurements, the sensor data is collected with a TRF7970A reader and displayed on a PC.

The effect of human body towards read range has been investigated in [21], revealing that the influence of skin contact is slight enough to be neglected. As shown in Fig. 5-9(a), the proposed sensing system is placed slightly below the arm pit since not only axillary

temperature is one of the most accurate measurements for body temperature, but the arm pit also generates great percentage of body sweat [30]. Other than general health conditions, the proposed system is also applicable during exercise to monitor body temperature rise and increment of sweat as the oxygen intake (exercise intensity) increases [31]. The sensing device is positioned to make the sensors face towards human body. In this case, the sensors are protected by the cotton substrate and ensured for more accurate measurements.

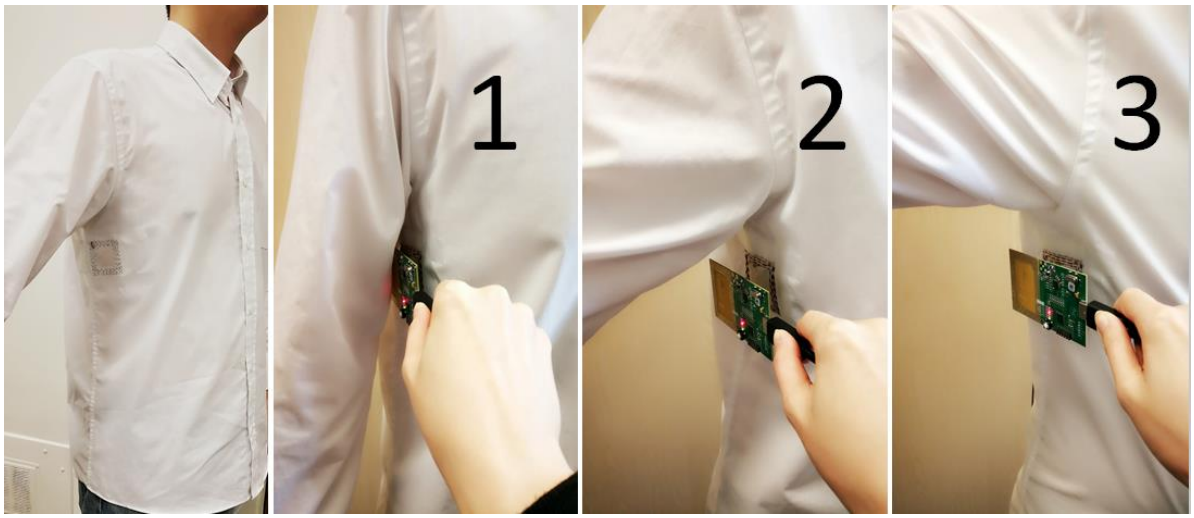

(a) (b) (c) (d)

Fig. 5-9. (a) Overview of the smart textile NFC sensing system integrated with a shirt, and NFC sensing system read with (b) 15°, (c) 60° and (d) 90°angle between arm and body

In order to investigate how the temperature measurements are affected by body movements, Fig. 5-9(b), (c) and (d) demonstrate three different arm positions for the temperature sensor to be read (labelled as 1, 2 and 3), where the arm is lifted from the body by 15°, 60°and 90°. The read temperature results are presented in Fig. 5-10, and the average measured temperature is 36.8°C, 34.4°C and 33.4°C, respectively. Naturally, the closer the textile NFC sensing system stays to the body, the higher and more accurate the measured temperature is. Since the sensor is placed most closely to the body for position 1, it tends to introduce small fluctuation to the results due to inevitable breathing action. On the other hand, the measurements from position 2 and 3 have fluctuation since there is less and less direct contact between the sensor and skin surface. However, these results are much less reliable and tend to vary with small changes of body position. In comparison, position 1 is considered the most suitable way for measurements since all the ripples shown in the test are less than ±0.5°C.

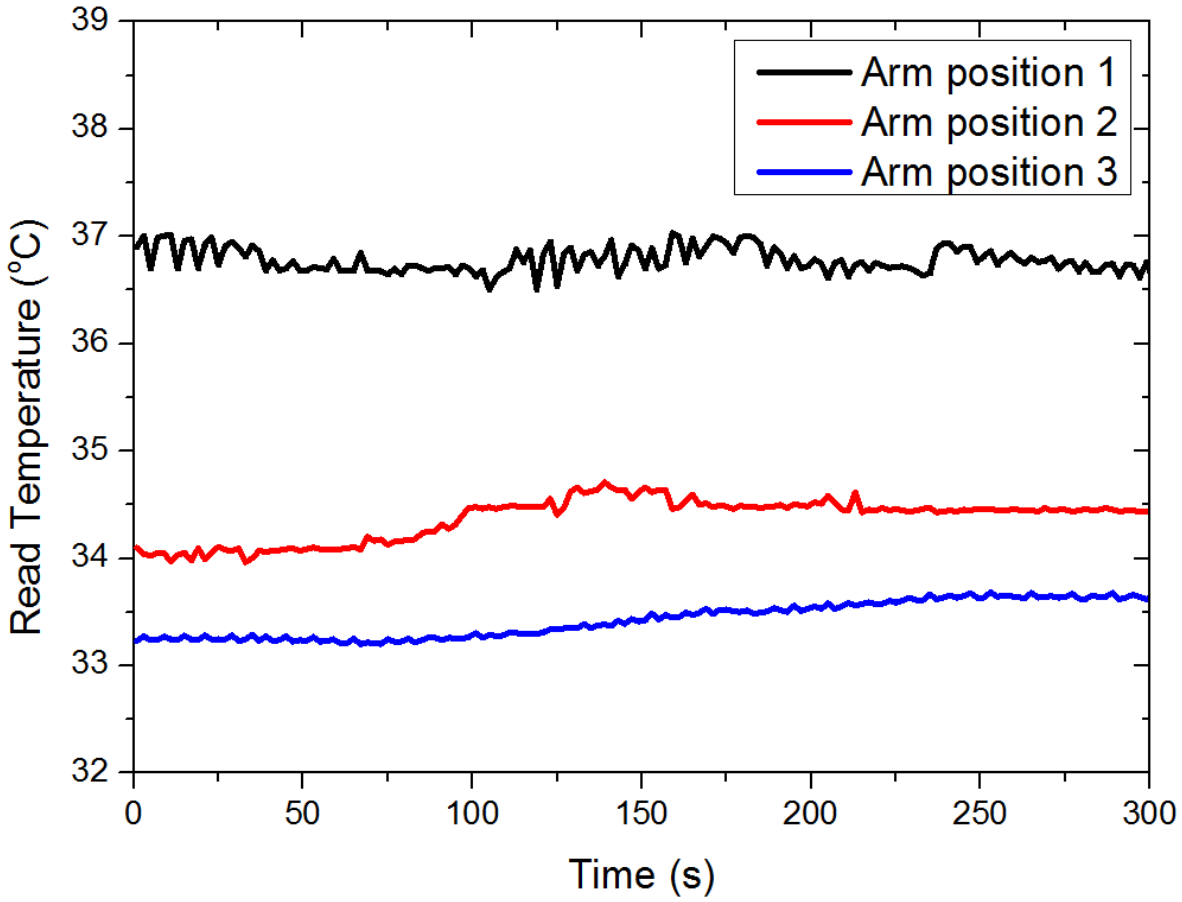

Fig. 5-10. Body temperature measured with three arm positions in Fig. 5-9 (b), (c) and (d)

5.3.2. Sweat sensor

The NFC transponder (RF430FRL152H, Texas Instruments) has two ADC ports, including ADC1 (reference resistor) and ADC2 (thermistor), mainly for determining an external thermistor value. In the resistive bias mode, a current source is sent to both reference pin and thermistor pin in order to obtain their resistance. Since the humidity sensor (HIH-5031, Honeywell) (used as sweat sensor) now connected to ADC2 operates on voltage bias, the current source is terminated for the data obtained from the transponder to completely depend on the voltage variation. Fig. 5-11 shows the results of how the sweat sensor voltage output varies with detected moisture level. The change rate of humidity factor calculated from this trend is 91.3%/V, which is applied into the coding of the ADC input data of the NFC transponder.

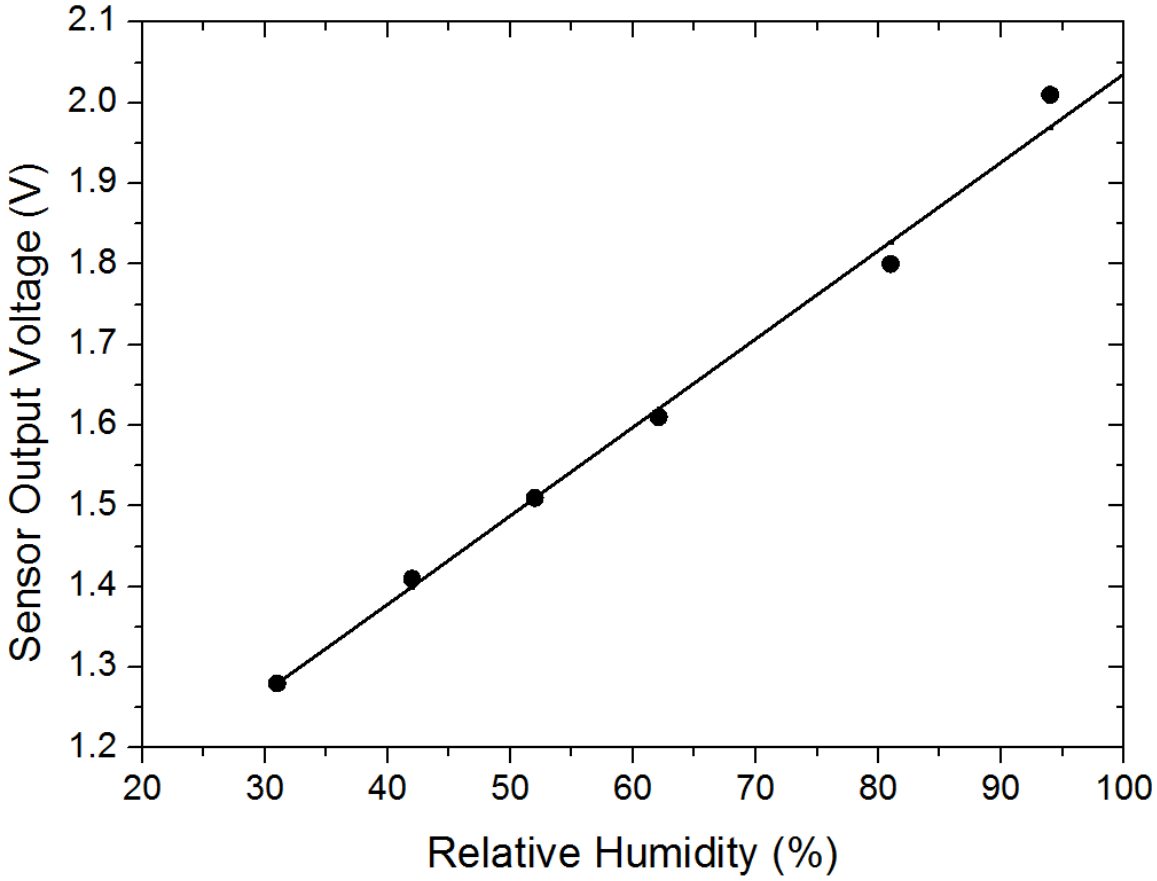

Fig. 5-11. Sweat sensor test results

The real time humidity was measured wirelessly by a reader for three different conditions: room environment, normal body humidity and body after workout humidity (under the armpit area) as presented in Fig. 5-12. Different from body temperature results, the humidity measurements are hardly affected by slight variation of arm positions since the humidity level around the armpit area is much more stable than temperature. The measured data indicates that for measuring environments where the humidity level is relatively steady, the sensor works smoothly in a ten-minute period with ripples less than ±0.2%. In the cool down process of a body workout, although the basic trend gradually drops from 77.9% to 38.1% as expected, some fluctuations still occur during this time period possibly due to slight body movements.

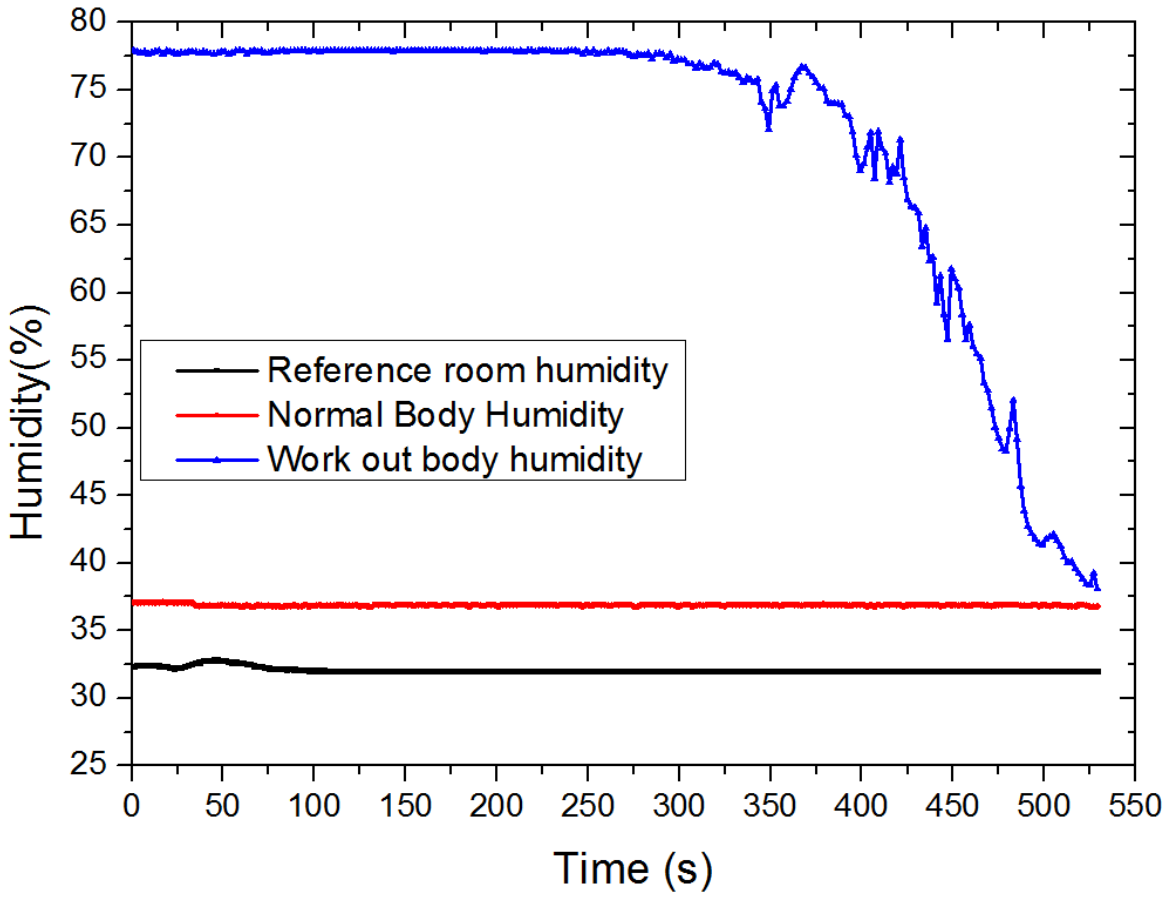

Fig. 5-12. Wireless measured humidity at room environment (32.1% moisture level), normal body (36.9% moisture level) and body after work out (77.9% moisture level)

5.4. Applications

5.4.1 Mobile handset reading

For the sensor data to be accessed by smart phones, we have developed an Android program that reads and displays body temperature and sweat continuously from RF430FRL152H, enabling the data to be transferred into cloud storage in order to keep a record of the user's health status. As it presents in Fig. 5-13(a), the App uses "start" and "stop" buttons that launch and terminate the reading progress, respectively. The software interface displays four types of messages showing the tag connection status, including "Place phone on tag", "Tag connected", "Reintroducing the phone" and "Tag disconnected". It is also able to save readings by time and date.

(a) (b)

Fig. 5-13. NFC reader software on Android (a) Basic functions (b) Verification of the accuracy of the mobile temperature reading.

Fig. 5-13(b) presents our App works on an NFC enabled Huawei Mate 7 mobile phone. The measured room temperature (24.44°C) shown on screen agrees with the one measured with a Fisher Scientific thermometer (24°C).

5.4.2. Wound Healing Monitoring

It has been stated in [32] and [33] that once wound tissue temperature falls below 33°C, the activity of fibroblast and epithelial cells decreases, which might lead to a delay in the healing progress. Research about how dressing methods can affect wound healing rate has been reported [32]. However, monitoring the healing always requires multiple measurements taken before and after the clothing is changed. On the other hand, if the wound temperature goes higher than normal body temperature for certain duration, it might indicate an infection has occurred [34]. Furthermore, a high moisture environment also prevents wounds from healing [35]. For all these conditions, the proposed smart textile NFC sensing system can be a suitable tool to wirelessly detect the temperature and humidity of trauma such as wounds caused by surgical debridement and accidental injury, in order to maintain normothermia as well as prevent and detect infections.

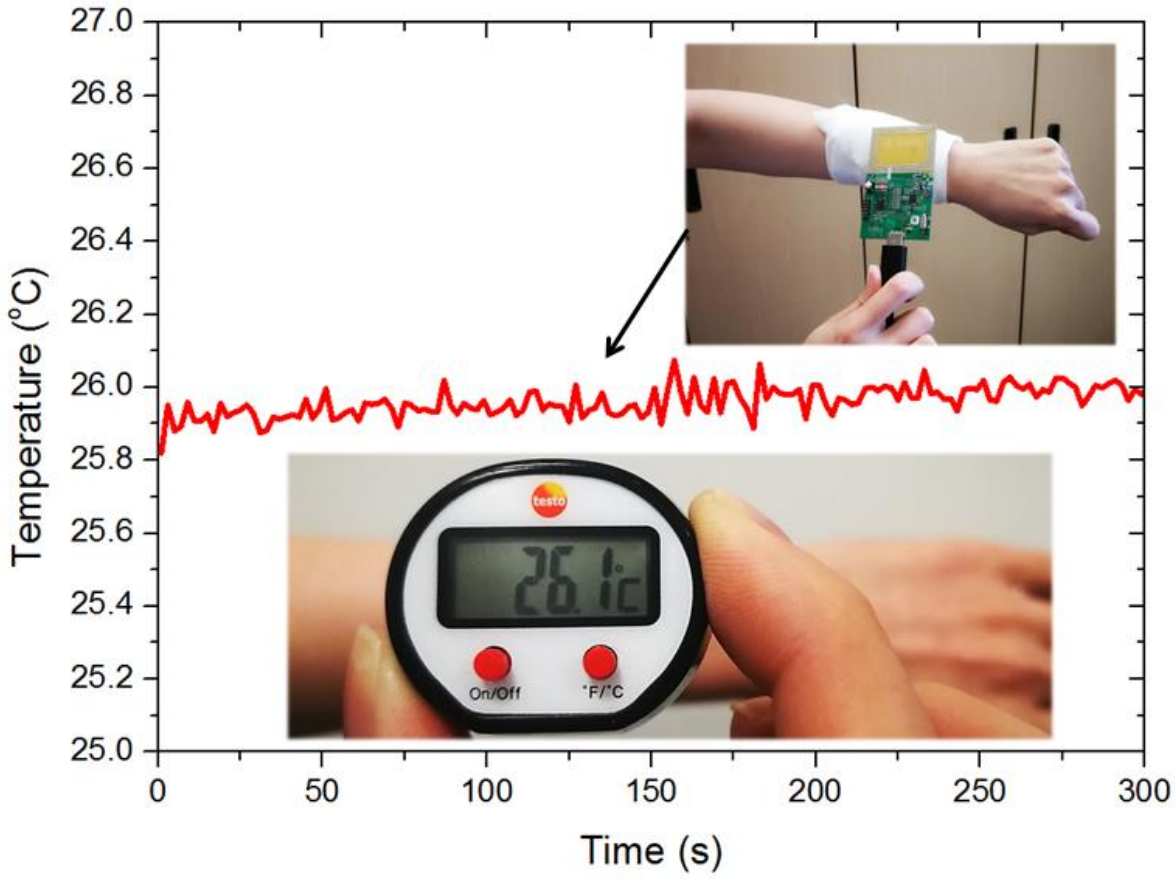

Fig. 5-14. Comparison between wrist (‘wound’) temperatures by wireless NFC sensor and Testo surface thermometer.

In Fig. 5-14, the temperature of a ‘wound’ on a wrist is measured with the NFC sensing system. The proposed smart textile NFC enabled sensing device is embedded between layers of gauze that are tightly wrapped around a wrist. The measured wrist (‘wound’) temperature (25.96°C) is compared with the temperature measured by Testo surface thermometer for validation. As a result, the accuracy of the wrist temperature measurements is ±0.14°C.

5.5. Conclusion

This paper has presented design, fabrication implementation and measurements of smart textile NFC antennas and a battery-free wireless NFC body temperature and sweat sensing device. The textile antenna is integrated with daily garments and the sensing system is wirelessly powered, aiming for truly ubiquitous wireless health and wellbeing monitoring. The measurement results have shown that the textile NFC antennas can still perform properly under bending up to 150^{o}. Both temperature and sweat sensors powered wirelessly by the reader are able to provide accurate and reliable results. Potential real-life applications relating

to this smart textile sensing device, including mobile application and wound healing monitoring, have also been proposed. It is believed that the wireless powered smart textile sensing system reported here possesses potential to be widely applied into daily health care system and wellbeing monitoring.

5.6. References

[1] S. Schneegass and O. Amft. Smart Textiles, Springer International Publishing, 2017, pp. 49-185.

[2] Y. Yun, W. Hong, D. Kim, H. Kim, Y. Jun, and H. Lee, "E-textile gas sensors composed of molybdenum disulfide and reduced graphene oxide for high response and reliability," Sensors and Actuators B: Chemical, vol. 248, pp. 829-835, Sept. 2017.

[3] A. Abdelgawad, and K. Yelamarthi, "Internet of things (IoT) platform for structure health monitoring," Wireless Communications and Mobile Computing, vol. 2017, pp. 1-10, Jan. 2017.

[4] N. Bui and M. Zorzi, "Health care applications: A solution based on the internet of things," ISABEL, Oct. 2011, Art. no. 131.

[5] S. Coyle and Y. Wu, "Bio-sensing textiles - wearable chemical biosensors for health monitoring," IFMBE Proceeding, vol. 13, pp. 35-39, 2007.

[6] G. Medrano and L. Beckmann, "Bioimpedance spectroscopy with textile electrodes for a continuous monitoring application," IFMBE Proceedings, vol. 13, pp. 23-28, 2007.

[7] T. Linz and L. Gourmelon, "Contactless EMG sensors embroidered onto textile," IFMBE Proceeding, vol. 13, pp.29-34, 2007.

[8] J. Meyer, B. Arnrich, J. Schumm and G. Troster, "Design and modeling of a textile pressure sensor for sitting posture classification," IEEE Sensors Journal, vol. 10, no. 8, pp. 1391-1398, Aug. 2010.

[9] W. Xu, M. Huang, N. Amini, L. He and M. Sarrafzadeh, "eCushion: A textile pressure sensor array design and calibration for sitting posture analysis". IEEE Sensors Journal, vol. 13, no. 10, pp. 3926-3934, Oct. 2013.

[10] A. Mason, S. Wylie, O. Korostynska, L. Cordova-Lopez and A. Al-Shamma'a, "Flexible e-textile sensors for real-time health monitoring at microwave frequencies," International Journal on Smart Sensing and Intelligent Systems, vol. 7, no. 1, pp. 32-47, Mar. 2014.

[11] M. Parrilla, R. Cánovas, I. Jeerapan, F. Andrade and J. Wang, "A textile-based stretchable multi-Ion potentiometric sensor," Advanced Healthcare Materials, vol. 5, no. 9, pp. 996-1001, Mar. 2016.

[12] X. Yang, Z. Chen, C. Elvin, L. Janice, S. Ng, J. Teo and R. Wu, "Textile fiber optic microbend sensor used for heartbeat and respiration monitoring," IEEE Sensors Journal, vol. 15, no. 2, pp. 757-761, Feb. 2015.

[13] E. Foo, R. Pettys-Baker, S. Sullivan and L. Dunne, "Bi-metallic stitched e-textile sensors for sensing salinized liquids," Proceedings of the 2017 ACM International Symposium on Wearable Computers - ISWC '17, Sept. 2017.

[14] M. Husain and R. Kennon, "Preliminary investigations into the development of textile based temperature sensor for healthcare applications," Fibers, vol. 1, no. 1, pp. 2-10, Apr. 2013.

[15] R. Soukup, A. Hamacek, L. Mracek and J. Reboun, "Textile based temperature and humidity sensor elements for healthcare applications," IEEE 37th Int. Spring Seminar on Electronics Technology, vol. 13, no. 10, May 2014.

[16] A. Lazaro, R. Villarino and D. Girbau, "A survey of NFC sensors based on energy harvesting for IoT applications," Sensors, vol. 18, no. 11, p. 3746, Oct. 2018.

[17] E. Strömmer, and J. Kaartinen, "Application of near field communication for health monitoring in daily life," Proceedings of the 28th IEEE EMBS Annual International Conference, p. 3249, Dec. 2006.

[18] S. Cecil, M. Bammer, G. Schmid, K. Lamedschwandner and A. Oberleitner, "Smart NFC-sensors for healthcare applications and further development trends," e & i Elektrotechnik und Informationstechnik, vol. 130, no. 7, pp.191-200, Nov. 2013.

[19] T. Leikanger, J. Häkkinen and C. Schuss, "Interfacing external sensors with Android smartphones through near field communication," Measurement Science and Technology, vol. 28, no. 4, Feb. 2017.

[20] J. Kim, G. Salvatore, H. Araki, A. Chiarelli and Z. Xie, “Battery-free, stretchable optoelectronic systems for wireless optical characterization of the skin,” Science Advances, vol. 2, no. 8, Aug. 2016.

[21] Y. Jiang, L. Xu, K. Pan, T. Leng, Y. Li, L Danoon and Z. Hu, “e-Textile embroidered wearable near-field communication RFID antennas,” IET Microwaves, Antennas & Propagation, vol. 13, no. 1, pp. 99-104, Sept. 2018.

[22] R. Del-Rio-Ruiz, and J. Lopez-Garde, “Design and performance analysis of a purely textile spiral antenna for on-body NFC applications,” IEEE MTT-S International Microwave Workshop Series on Advanced Materials and Processes, Sept. 2017.

[23] D. Ogoina, “Fever, fever patterns and diseases called ‘fever’ – A review,” Journal of Infection and Public Health, vol. 4, no. 3, pp.108-124, Aug. 2011.

[24] T. Tanzawa and T. Tanaka, “A dynamic analysis of the Dickson charge pump circuit,” IEEE Journal of Solid-State Circuits, vol. 32, no. 8, pp.1231-1240, Aug. 1997.

[25] D. Waidelich, and C. Shackelford, “Characteristics of voltage-multiplying rectifiers,” Proceedings of the IRE, vol. 32, no. 8, pp.470-476, Aug. 1944.

[26] J. Dickson, “On-chip high-voltage generation in MNOS integrated circuits using an improved voltage multiplier technique,” IEEE Journal of Solid-State Circuits, vol. 11, no. 3, pp.374-378, Jun. 1976.

[27] D. Baderna, A. Cabrini and G. Torelli, “Efficiency comparison between doubler and dickson charge pumps,” 2005 IEEE International Symposium on Circuits and Systems, pp.1891-1894, Jul. 2005.

[28] D. Jan, “Fully Integrated High-Voltage Generators with Optimized Power Efficiency,” Journal of Computer and Communications, vol. 2, no. 13, pp.1-8, Aug. 2014.

[29] S. John, “The best thermometers you can buy to check for fevers,” Business Insider, Feb. 13, 2018. [Online]. Available: http://uk.businessinsider.com/best-thermometer?r=US&IR=T/#the-best-thermometer-overall-1 [Accessed 11 Sep, 2018].

[30] T. Togawa, “Body temperature measurement,” Clinical Physics and Physiological Measurements, vol. 6, no.2, pp. 83-108, Oct. 1985.

[31] C. Davies, C. Barnes and A. Sargeant, “Body temperature in exercise,” Internationale Zeitschrift fur Angewandte Physiologie Einschlieulich Arbeitsphysiologie, vol. 30, no. 1, pp.10-19, Mar. 1971.

[32] W. McGuiness, E. Vella and D. Harrison, “Influence of dressing changes on wound temperature,” Journal of Wound Care, vol. 13, no. 9, pp.383-385, Oct. 2004.

[33] A. Kurz, D. Sessler and R. Lenhardt, “Perioperative normothermia to reduce the incidence of surgical-wound infection and shorten hospitalization,” New England Journal of Medicine, vol. 334, no. 19, pp.1209-1216, May 1996.

[34] Advanced Tissue, “6 Signs You Have an Infected Wound,” Advanced Tissue, Aug. 28, 2015. [Online]. Available: https://www.advancedtissue.com/6-signs-you-have-an-infected-wound/ [Accessed 1 May, 2018].

[35] S. Thomas and B. Pharm, “The effect of the weather and other environmental factors on the performance of surgical dressings,” Wounds : a Compendium of Clinical Research and Practice, vol. 24, no. 12, pp.335-338, Dec. 2012.

Chapter 6 Machine Embroidered Antenna Designs for On-Body Data Communications and RF Energy Harvesting

This chapter includes two conference papers in the same category which presents the design and performance of two types of machine embroidered e-textile antennas: a wideband UHF RFID tag antenna and a novel wideband monopole antenna, which aim to realize on-body data communication and wearable RF energy harvesting, respectively.

Machine Embroidered Wearable e-textile Wideband UHF RFID Tag Antenna

2019 IEEE International Symposium on Antennas and Propagation and USNC-URSI Radio Science Meeting, Atlanta, GA, USA, 2019, pp. 643-644

My contributions:

I have simulated and fabricated the proposed device, performed all of the measurements, analysed data, and prepared all the graphs.

6.1. Machine Embroidered Wearable e-textile Wideband UHF RFID Tag Antenna

Yutong Jiang, Ting Leng, Yixian Fang and Zhirun Hu

EEE Department

The University of Manchester

Manchester, UK

yutong.jiang@manchester.ac.uk; ting.leng@manchester.ac.uk;
yixian.fang@manchester.ac.uk; z.hu@manchester.ac.uk

Lulu Xu

School of Materials

The University of Manchester

Manchester, UK

Lulu.xu@postgrad.manchester.ac.uk

Abstract

The design and fabrication of a novel e-textile wideband UHF RFID tag antenna is presented. The proposed antenna is verified by simulation and measurements. The RFID tag read range is over 6.5 m in the frequency band between 860 and 960 MHz. The maximum read range is measured at 7.23 m in air and 4.71 m on body.

6.1.1. Introduction

In the past decade, conductive fabric integrated UHF RFID tags are highly desirable due to their wearability and flexibility and have been applied into body area communication networks and body sensing systems [1-3]. Most recently, the conductive threads fabricated contour RFID tag presented in [4] is able to achieve a read range of 7 m.

In this work, we propose a novel RFID antenna structure fabricated with silver coated conductive threads and cotton substrate, which achieves a steady read range over 6.5 m from 860 to 960 MHz. Due to the wideband operation, the proposed tag is able to applied for the two main RFID frequency bands: EU (865-868 MHz) and US (902-928 MHz).

This paper will present the antenna design, matching and simulation in Section II and read range measurements in Section III. The conclusions are drawn in Section IV.

6.1.2. RFID antenna design

The antenna layout is presented in Fig. 1. The proposed structure is a dipole integrated with an inductive matching loop. The gaps on each side are designed for the tag inductance to be conjugately matched to the chip capacitance.

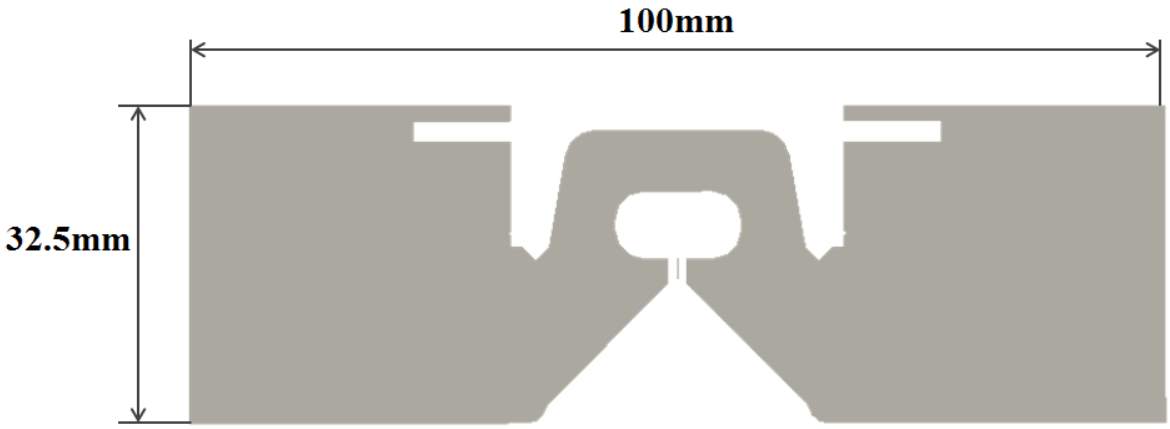

Fig. 6-1. RFID tag antenna layout

The read rage of the tag can be calculated with (6-1)

$$r = \frac{\lambda}{4\pi}\sqrt{\frac{P_t G_t G_r \tau}{P_{th}}} \tag{6-1}$$

where λ is the wavelength, P_t is the power transmitted by the reader, G_t is the gain of the transmitting antenna, G_r is the gain of the receiving tag antenna, P_{th} is the minimum threshold power necessary to provide enough power to the RFID tag chip, and τ is the power transmission coefficient that is expressed by (6-2)

$$\tau = \frac{4R_c R_a}{|Z_c + Z_a|^2}, \quad 0 \leq \tau \leq 1 \tag{6-2}$$

where $z_c = R_c + jX_c$ is chip impedance and $z_a = R_a + jX_a$ is antenna impedance.

The tag resonant frequency is determined by τ as the imaginary impedance of the antenna and chip are conjugated matched. The measured chip capacitance is 1.45 pF. As it shows in Fig. 6-2, the reactance of the antenna (X_A) and chip (X_c) are matched at 870 and 952 MHz, which indicates a relatively wideband behavior of the RFID tag.

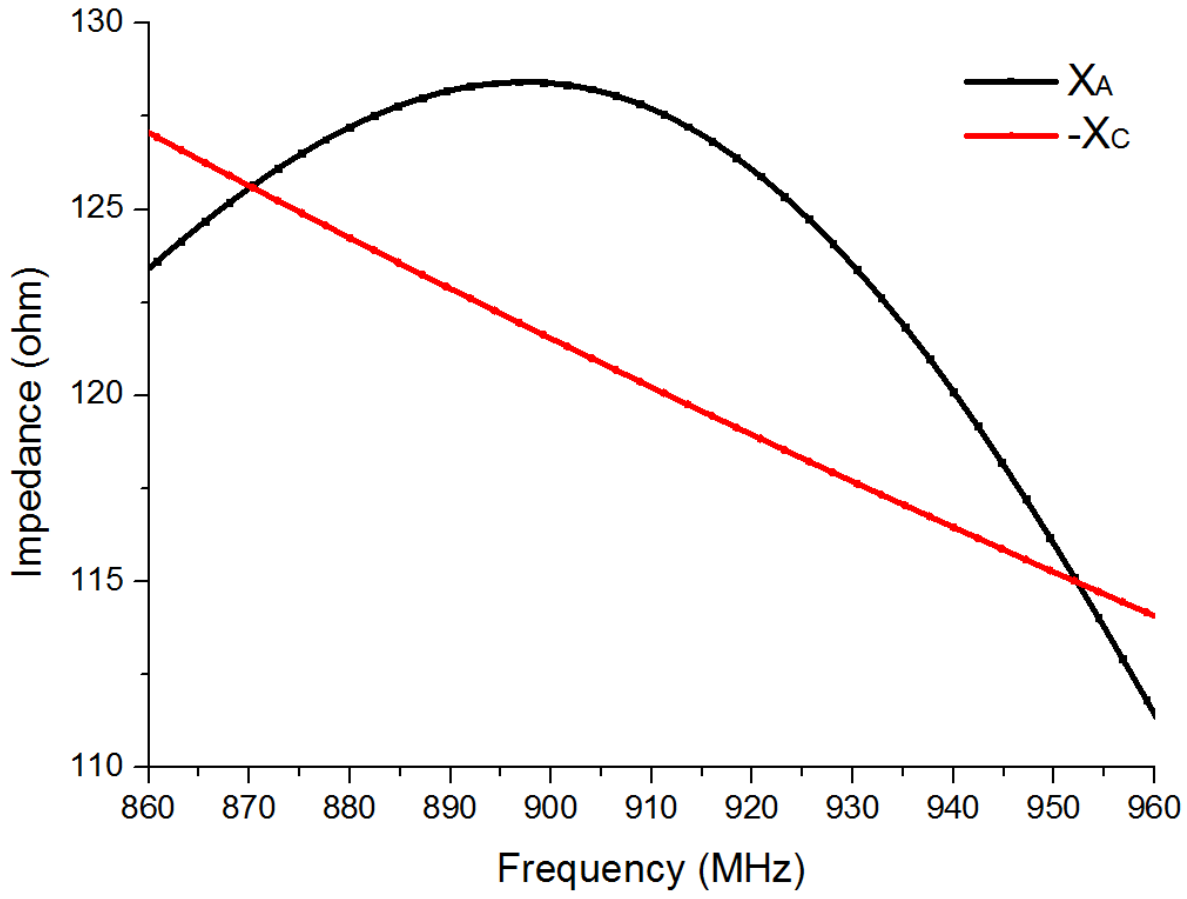

Fig. 6-2. Antenna and chip reactance

The simulated power transmission coefficient and antenna realized gain are presented in Fig. 6-3. τ achieves peak value (0.86) at 846 MHz instead of the resonant frequencies since the antenna resistance at higher frequencies simulated with conductive yarns are higher than conventional metal antennas. However, the simulated realized gain achieves 0.7 dB at 900 MHz, showing a desirable efficiency of the antenna.

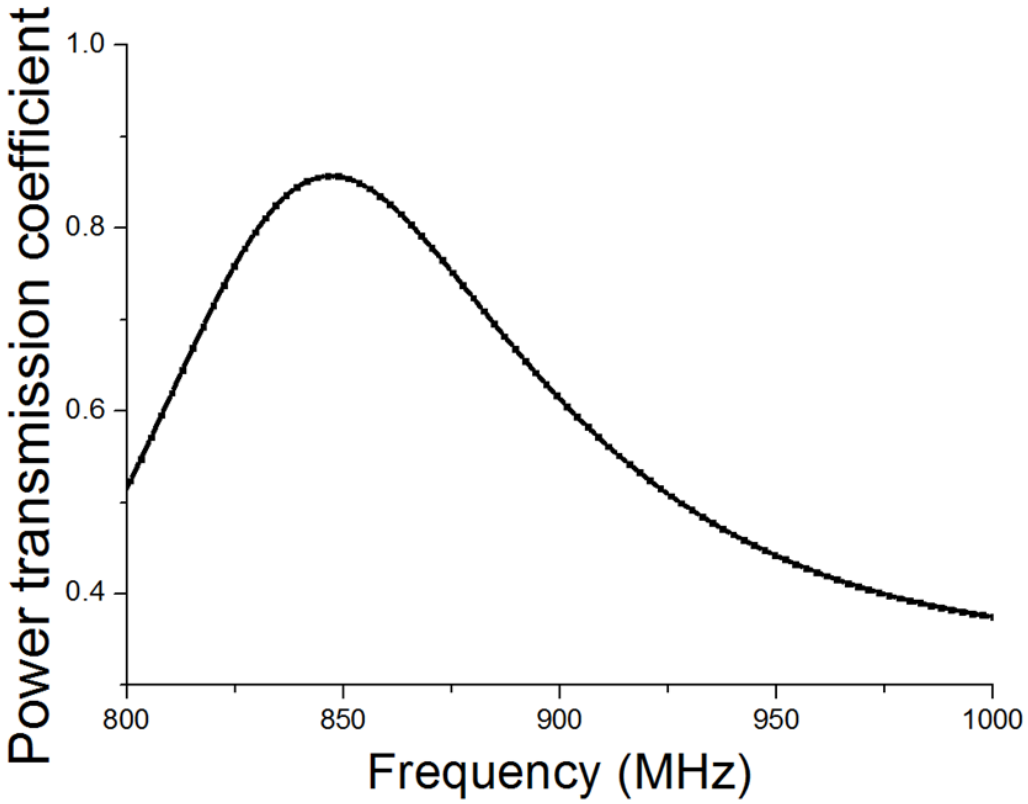

(a)

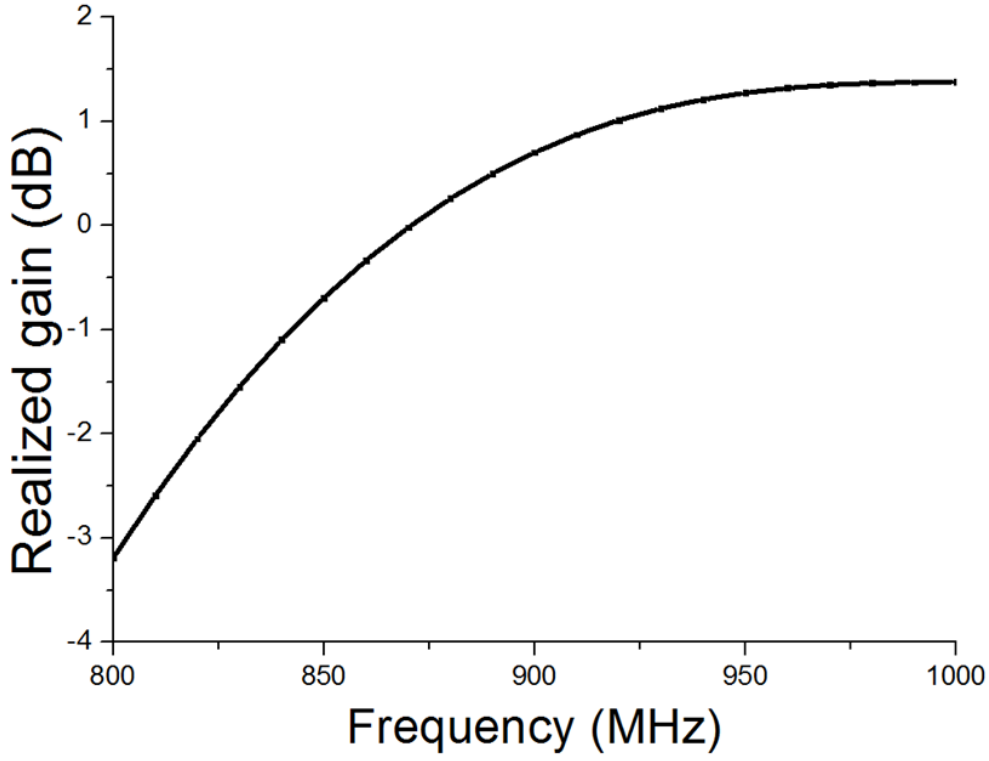

(b)

Fig. 6-3. Simulated results of (a) power transmission coefficient and (b) realized gain

6.1.3. Antenna measurements

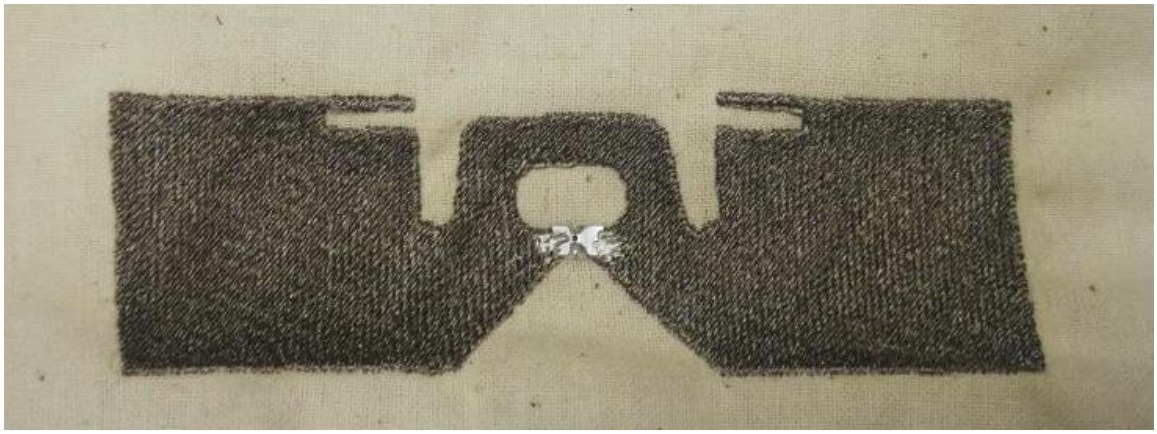

Fig. 6-4. Fabricated RFID tag

Fig. 6-4 presents the fabricated RFID antenna prototype. The antenna is embroidered with silver coated conductive threads (Silverpam 250 from TIBTECH Innovation) on cotton substrate using embroidery machine (JCZA 0109-550, ZSK). An IC chip (Monza R6) is connected to the antenna using conductive epoxy. The measured sheet resistance of the conductive yarn is 0.4 Ω/sq.

The read range of the RFID antenna is measured with Tagformance Lite RFID measurement unit from Voyantic and the results for the tag placed in air, 1 cm from human body and on body (sleeve) are presented in Fig. 6-5. When the tag is placed in air, the read range varies between 6.5 and 7.23 m from 860 to 960 MHz and achieves the peak value at 895 MHz. As the tag is placed closer to human body, a part of the transmitted power is absorbed by the skin, which results in decrements of read range. When the tag is placed 1 cm away from body and directly on body, the read range is between 5 to 6.4 m with the maximum value at 870 MHz and between 3.73 and 4.71 m with the maximum value at 885 MHz, respectively. Such results show that the proposed antenna is suitable for wearable applications.

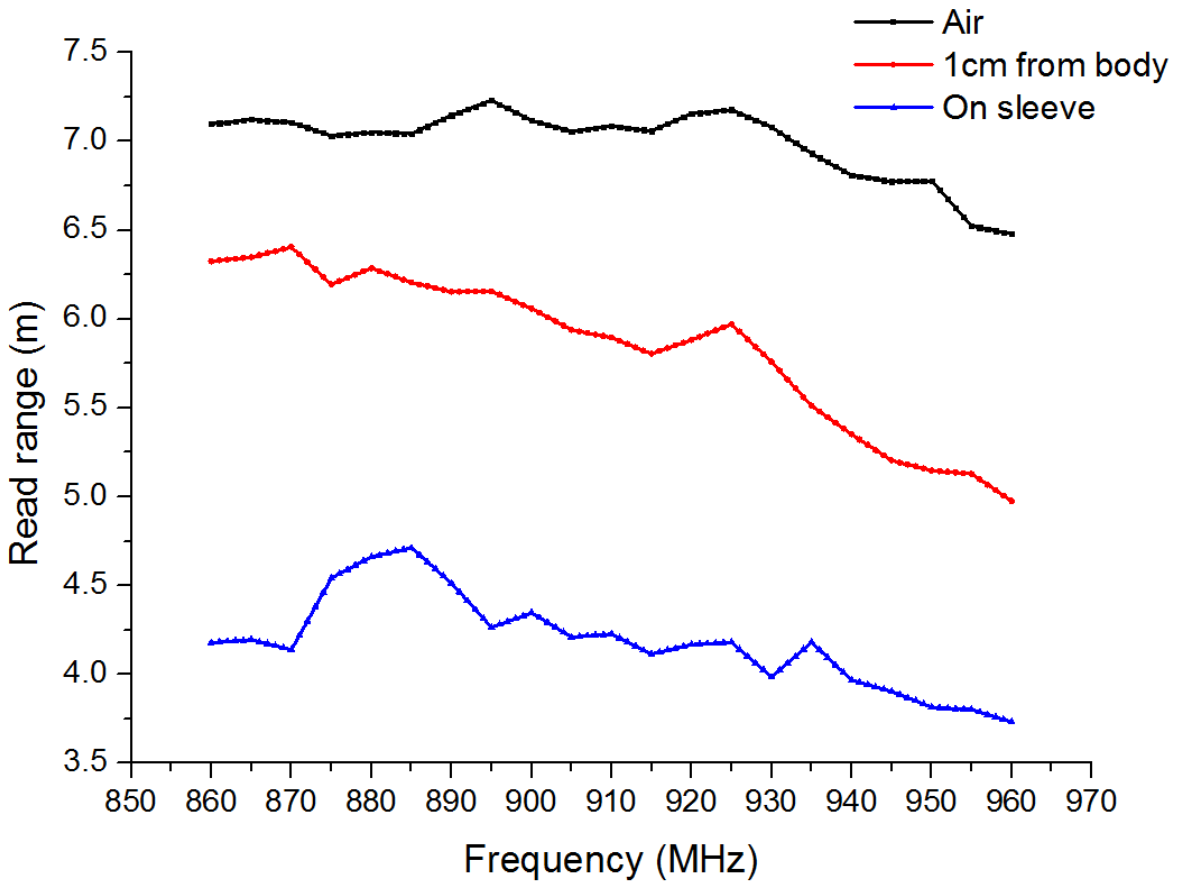

Fig. 6-5. Measured read range

6.1.4. Conclusion

A wearable wideband UHF RFID tag antenna fabricated with conductive textile has been proposed. Simulation results and measured read rage have been presented and discussed. As an antenna fabricated with relatively less conductive material, it possesses a high and steady read range (6.5-7.23m) over the RFID band (860-960MHz) and performs well while placed on human body with the best read range of 4.71m.

A Novel e-textile Integrated Wideband Monopole Antenna for Body-worn Energy Harvesting Systems

2019 IEEE International Symposium on Antennas and Propagation and USNC-URSI Radio Science Meeting, Atlanta, GA, USA, 2019, pp. 1287-1288

My contributions:

I have designed and fabricated the proposed devices, performed all of the measurements and data analyzation, and prepared all the graphs.

6.2 A Novel e-textile Integrated Wideband Monopole Antenna for Body-worn Energy Harvesting Systems

Yutong Jiang[#1], Ting Leng[#2], Yixian Fang[#3], Lulu Xu[$4], Kewen Pan[#5], Zhirun Hu[#6]

[#]School of Electrical and Electronic Engineering, the University of Manchester, UK

[$]School of Materials, the University of Manchester, UK

[1]yutong.jiang@manchester.ac.uk, [2]ting.leng@manchester.ac.uk,

[3]yixian.fang@manchester.ac.uk, [4]lulu.xu@postgrad.manchester.ac.uk,

[5]kewen.pan@manchester.ac.uk, [6]z.hu@manchester.ac.uk

Abstract

A novel e-textile integrated wideband monopole antenna designed for body-worn energy harvesting systems is presented. The proposed antenna is constructed with silver coated conductive threads woven into cotton substrate, and the operation bandwidth of which covers GSM bands (range 870.4-915 MHz and 1.7-1.9 GHz), LTE bands (range 0.79–0.96 GHz; 1.71–2.17 GHz; and 2.5–2.69 GHz) and Wi-Fi frequencies (2.4 and 3.6 GHz).

6.2.1. Introduction

In recent years, with the increasing popularity of body worn electronics such as sensors, e-textile based electrodes and antennas, a demand for wearable energy sources has arisen in order to power these devices continuously and complete a self-supplying personal communication network. RF energy harvesters are considered an excellent power source since ambient energy is available in an increasing number of frequency bands [5-6]. Therefore a well-designed energy harvesting device can be both effective and environmental friendly.

The receiving antenna for a wearable RF energy harvesting system is expected to be light weight, conformable and effective for a wide range of frequencies [7]. To meet these expectations, we present a monopole antenna fabricated with textile materials including silver coated conductive threads for the antenna body and cotton for the substrate, which is flexible and provides high comfort level for human body.

Due to the large available on-body area, the size of wearable textile antennas is not strictly limited. The proposed antenna possesses an active area of 20×16 cm, which is constructed in circular shape in order to achieve wide operation bandwidth [8-11]. The operation bandwidth of this antenna is designed to cover some of the most occupied frequency band in RF communication including GSM bands (range 870.4-915 MHz and 1.7-1.9 GHz), LTE bands (range 0.79–0.96 GHz; 1.71–2.17 GHz; and 2.5–2.69 GHz) and Wi-Fi frequencies (2.4 and 3.6 GHz).

This paper will present the antenna design and S11 performance in Section II and far-field radiation measurements in Section III. The conclusions are drawn in Section IV.

6.2.2. Design and procedures

A. Antenna structure

In Fig. 6-6(a) and (b), the layout of the proposed antenna is presented. The designed monopole antenna consists of a slotted circular patch with a radius of 71 mm and a smaller circular patch with a radius of 25.2 mm. The antenna body is fed by a micro-strip transmission line matched to 50 Ω. In simulation, the antenna performance highly depends on the smaller patch radius R_2 and the slot angle θ labelled in Fig. 1(a), and the operation frequency bands are optimized by tuning these two parameters.

Fig. 6-7 presents the fabricated antenna prototype. The silver coated conductive threads selected for the embroidered antenna is Silverpam 250 silver coated conductive threads from TIBTECH Innovation, which possesses line resistivity of 3 Ω/cm and thickness of 0.2 mm. The antenna is fabricated with embroidery machine (JCZA 0109-550, ZSK). The substrate consists three layers of cotton (ε_r=1.4) including the front plane, ground plane and a middle layer for isolation. In order to minimize the effect towards surface current flow caused by single weaving direction, the gap between parallel threads is set at 0.1mm so that threads are weaved together tightly enough to be considered as a metal patch. All three layers are sewed together with cotton threads and the overall thickness is about 1.2 mm. An SMA connector is connected to the antenna using conductive epoxy for measurements.

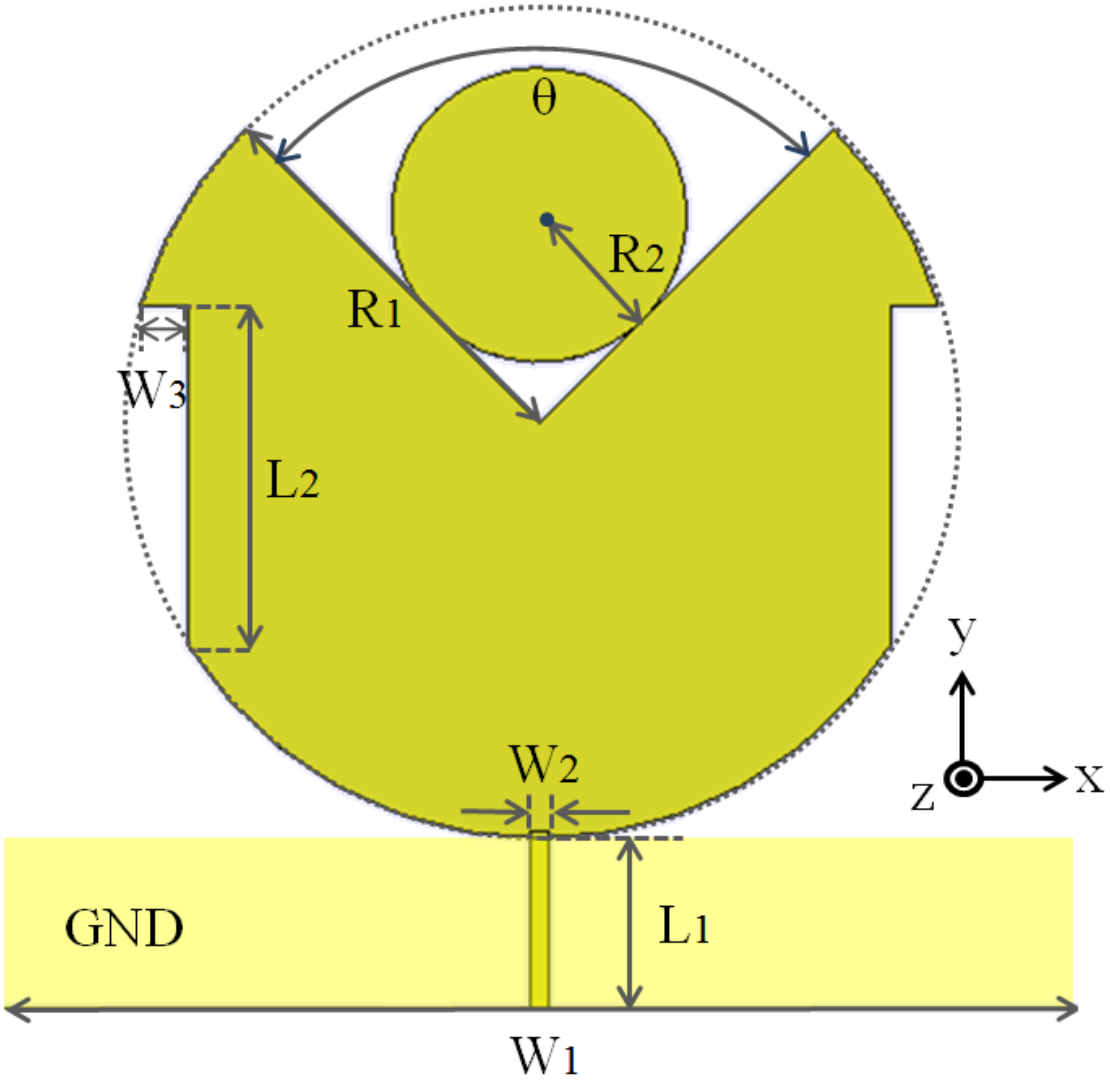

(a)

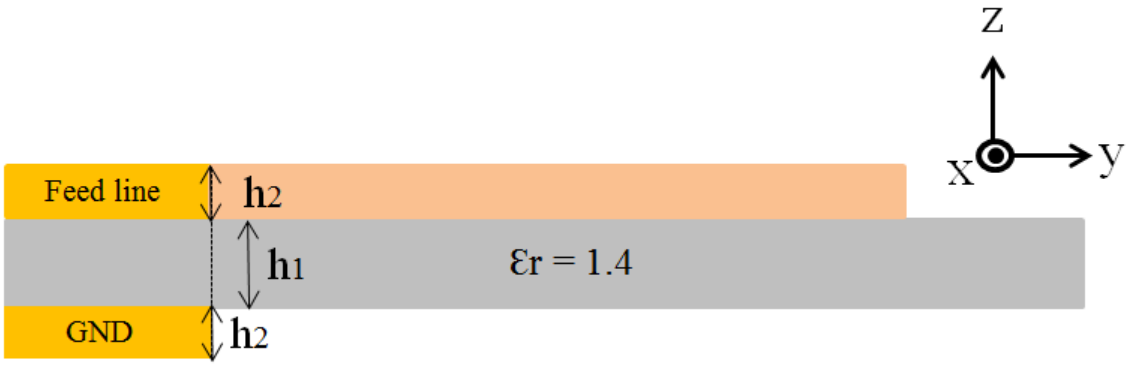

(b)

Fig. 6-6. Layout of the antenna prototype (a) Front view: θ=$\boldsymbol{90^o}$, $\boldsymbol{R_1}$=71 mm, $\boldsymbol{R_2}$=25.2 mm, $\boldsymbol{W_1}$=200 mm, $\boldsymbol{W_2}$=3.2 mm, $\boldsymbol{W_3}$=8.12 mm, $\boldsymbol{L_1}$=30 mm, $\boldsymbol{L_2}$=57.96 mm. (b) Side view: $\boldsymbol{h_1}$= 0.8 mm, $\boldsymbol{h_2}$=0.2 mm

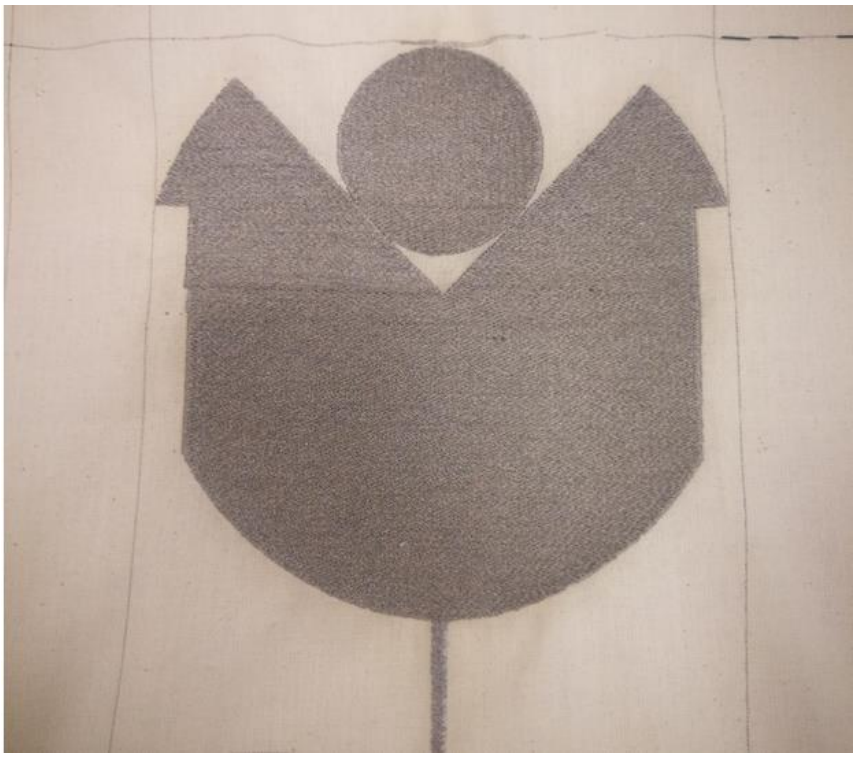

(a)

(b)

Fig. 6-7. Antenna embroidered with SILVERPAM 250 on cotton substrate (a) Front view. (b) Back view.

B. Return loss characteristics

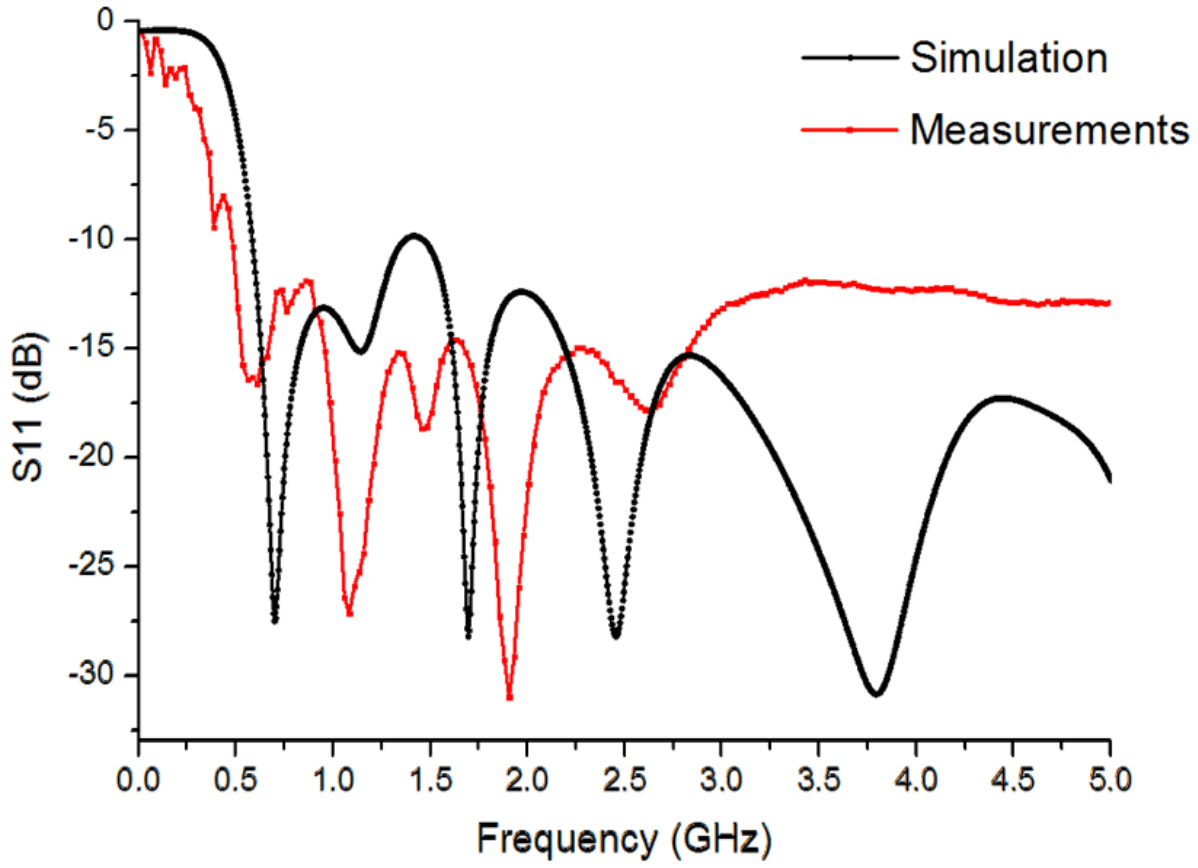

Fig. 6-8. Simulated and measured $\boldsymbol{S_{11}}$ magnitude for the fabricated antenna prototype.

Fig. 6-8 presents the simulated and measured magnitude of reflection coefficient (S_{11}) for the fabricated antenna. The simulated antenna operates at a first frequency band from 0.59 GHz to 1.37 GHz with resonant frequency of 0.7 GHz and a second band from 1.46 GHz to 5 GHz with resonant frequencies of 1.7 GHz, 2.45 GHz and 3.79 GHz. Due to the relatively high power loss in conductive threads and the inevitable misshape of the antenna, it can be seen that the measured results do not match well at higher frequencies around 3.79 GHz. However, since the antenna operates at a wide bandwidth between 0.5 GHz and 5 GHz, all the desired frequency bands are covered under -10 dB bandwidth.

6.2.3. Far field radiation characteristics

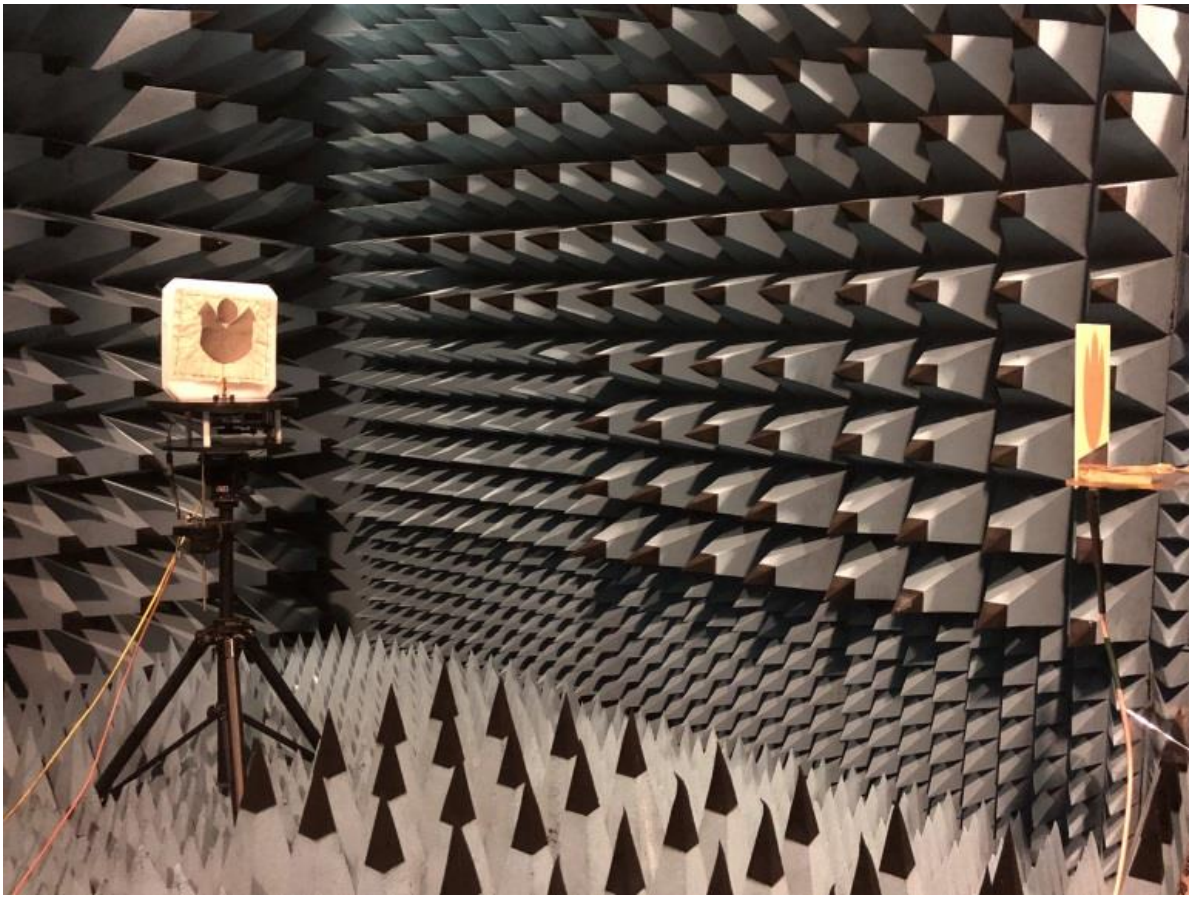

Fig. 6-9. Fabricated textile antenna being measured in the anechoic chamber.

The far-field radiation characteristics of the antenna prototype were measured in an anechoic chamber with a fully calibrated ENA E5071B as presented in Fig. 6-9. The transmitting antenna applied in the measuring process is the same proposed structure fabricated with FR4 substrate and copper film. The simulated and measured radiation patterns for both E-plane (y-z plane) and H-plane (x-z plane) are presented in Fig. 6-10 at four selected frequencies: 0.7 GHz, 1.7 GHz, 2.4 GHz and 3.6 GHz. The patterns of simulation and measurements for both planes correspond better between 0° and 180°. At lower frequencies, the radiation pattern on E-plane appears directive towards between 0° and 180° while the H-plane is perfectly omnidirectional as it shows in Fig. 6-10(a). As the frequency increases, the H-plane patterns become increasingly directive to 90° and 270° and the main lobe direction of E-plane patterns moves gradually towards 90°. Such results indicate that the antenna becomes more directional as the frequency increased within the selected range. The measured gains at the

four selected frequencies are 2.73 dBi, 3.56 dBi, 2.17 dBi and 5.64 dBi at 0.7 GHz, 1.7 GHz, 2.4 GHz and 3.6 GHz, respectively.

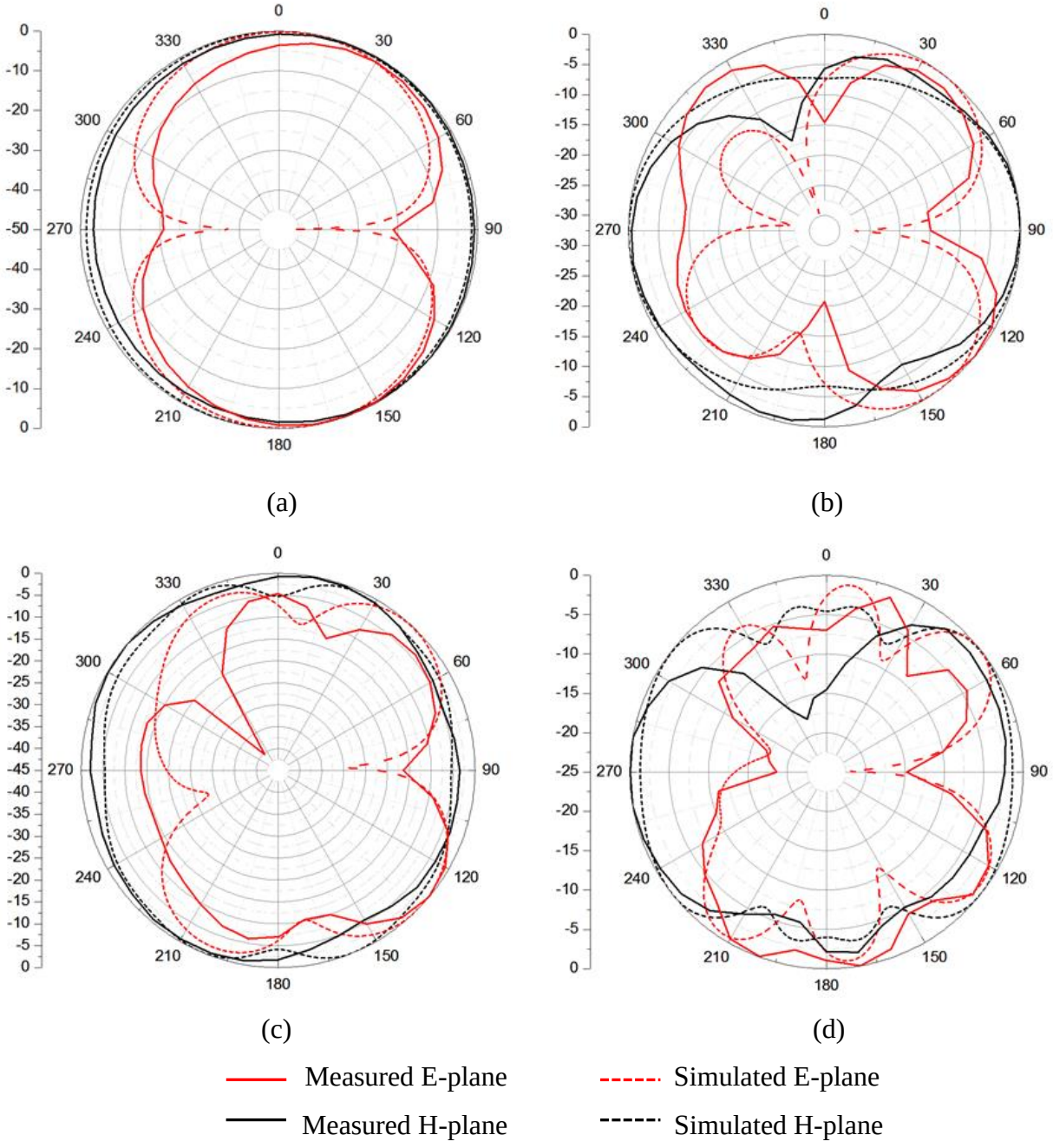

Fig. 6-10. Simulated and measured textile antenna radiation patterns for E-plane and H-plane at four different frequencies (a) 0.7 GHz, (b) 1.7 GHz, (c) 2.4 GHz, (d) 3.6 GHz.

6.2.4. Conclusion

A wideband circular structured monopole antenna fabricated with e-textile has been proposed. Results for reflection coefficient and radiation patterns have been presented and discussed.

The proposed antenna operates for 0.78 GHz from 0.59 GHz to 1.37 GHz and 3.54 GHz from 1.46 GHz to 5 GHz. The measured and simulated radiation patterns agree well for a conformal antenna made with relatively lossy material. Furthermore, the antenna achieves steady gain along a wide range of frequencies. The performance of the proposed structure makes it promising to be applied in effective power harvesting systems.

6.3. References

[1] Ukkonen, L. and Sydänheimo, L. (2011). Sewed Textile RFID Tag and Sensor Antennas for On-Body Use. 6th European Conference on Antennas and Propagation (EUCAP).

[2] K. Koski, L. Sydänheimo, Y. Rahmat-Samii and L. Ukkonen, "Fundamental Characteristics of Electro-Textiles in Wearable UHF RFID Patch Antennas for Body-Centric Sensing Systems," in IEEE Transactions on Antennas and Propagation, vol. 62, no. 12, pp. 6454-6462, Dec. 2014.

[3] W. M. Mongan, I. Rasheed, K. Ved, A. Levitt, E. Anday, K. Dandekar, G. Dion, T. Kurzweg, and A. Fontecchio, "Real-time detection of apnea via signal processing of time-series properties of RFID-based smart garments," in 2016 IEEE Signal Processing in Medicine and Biology Symposium (SPMB), 2016, pp. 1-6.

[4] Ginestet, G., Brechet, N., Torres, J., Moradi, E., Ukkonen, L., Bjorninen, T. and Virkki, J. (2017). Embroidered Antenna-Microchip Interconnections and Contour Antennas in Passive UHF RFID Textile Tags. IEEE Antennas and Wireless Propagation Letters, 16, pp.1205-1208.

[5] Niotaki, K., Kim, S., Jeong, S., Collado, A., Georgiadis, A. and Tentzeris, M. (2013). A Compact Dual-Band Rectenna Using Slot-Loaded Dual Band Folded Dipole Antenna. IEEE Antennas and Wireless Propagation Letters, 12, pp.1634-1637.

[6] Palazzi, V., Hester, J., Bito, J., Alimenti, F., Kalialakis, C., Collado, A., Mezzanotte, P., Georgiadis, A., Roselli, L. and Tentzeris, M. (2018). A Novel Ultra-Lightweight Multiband Rectenna on Paper for RF Energy Harvesting in the Next Generation LTE Bands. IEEE Transactions on Microwave Theory and Techniques, 66(1), pp.366-379.

[7] Zhang, L., Wang, Z. and Volakis, J. (2012). Textile Antennas and Sensors for Body-Worn Applications. IEEE Antennas and Wireless Propagation Letters, 11, pp.1690-1693.

[8] Siddiqui, J., Saha, C. and Antar, Y. (2014). Compact SRR Loaded UWB Circular Monopole Antenna With Frequency Notch Characteristics. IEEE Transactions on Antennas and Propagation, 62(8), pp.4015-4020.

[9] Kumar, A. and Raghavan, S. (2017). Design of a broadband planar cavity-backed circular patch antenna. AEU - International Journal of Electronics and Communications, 82, pp.413-419.

[10] Chen, J. and Liu, J. (2016). A new broadband dual-layer monoplolar circular patch antenna with slot coupling. Microwave and Optical Technology Letters, 59(1), pp.40-43.

[11] Seo, Y., Jung, J., Lee, H. and Lim, Y. (2012). Design of circular monopole antenna with symmetrically folded stub for WLAN operation. Microwave and Optical Technology Letters, 54(7), pp.1549-1552.

Chapter 7 A Novel Body-Worn Energy Harvesting System Based on e-Textile Antenna Array and Compact Multiband Rectifier

Yutong Jiang, Kewen Pan, Ting Leng and Zhirun Hu, Member, IEEE

My contributions:

I have designed and fabricated the proposed devices, performed all of the measurements and data analyzation, and prepared all the graphs.

Abstract

Ambient energy harvesting is a rising technology that converts EM energy in air into electricity, which has become a great solution for replacing batteries and providing steady and lasting power source for electronic devices. The work reported here demonstrates the development of a novel wearable energy harvesting system constructed with a pure e-textile broadband dual-antenna array and a compact six-band rectifier. The textile antennas are seamlessly integrated with skin friendly cotton substrate, which is wearable for relatively large body area in order to harvest ambient RF energy. The operating bandwidth of the proposed device covers the most occupied RF power generating frequency bands, including digital TV bands (470–610 MHz), GSM bands (range 870.4–915 MHz and 1.7–1.9 GHz), LTE bands (range 0.79–0.96 GHz; 1.71–2.17 GHz; and 2.5–2.69 GHz), 3G bands (1.92–1.98 GHz and 2.11–2.17 GHz) and Wi-Fi frequency (2.4 GHz). This system aims for providing constant DC power for body sensors, which has the potential to be applied in various fields as a part of body area network.

7.1. Introduction

During the past decade, wearable e-textile technology has become increasingly popular for the market. E-textile produced with various fabrication techniques has been developed with functionalities such as heat regulation, luminescent and most of all, sensor embedded [1]. With the rapid development of body sensor networks (BSN), wearable sensors have made

tremendous contribution in a variety of fields, such as physiological signals real-time monitoring in healthcare [2-4] and human surveillance for personal safety [5]. Since most of the wearable sensors require a stable power source, integration of energy harvesting technology has been considered a great solution to replace batteries and prolong the life time of wearable devices as well as reduce chemical waste by acquiring energy from ambient environment constantly.

Wearable energy harvesting techniques can take many forms, such as transferring electrical energy from body movements and human motions by employing triboelectric e-textile [6-8], light energy harvesting [9] and RF energy harvesting [10]. The ambient RF energy harvesting technique operates by converting energy from electromagnetic waves into DC power, the state-of-art development of which is stated in [11]. This technique has attracted tremendous attention due to the intense density of wireless communication. The average power density of the largest RF contributors in London is summarized in [12], which shows that the most intense density of ambient RF power lies in the operation bands of GSM1800 (base station transmitter) and GSM900 (base station transmitter) with 84 nW/cm^2 and 36 nW/cm^2, respectively.

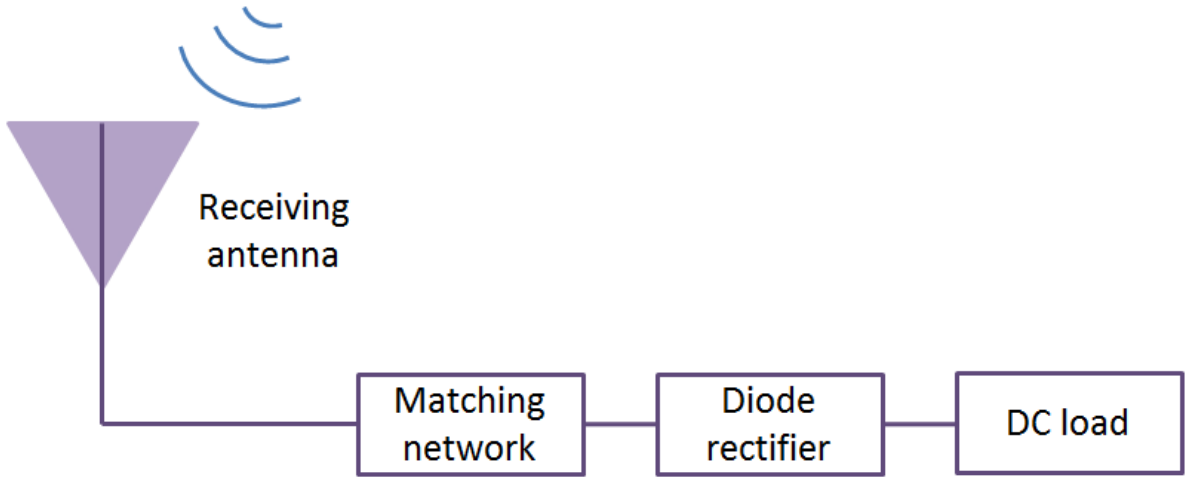

Fig. 7-1. The overall architect of an RF energy rectifier

As it presents in Fig. 7-1, RF energy harvesters are usually constructed with receiving antennas, matching circuits and RF rectifiers, which are also called rectennas. The latest researches of wearable RF energy harvesters designed for powering wearable sensors are listed in [13-18]. Most of the existing wearable rectennas are designed for single and dual

band operation, for which the received RF power can be limited and the device would require a closed-by power source.

In this paper, we propose a six-band operating body worn RF energy harvester composed with an e-textile broadband dual monopole antenna array and a six-band rectifier. The antenna array is constructed with two identical monopole antennas designed in a plier shape with thin outlines, which aims to achieve high realized gain and broad operating bandwidth with minimal cost. The antenna circuit is light weight and skin friendly for it is fabricated with silver coated conductive threads (0.3 mm cross-section diameter) and cotton substrate. In order to maximize the RF to DC conversion from ambient sources, the rectifier is constructed with three parallel dual-band matching branches [19]. For the interest of reducing effect from natural body movements due to the deformable structure and relatively large size of the textile antenna array, the proposed device is designed to be implanted on the back body area, where the clothing takes less distorting forces.

This paper is structured as follows. Section II will demonstrate the design, fabrication and performance of the e-textile dual antenna array. In Section III, the design and performance of the six-band rectifier are presented. Section IV will demonstrate the ambient harvesting performance of the rectenna and propose potential applications of the proposed device. Section V summarizes the key results and overall circuit performance.

7.2. e-textile duo antenna array

7.2.1. Antenna design

Fig. 7-2 presents the layout of the antenna designed for the wearable energy harvesting system, which is a dual-antenna array composed of two identical monopole antennas. The antennas are designed in the shape of slotted elliptical rings in order to achieve broadband operation as well as to minimize the usage of conductive textile. The slots at the top of the antennas are optimized for the desired operation frequencies, and the distance between the two antennas are designed as 200mm for a trade-off between minimizing the crosstalk and the overall antenna size. The substrate material is selected as cotton (ε_r=1.4) with 0.4mm thickness. The antennas are feed with transmission lines matched to 50 Ω. The separating distance between the antenna elements is set to 0.25λ at 750 MHz (the lowest expected operating frequency).

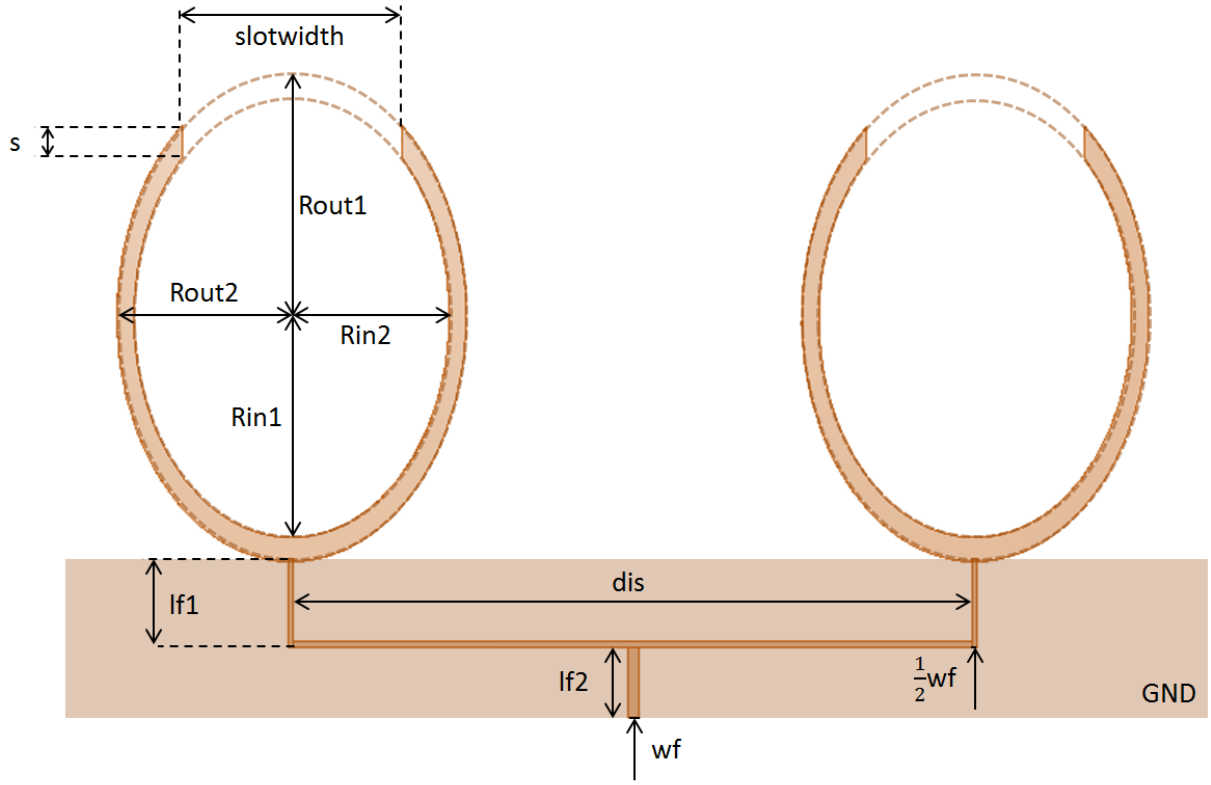

Fig. 7-2. The antenna array layout: Rout1=71 mm, Rout2=51 mm, Rin1=64 mm, Rin2=46 mm, slotwidth=64 mm, s=9.31 mm, lf1=25 mm, lf2= 20 mm, wf= 3.1mm, dis=200mm, ground plane =350 mm×45 mm

As presented in Fig. 7-3, the array antenna prototype is fabricated using embroidery machine (JCZA 0109-550, ZSK), integrating silver coated conductive threads (Silverpam 250 from TIBTECH Innovation) with cotton substrate. A cotton layer is placed between the antenna and the ground plane for electrical isolation. The e-textile feedline is connected to an SMA port using conductive epoxy.

The S-parameters of the antenna is measured with Keysight Fieldfox VNA N9918A. Fig. 7-4 presents the simulated and measured S11 results of the antenna array from 0 to 5 GHz. In simulation, the antenna shows a multiband behaviour within the frequency bands of 560-725 MHz, 880-1020 MHz, 1.42-1.58 GHz, 1.74-2.03 GHz, 2.44-3.03 GHz, 3.59-4.04 GHz, 4.4-4.54 GHz and 4.81-5 GHz. In the measurements, the magnitude of reflection coefficient is generally lower than the simulation results and the antenna presents a broad operation bandwidth from 0.56 GHz to 5 GHz, covering most of the frequency bands required for ambient RF energy harvesting. The simulated gain trend of the antenna array is presented in Fig. 7-5. The maximum gain achieves 7.68 dBi at 1.45 GHz, and the average gain from 0.5

GHz to 5 GHz is 5.55 dBi. This trend shows a high and stable gain pattern over the broad operating band, which is considered suitable for the multiband rectifier implantation that will be discussed in Section III.

(a)

(b)

Fig. 7-3. Fabricated textile dual-array monopole antenna: (a) front (b) back

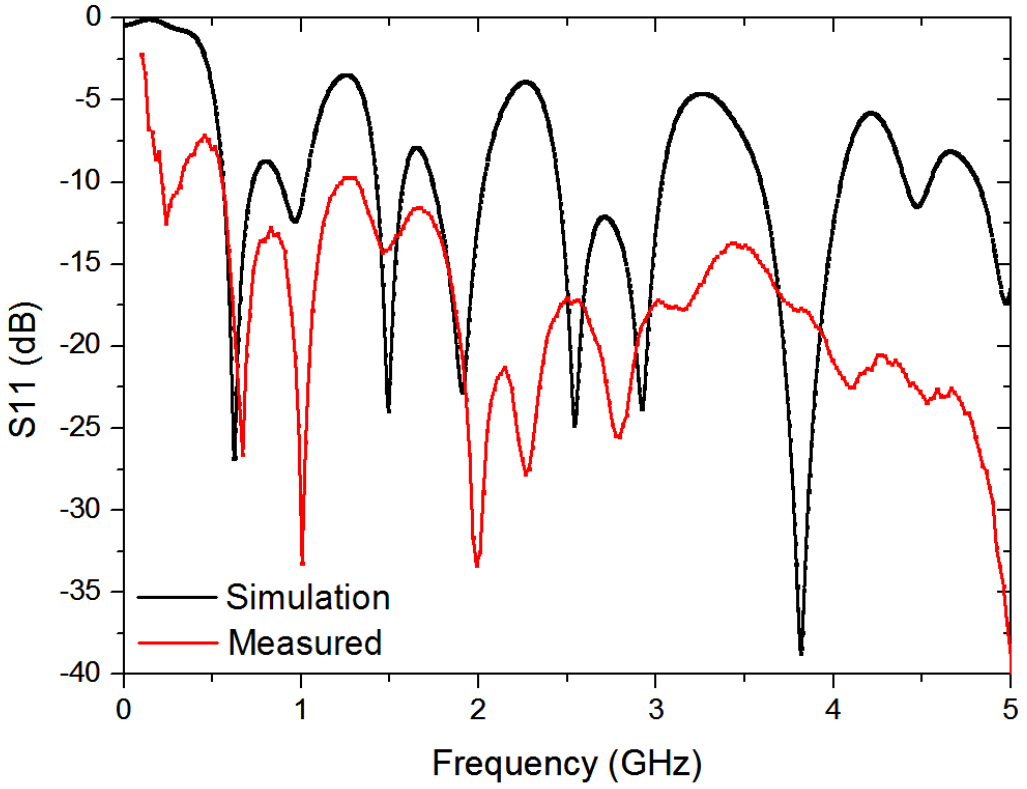

Fig. 7-4. Simulated and measured S11 results for textile antenna array

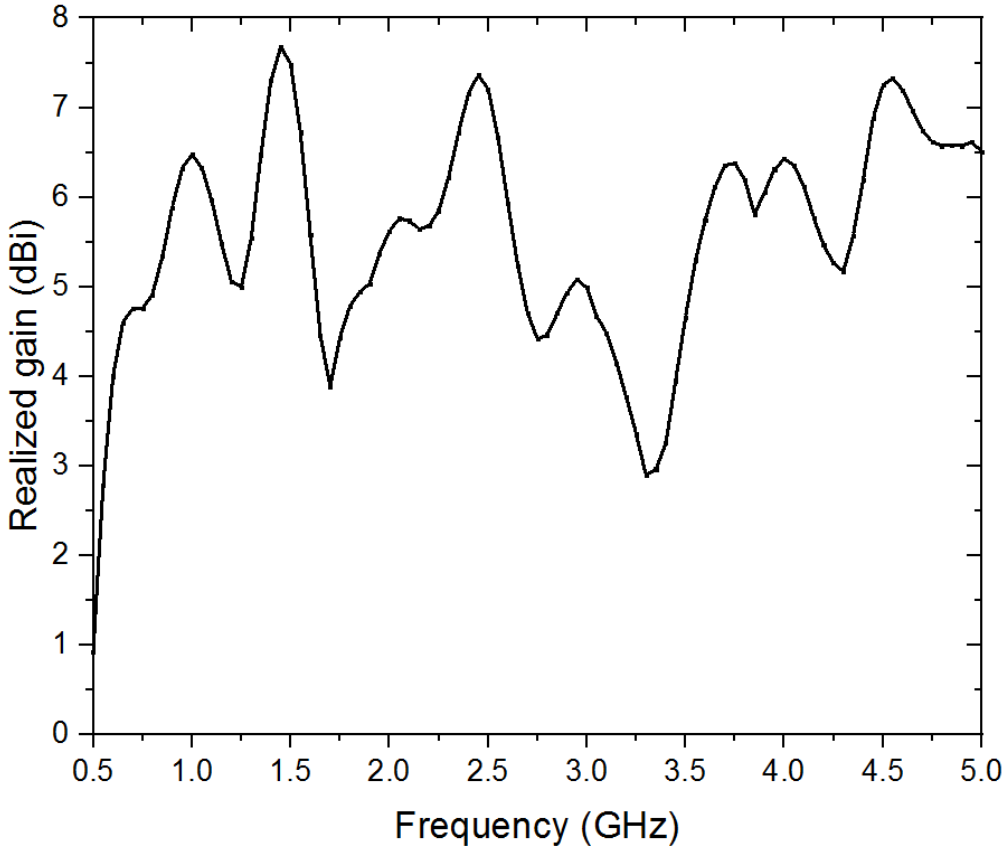

Fig. 7-5. Simulated antenna gain over frequency

7.2.2. Far field radiation

The far-field radiation patterns of the antenna array were measured in an anechoic chamber with a fully calibrated ENA E5071B as it shows in Fig. 7-6. A broadband monopole antenna fabricated with FR4 substrate and copper film is applied as the transmitting antenna in the measuring process. The simulated and measured radiation patterns for both E-plane (y-z plane) and H-plane (x-z plane) are presented in Fig. 7-7 at six selected frequencies: 0.6 GHz, 1.5 GHz, 1.9 GHz, 2.45 GHz, 2.9 GHz and 3.6 GHz. The maximum gain measured at these frequency points are 3.99 dBi, 7.51 dBi, 5.04 dBi, 7.36 dBi, 4.56 dBi and 2.64 dBi, respectively. The discrepancy between the measured and simulated results is mainly due to instability induced by the flexible structure of the e-textile antenna. As the operation frequency increases, the angular width of the main lobe narrows down gradually for both E-plane and H-plane patterns, which indicates antenna becomes more directional over the selected frequency range.

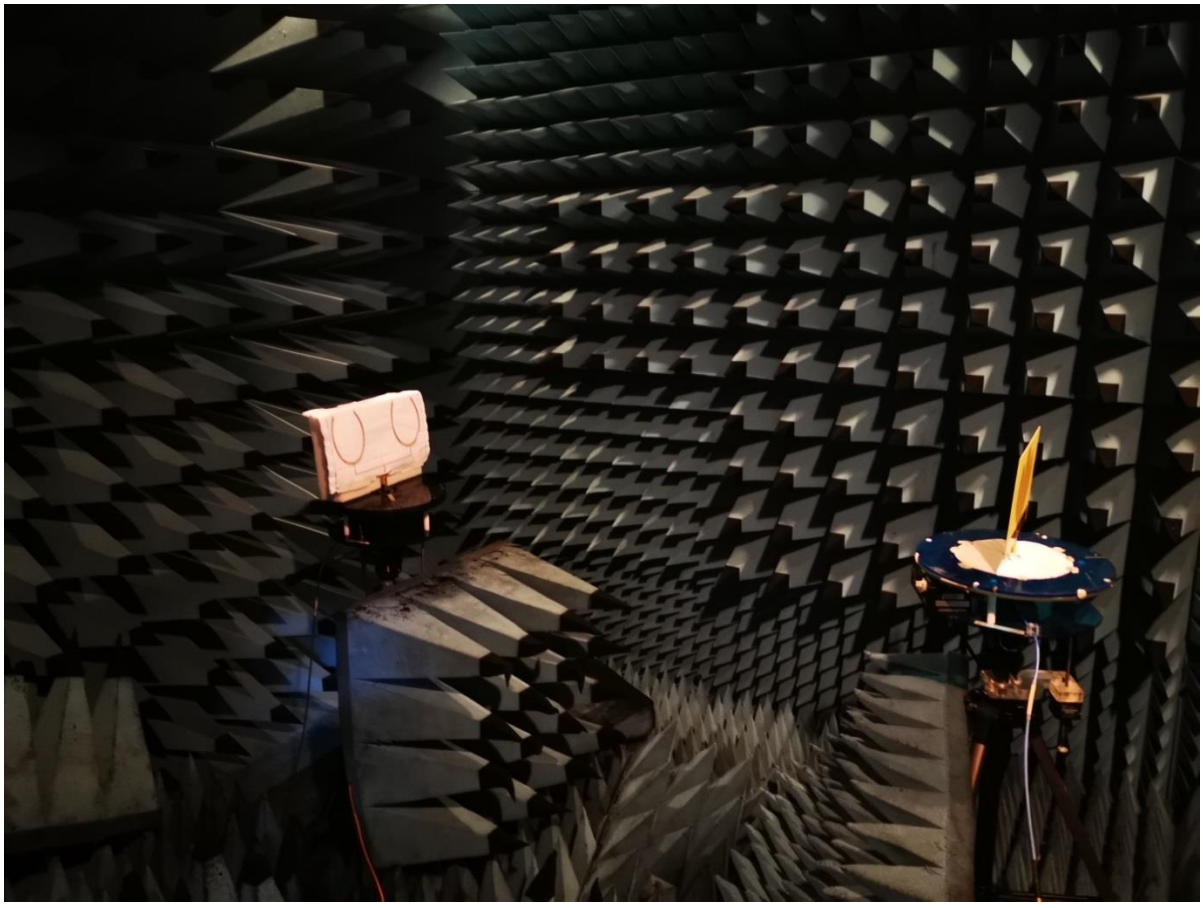

Fig. 7-6. Measurement setup for far field radiation

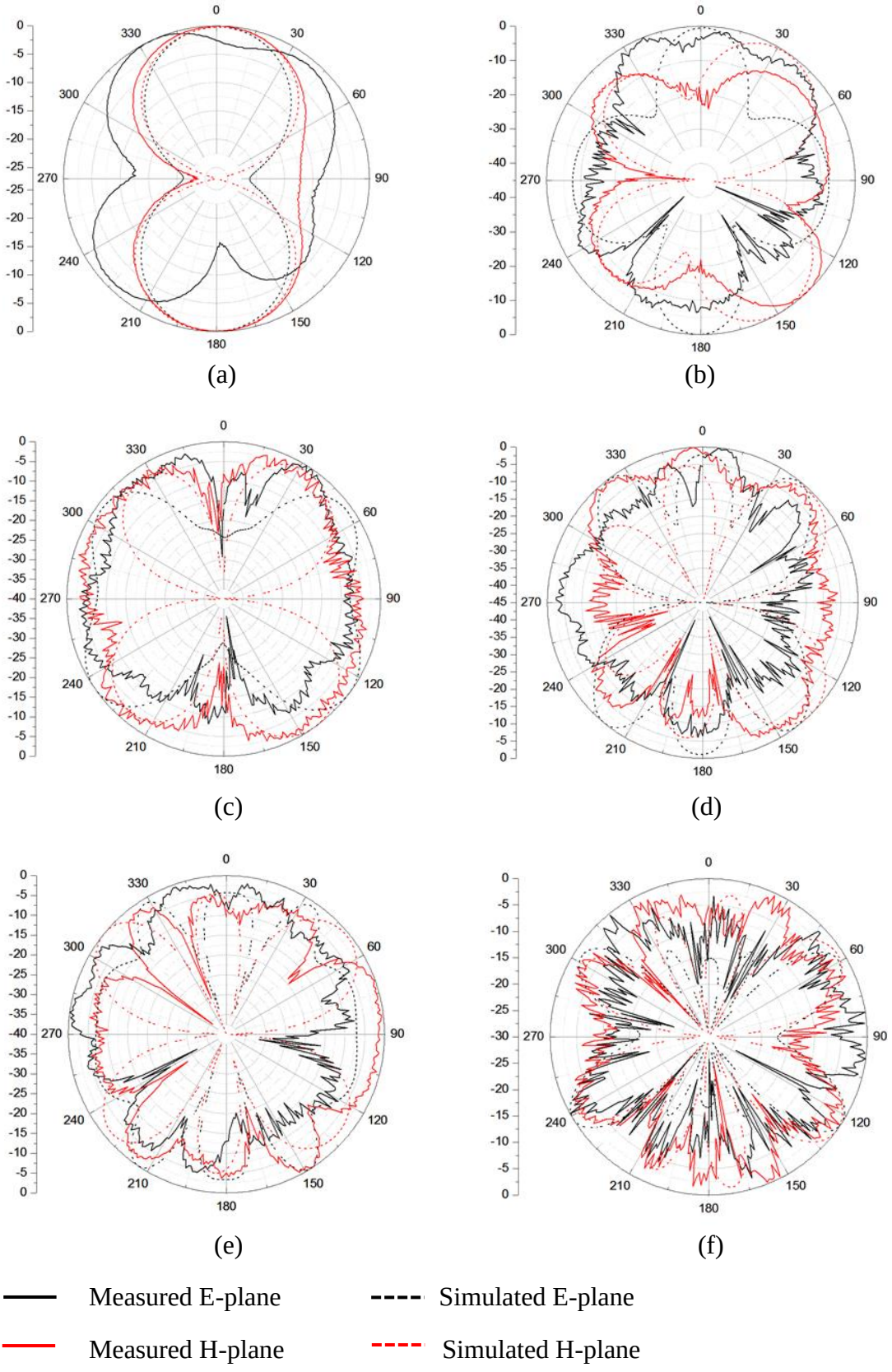

Fig. 7-7. Simulated and measured textile antenna array radiation patterns for E-plane and H-plane at six different frequencies (a) 0.6 GHz, (b) 1.5 GHz, (c) 1.9 GHz, (d) 2.45 GHz, (e) 2.9 GHz and (f) 3.6 GHz

The simulated antenna total efficiency is presented in Fig. 7-8. The trend possesses a periodic pattern at the selected frequency range with peak efficiencies at 0.65 GHz, 1.8 GHz, 2.95 GHz and 3.9 GHz. At the selected frequencies for radiation pattern measurements, the radiation efficiencies are 86.9%, 85.7%, 84.5%, 72.1%, 91.5% and 74.1%, respectively.

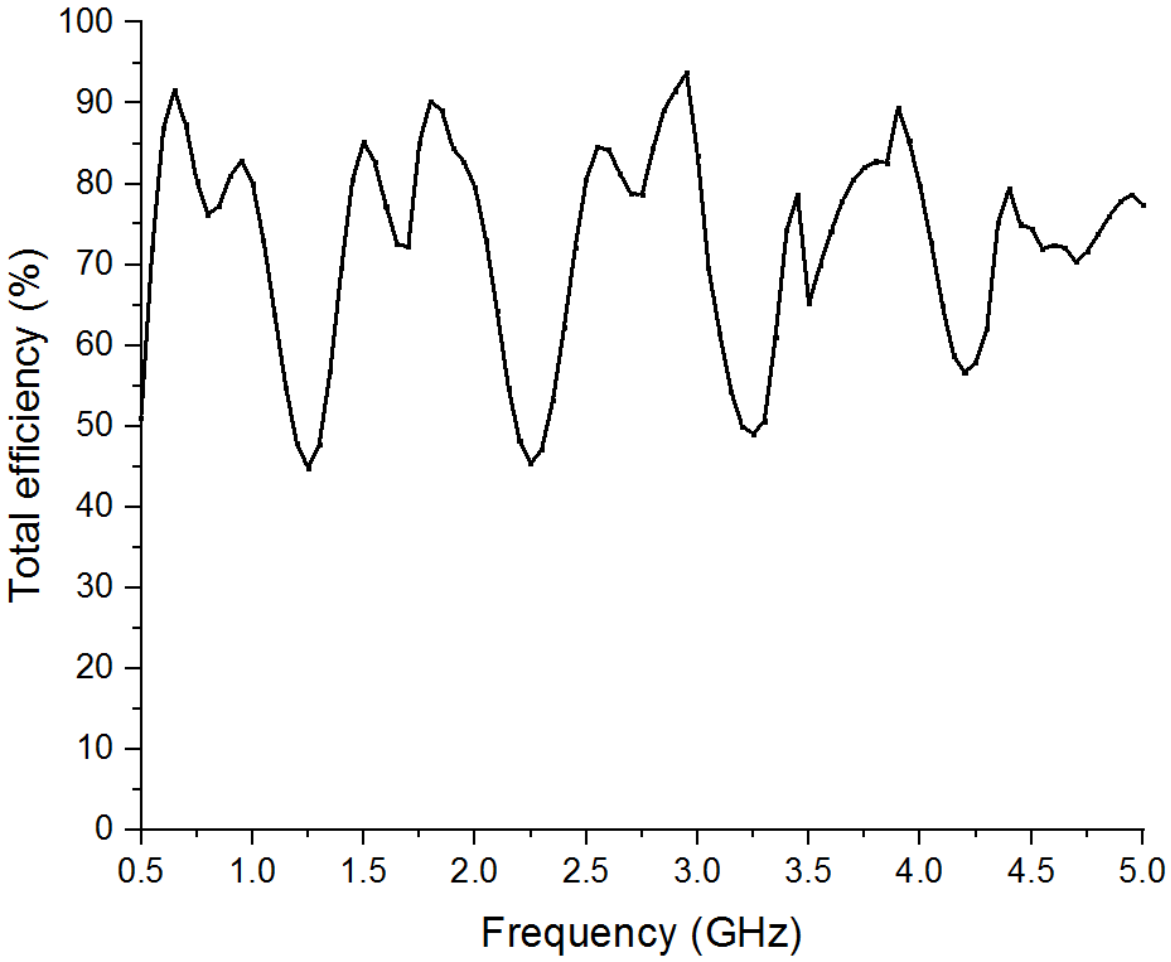

Fig. 7-8. Simulated antenna efficiency over frequency

7.3. Multiband RF rectifier

7.3.1. Rectifier design

In order to coordinate the broad operating bandwidth of the textile antenna and increase the efficiency in harvesting ambient energy, a multiband rectifier structure is chosen for the design. The proposed rectifier aims to cover 6 frequency bands that include UHF TV bands (470–806 MHz), GSM bands (870.4-915 MHz and 1.7-1.9 GHz), LTE bands (0.79–0.96 GHz;

1.71–2.17 GHz; and 2.5–2.69 GHz) and Wi-Fi frequency (2.4 GHz). The six-band matching technique is discussed in [19].

The rectifier circuit consists three branches. A dual band matching circuit is connected to a four-stage diode rectifier at each branch as it presents in the designed circuit schematic shown in Fig 7-9. The value of the lumped components at each branch is calculated based on CRLH (composite right/left-handed) dual-band principle [20] and dual-band impedance matching theory described in [21]. The optimized value of lump components in the matching network is listed in Table 7-1.

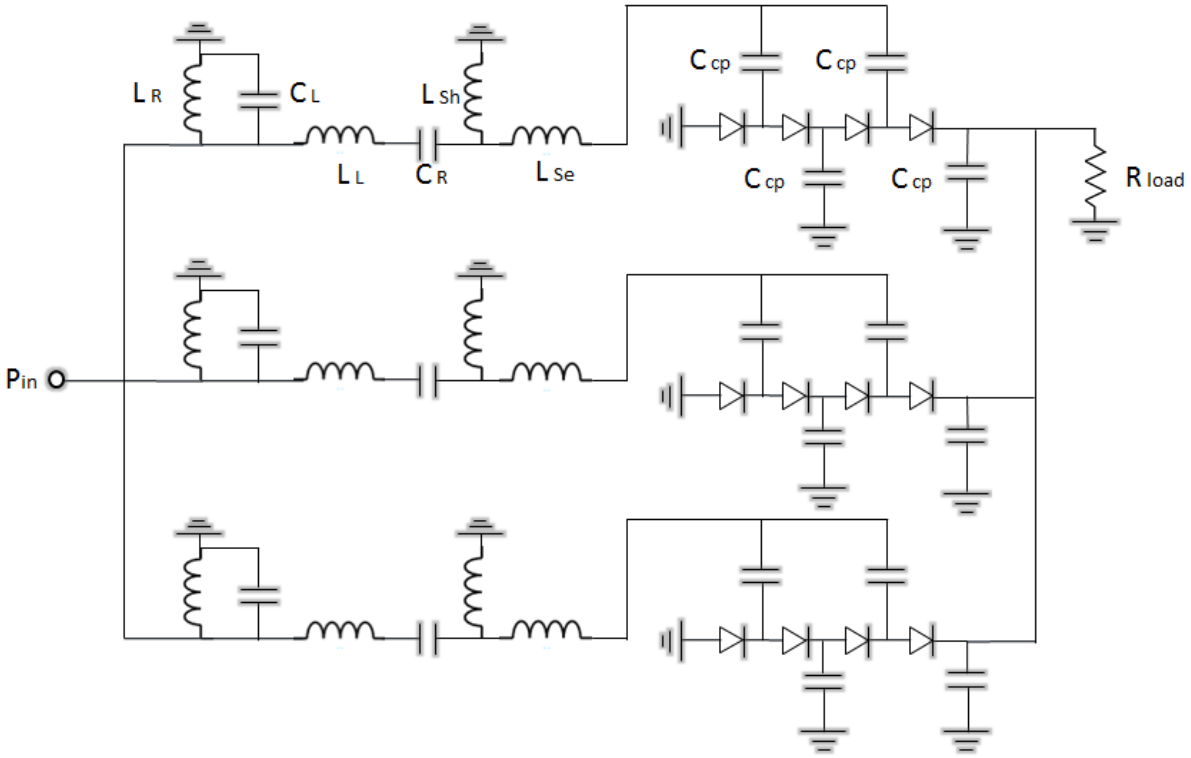

Fig. 7-9. Six-band rectifier layout

Fig. 7-10 presents the fabricated rectifier with FR4 substrate and copper film. The diodes in this circuit are selected as Schottky diodes (SMS7630, Skyworks) for a low barrier, and the coupling capacitance and load resistance are selected as 100 nF and 6.2 kΩ, respectively.

Table 7-1. Lump Component Parameters for the Fabricated Multiband Rectifier

	Branch 1	Branch 2	Branch 3
L_R (nH)	6.3	2.3	30
C_L (pF)	4.8	1.6	1
L_L (nH)	1	1	4
C_R (pF)	2.5	4.5	1.1
L_{sh} (nH)	12.8	2.8	1
L_{se} (nH)	32.4	7.8	1.6

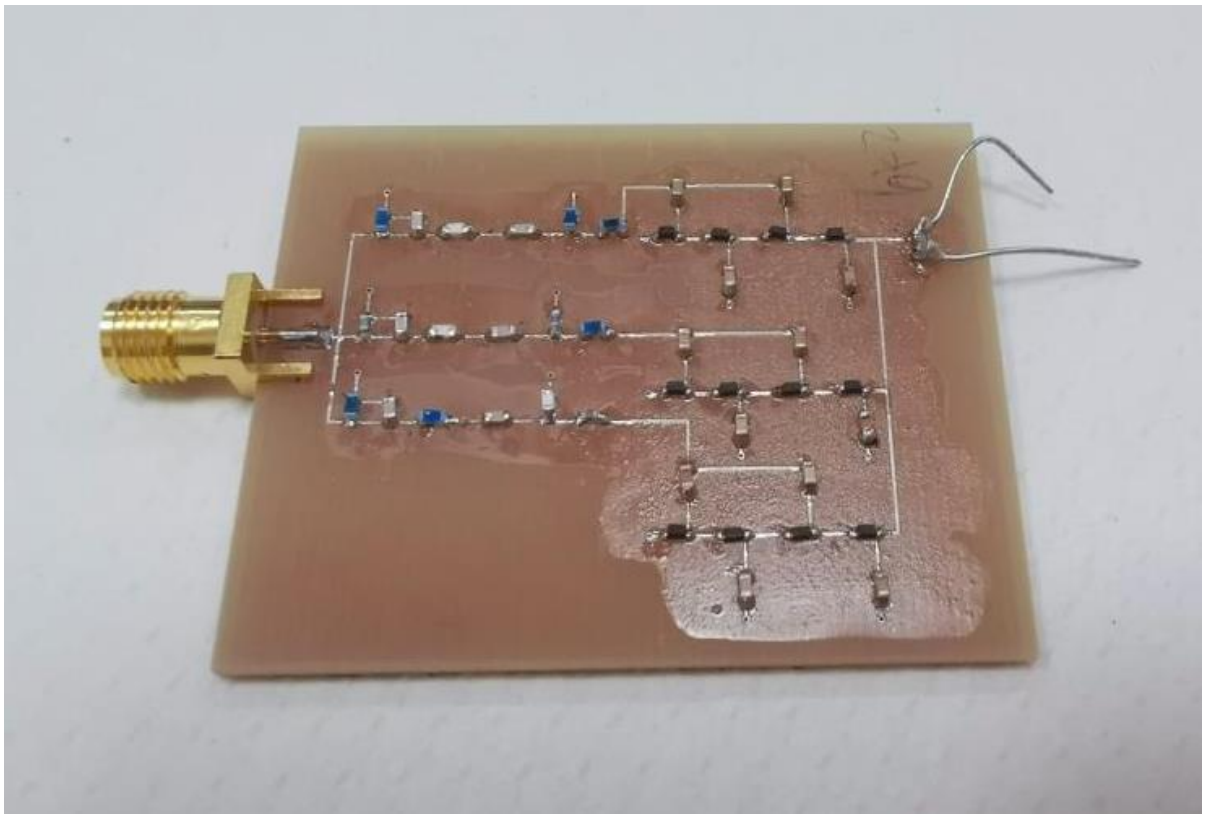

Fig. 7-10. Fabricated six-band rectifier

7.3.2. Rectifier performance

The simulated and measured reflection coefficient (S11) results are presented in Fig. 7-11, where the simulation results are calculated using the measured input impedance of the diode circuits. In simulation, the rectifier operates at 6 frequency bands around 0.62 GHz, 0.86 GHz, 1.46 GHz, 1.92 GHz, 2.22 GHz and 2.45 GHz. The measured operating frequencies are 0.53

GHz, 0.9 GHz, 1.61 GHz, 1.96 GHz, 2.11 GHz and 2.45 GHz. The results matches better at the higher three frequencies than the lower ones. Due to the non-linear properties of the rectifier circuit, the reflection coefficient is dependent on the input power level. However the S-parameter simulation in ADS generates constant results disregarding the input power level while in actual measurements the input power level of VNA measuring is fixed at -15 dBm. This might be the main reason for the mismatch between the simulation and measurement results.

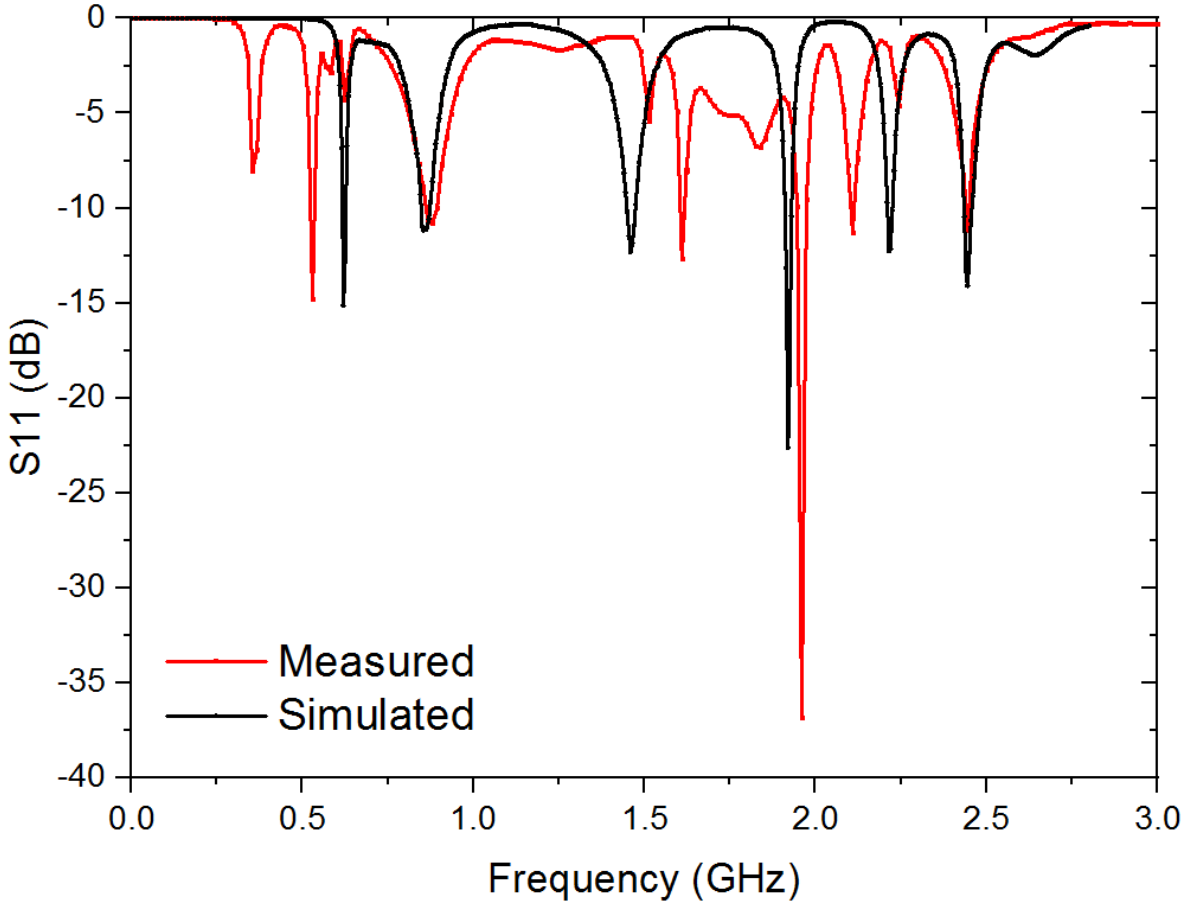

Fig. 7-11. Simulated and measured S11 results of the proposed rectifier

The RF to DC conversion efficiency can be calculated with (7-1)

$$\eta = \frac{P_{DC}}{P_{in}} \tag{7-1}$$

where P_{DC} is the output DC power, and P_{in} is the input power.

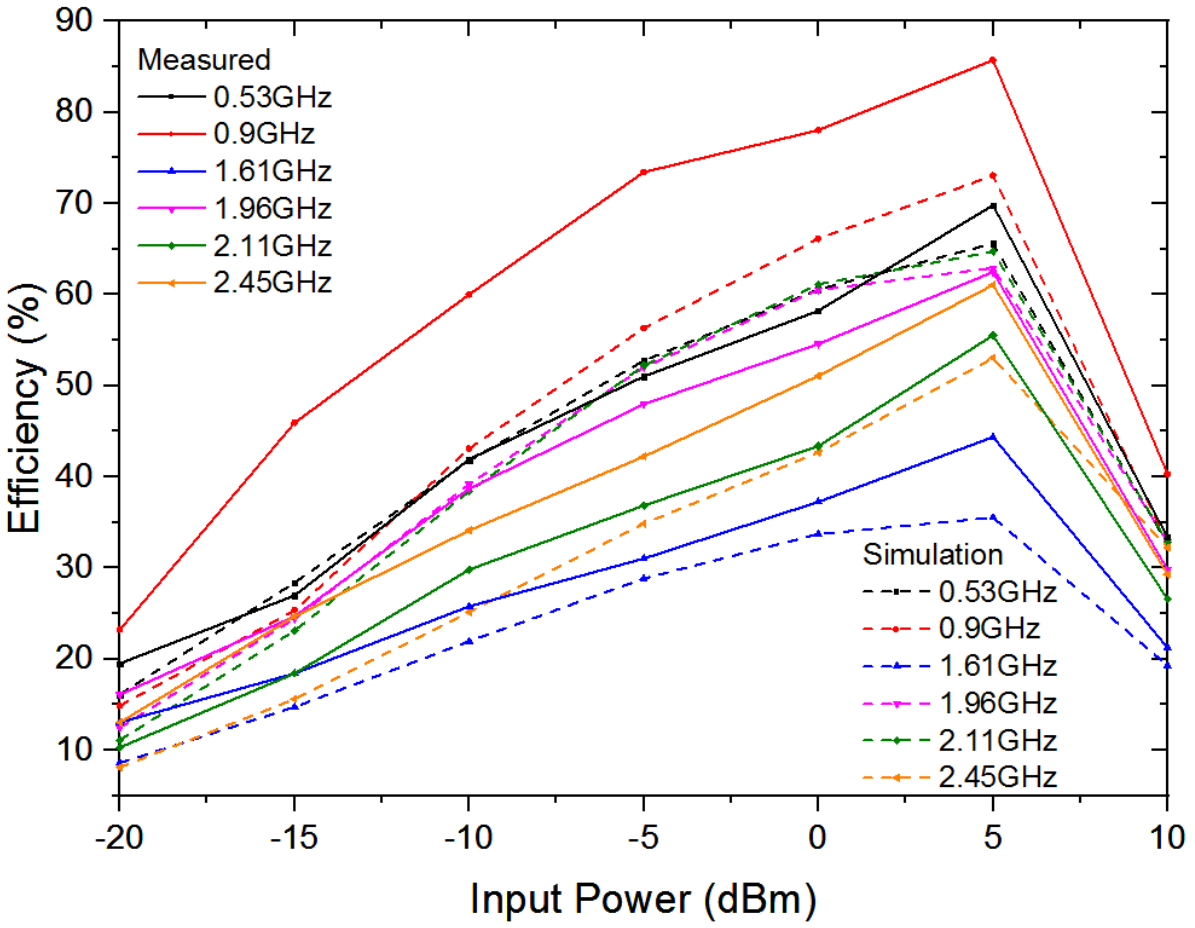

Fig. 7-12. Simulated and measured RF to DC conversion efficiency verses input power level at 6 selected frequencies

The simulated and measured conversion efficiencies at the measured resonant frequencies are presented in Fig. 7-12. The simulated efficiencies are obtained using the equivalent circuit model designed in ADS, and the actual efficiencies are obtained by measurements taken with an RF signal generator (Marconi Instruments 6200) and a DC-mode multi-meter. It shows that the rectifier works well over the wide range of frequencies with the input power level from -20 dBm to 10 dBm. It has been noticed that some of the measured efficiencies are considerably higher than the simulated ones, which might be due to the errors existing in the configuration between the actual and ADS SPICE models of Schottky diodes (SMS7630, Skyworks). The efficiencies approach peak values as the input power is 5 dBm with maximum value of 85.7% at 0.9 GHz. As the input power is between -20 and -10 dBm, the measured conversion efficiencies are 19.52%-41.95%, 23.23%-60.02%, 13.06%-25.81%, 16.13%-38.73%, 10.32%-29.82% and 13.06%-34.13% at the selected frequencies, respectively.

7.4. Ambient RF Energy Harvesting

The completed energy harvester is presented in Fig. 7-13(a), where the rectifier is connected to the antenna array through an SMA connector. In order to examine performance of device harvesting energy in air, a wireless power transfer experiment is performed as it presents in Fig. 7-13(b). A broadband antenna is connected to RF power generator (Marconi Instruments 6200) as a power source, and the proposed device is positioned 50 cm away from the source. The input power generated is set at 5 dBm, and the output DC voltage is measured with a multimeter (Fluke 87 III).

Table 7-2. Measured DC Output

Frequency (GHz)	Output DC voltage (mV)	Output Power (dBm)
0.53	168	-23.42
0.9	650	-11.67
1.61	83	-29.55
1.96	120	-26.32
2.11	66	-31.53
2.45	140	-25

The measured output DC voltage and DC power at each operating frequency are listed in Table 7-2. It shows that the greatest DC power harvested is -11.67 dBm at 0.9 GHz. The power acquired from the rectenna is able to power a variety of wearable low power sensors, such as ECG sensors [22] [23], spirometers [24], gas sensors [25] and GPS sensors. In future developments, the proposed energy harvesting system can be applied as a power source for wireless body sensing networks in various fields, such as real-time health monitoring and personnel locating for special professions.

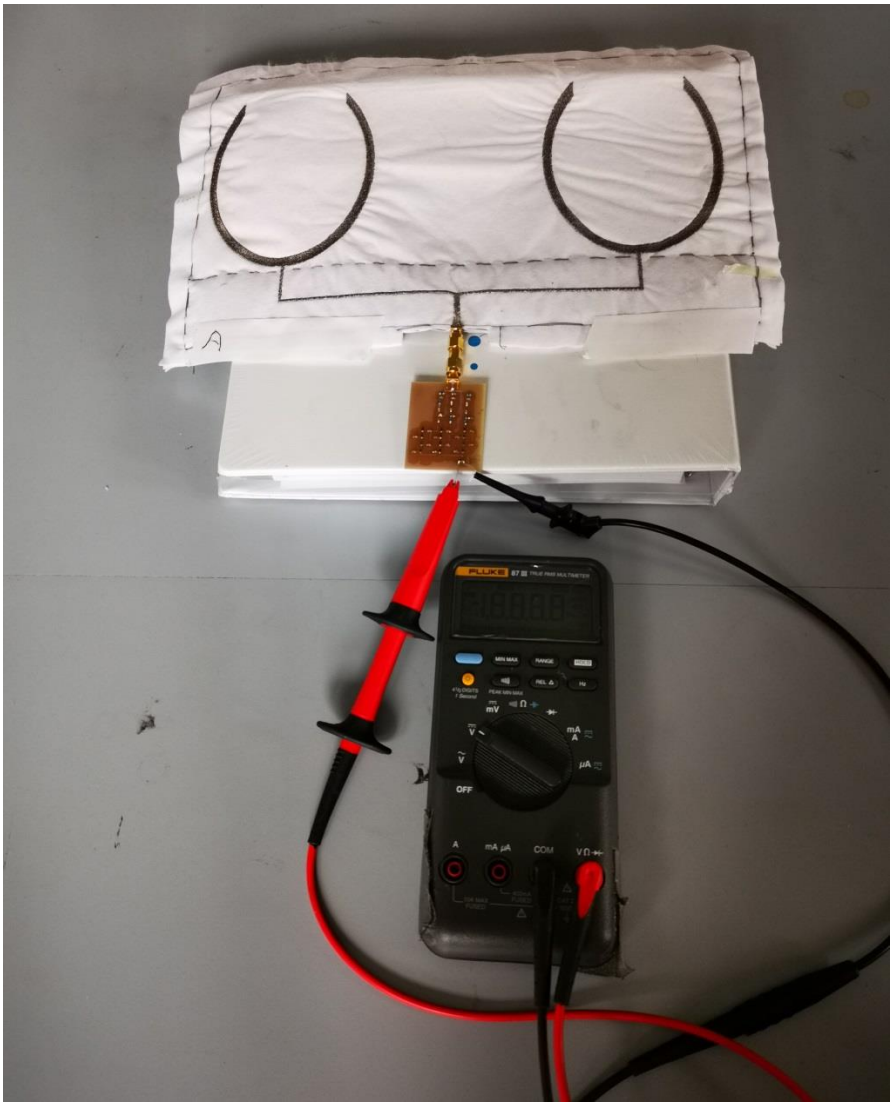

(a)

(b)

Fig. 7-13. Experimental setup of wireless power transfer

7.5. Conclusion

This paper has presented design, fabrication and measurements of a six-band operating e-textile integrated RF energy harvester. The reported device is integrated with daily garments, aiming for an environmental-friendly and steady power source for wearable sensors.

The measurement results have shown that the e-textile antenna array has a broadband operation that cover most of the ambient RF generators, and the six-band rectifier connected to the antenna operates at corresponding frequency bands, which has a tested maximum conversion efficiency of 60.02% and 23.23% at -10 dBm and -20 dBm input power, respectively. The harvester is able to generate highest DC power of -11.67 dBm with an ambient power source at a single frequency (0.9 GHz). It is believed that the wearable energy harvesting system reported here would make great contribution to BSN and personal health care.

7.6. References

[1] Gonçalves, Carlos et al. "Wearable E-Textile Technologies: A Review On Sensors, Actuators And Control Elements". Inventions, vol 3, no. 1, 2018, p. 14. MDPI AG, doi:10.3390/inventions3010014.

[2] M. A. Hanson et al., "Body Area Sensor Networks: Challenges and Opportunities," in Computer, vol. 42, no. 1, pp. 58-65, Jan. 2009, doi: 10.1109/MC.2009.5.

[3] Yao, Shanshan et al. "Nanomaterial-Enabled Wearable Sensors For Healthcare". Advanced Healthcare Materials, vol 7, no. 1, 2017, p. 1700889. Wiley, doi:10.1002/adhm.201700889.

[4] Hatamie, Amir et al. "Review—Textile Based Chemical And Physical Sensors For Healthcare Monitoring". Journal Of The Electrochemical Society, vol 167, no. 3, 2020, p. 037546. The Electrochemical Society, doi:10.1149/1945-7111/ab6827.

[5] E. Kańtoch and P. Augustyniak, "Human activity surveillance based on wearable body sensor network," 2012 Computing in Cardiology, Krakow, 2012, pp. 325-328.

[6] G. Medrano and Li, Xian, and Ye Sun. "WearETE: A Scalable Wearable E-Textile Triboelectric Energy Harvesting System For Human Motion Scavenging". Sensors, vol 17, no. 11, 2017, p. 2649. MDPI AG, doi:10.3390/s17112649.

[7] Zhang, Mingchao et al. "Printable Smart Pattern For Multifunctional Energy-Management E-Textile". Matter, vol 1, no. 1, 2019, pp. 168-179. Elsevier BV, doi:10.1016/j.matt.2019.02.003.

[8] Balpande, Suresh S. et al. "Development Of Strain Energy Harvester As An Alternative Power Source For The Wearable Biomedical Diagnostic System". Micro & Nano Letters, vol 14, no. 7, 2019, pp. 777-781. Institution Of Engineering And Technology (IET), doi:10.1049/mnl.2018.5250.

[9] Lemey, Sam et al. "Wearable Flexible Lightweight Modular RFID Tag With Integrated Energy Harvester". IEEE Transactions On Microwave Theory And Techniques, vol 64, no. 7, 2016, pp. 2304-2314. Institute Of Electrical And Electronics Engineers (IEEE), doi:10.1109/tmtt.2016.2573274.

[10] S. Gomes et al., "Ultra-small energy harvesting microsystem forbiomedical applications," in Proc. 2014 44th European MicrowaveConf., Rome, pp. 660–663. doi: 10.1109/EuMC.2014.6986520.

[11] Xu, Guoyue et al. "Harvesting Electromagnetic Energy In Air: A Wireless Energy Harvester At 2.45 Ghz Using Inexpensive Materials". IEEE Microwave Magazine, vol 21, no. 6, 2020, pp. 88-95. Institute Of Electrical And Electronics Engineers (IEEE), doi:10.1109/mmm.2020.2979357.

[12] M. Piñuela, P. D. Mitcheson, and S. Lucyszyn, "Ambient RF energy harvesting in urban and semi-urban environments," IEEE Trans. Microw. Theory Techn., vol. 61, no. 7, pp. 2715–2726, July 2013. doi: 10.1109/TMTT.2013.2262687.

[13] A. Abdelraheem, M. Sinanis, S. Hameedi, M. Abdelfattah, and D. Peroulis, "A flexible virtual battery: A wearable wireless energy harvester," IEEE Microw. Mag., vol. 20, no. 1, pp. 62–69, Jan. 2019. doi: 10.1109/MMM.2018.2875629.

[14] Borges, Luís M. et al. "Radio-Frequency Energy Harvesting For Wearable Sensors". Healthcare Technology Letters, vol 2, no. 1, 2015, pp. 22-27. Institution Of Engineering And Technology (IET), doi:10.1049/htl.2014.0096.

[15] V. Talla, S. Pellerano, H. Xu, A. Ravi and Y. Palaskas, "Wi-Fi RF energy harvesting for battery-free wearable radio platforms," 2015 IEEE International Conference on RFID (RFID), San Diego, CA, 2015, pp. 47-54, doi: 10.1109/RFID.2015.7113072.

[16] D. Masotti, A. Costanzo and S. Adami, "Design and realization of a wearable multi-frequency RF energy harvesting system," Proceedings of the 5th European Conference on Antennas and Propagation (EUCAP), Rome, 2011, pp. 517-520.

[17] S. Nguyen and R. Amirtharajah, "A hybrid RF and vibration energy harvester for wearable devices," 2018 IEEE Applied Power Electronics Conference and Exposition (APEC), San Antonio, TX, 2018, pp. 1060-1064, doi: 10.1109/APEC.2018.8341146.

[18] Naresh B., V. K. Singh and V. Bhargavi, "Dual band RF energy harvester for wearable electronic technology," 2017 Third International Conference on Advances in Electrical, Electronics, Information, Communication and Bio-Informatics (AEEICB), Chennai, 2017, pp. 274-277, doi: 10.1109/AEEICB.2017.7972428.

[19] C. Song et al., "A Novel Six-Band Dual CP Rectenna Using Improved Impedance Matching Technique for Ambient RF Energy Harvesting," in IEEE Transactions on Antennas and Propagation, vol. 64, no. 7, pp. 3160-3171, July 2016, doi: 10.1109/TAP.2016.2565697.

[20] Caloz, Christophe, and Tatsuo Itoh. Electromagnetic Metamaterials. John Wiley & Sons, 2013, pp. 193-205.

[21] Kim, Phirun et al. "A DUAL-BAND RF ENERGY HARVESTING USING FREQUENCY LIMITED DUAL-BAND IMPEDANCE MATCHING". Progress In Electromagnetics Research, vol 141, 2013, pp. 443-461. EMW Publishing, doi:10.2528/pier13061704.

[22] C. Park, P. H. Chou, Y. Bai, R. Matthews and A. Hibbs, "An ultra-wearable, wireless, low power ECG monitoring system," 2006 IEEE Biomedical Circuits and Systems Conference, London, 2006, pp. 241-244, doi: 10.1109/BIOCAS.2006.4600353.

[23] R. F. Yazicioglu et al., "Ultra-low-power wearable biopotential sensor nodes," 2009 Annual International Conference of the IEEE Engineering in Medicine and Biology Society, Minneapolis, MN, 2009, pp. 3205-3208, doi: 10.1109/IEMBS.2009.5333154.

[24] J. Dieffenderfer et al., "Low-Power Wearable Systems for Continuous Monitoring of Environment and Health for Chronic Respiratory Disease," in IEEE Journal of Biomedical and Health Informatics, vol. 20, no. 5, pp. 1251-1264, Sept. 2016, doi: 10.1109/JBHI.2016.2573286.

[25] H. Li, X. Mu, Y. Yang and A. J. Mason, "Low Power Multimode Electrochemical Gas Sensor Array System for Wearable Health and Safety Monitoring," in IEEE Sensors Journal, vol. 14, no. 10, pp. 3391-3399, Oct. 2014, doi: 10.1109/JSEN.2014.2332278.

Chapter 8 Conclusions and Future Work

8.1. Conclusions

This thesis focuses on the development of e-textile antennas and antenna integrated electronic devices. The design, fabrication, electronic properties and performance of e-textile integrated antennas including NFC antennas, a UHF RFID antenna, a wideband monopole antenna and a broadband dual antenna array have been under research. Based on the e-textile NFC tag, a wireless body temperature and humidity sensing device has been developed, and the sensing performance under various circumstances and potential application of the device have been investigated. A body-worn RF energy harvesting system has been proposed based on the e-textile dual antenna array with integration of a six-band RF rectifier, and the RF-to-DC conversion performance at 6 frequency bands has been presented. Detailed conclusions and key findings are shown in the following sections.

8.1.1. e-Textile embroidered wearable NFC antennas and wireless powered NFC body temperature and sweat sensing system

Since an e-textile NFC antenna for everyday wear might be constantly under external forces such as bending, it requires a wider operation bandwidth than conventional NFC tags to maintain a stable read range. It has been found that a lower inductance of an NFC coil results in a lower antenna quality factor (Q) and therefore a wider bandwidth. Moreover, a lower inductance value of an NFC tags usually means a smaller size, which makes the tags easier to wear and affected less from bending and stretching. The proposed e-textile NFC tag in this thesis has a 10 dB bandwidth of 3.787 MHz and a Q factor of 8.85. The best read range of the tag is 5.57 cm and 6.09 cm while matched to an NXP diode (NXP SL2S2102FTB) and an NFC transponder (RF430FRL152H), respectively, and tag is able to be read within 0.5cm when it is completely folded (180° bending angle).

The sensing device based on an e-textile antenna proposed in this thesis has applied two sensors: a built-in temperature sensor within the NFC transponder (RF430FRL152H) and an external humidity sensor (HIH-5031, Honeywell). Since the humidity sensor operates at a higher voltage level (3 V) than the minimum antenna voltage (1.5 V), a voltage booster (modifies 4-time Dickson charge pump) is modified and applied to increase the antenna

output voltage at the longest read distance up to 5.32 V. As a result, both temperature and sweat sensors powered wirelessly by the reader are able to realize real-time reading and to provide accurate results. Potential real-life applications relating to this smart textile sensing device, including mobile application and wound healing monitoring, have also been proposed.

8.1.2. e-Textile embroidered UHF RFID antenna

A machine embroidered UHF RFID antenna has been proposed. The RFID antenna is designed to be conjugate matched with the microchip over a wide bandwidth (840-1343 MHz). Comparing to conventional metal material, e-textile material possesses relatively higher sheet resistance which leads to a lower expected efficiency. Therefore, in order to reach a maximum read distance, a high embroidery density is applied in the fabrication process, and the obtained average sheet resistance of the antenna is 0.4 Ω/sq. In measurements, the proposed antenna achieves a long and steady read range (6.5-7.23 m) over the RFID band (860-960 MHz) and performs well while placed on human body with the best read distance of 4.71 m.

8.1.3. e-Textile Integrated Wideband Monopole Antenna for Body-worn Energy Harvesting Systems

A receiving antenna working in a wide bandwidth is desirable in a wearable RF energy harvesting system so that it can harvest power from multiple ambient RF frequency bands and obtain relatively high output power. An e-textile monopole antenna, designed in a slotted circular patch structure which achieves a working bandwidth from 0.51 GHz to 5 GHz, is proposed in this thesis. Despite the material loss, the antenna is able to achieve high efficiency over the wide operating bandwidth. The measured gains at four selected frequencies (0.7 GHz, 1.7 GHz, 2.4 GHz and 3.6 GHz) are 2.73 dBi, 3.56 dBi, 2.17 dBi and 5.64 dBi, respectively. The realized gain tends to increase at higher frequencies from 3 GHz to 5 GHz, which makes it particularly suitable to be applied in an RF energy harvester to compensate the higher loss of rectifiers at higher frequencies.

8.1.4. A Novel Body-worn Energy Harvesting System based on e-textile Antenna Array and compact Multiband Rectifier

To further investigate in the application of wearable RF energy harvesting, a novel e-textile integrated rectenna is proposed. The receiving antenna is designed as a dual monopole

antenna array in order to achieve a higher gain for higher energy harvesting efficiency. The proposed antenna structure is in a slotted plier shape, which restricts the usage of e-textile material while obtaining a broad operating bandwidth (0.56-5 GHz) within the frequency range up to 5 GHz. A modified six-band RF rectifier is designed for RF-to-DC power conversion for the most occupied ambient RF frequency bands, the performance of which is steady over the wide frequency range. The rectifier is tested to be most efficient at 900 MHz with maximum conversion efficiency of 60.02% and 23.23% at -10 dBm and -20 dBm input power, respectively. With an ambient power source at this frequency, the integrated harvester is able to generate a highest DC power of -11.67 dBm.

8.2. Key contributions

- Development of various novel e-textile antenna structures (NFC, UHF RFID, monopole, and array).
- Detailed study of e-textile characteristics: electrical properties, performance under bending, pressure and skin contact.
- Optimizing antenna performance by fully considering the unique properties of textile material in the design process: all proposed antennas possess relatively wide bandwidth, which stabilizes the performance when the antenna circuit is under external forces.
- Development of sensing and wireless powering devices based on e-textile antennas, including wireless power NFC sensing device and wearable RF energy harvester.
- Modification of the Dickson Charge Pump structure for high frequency AC voltage boosting.

8.3. Limitations and future work

Although the far field wearable antennas proposed in Chapter 6 and 7 have performed decently in measurements, in on-body applications, the radiated signal from the antennas could be easily absorbed by human body, which would affect the antenna performance on different levels. In future research, it would be necessary to develop an RF blocking layer between the antenna and body in order to ensure the functionality of the wearable circuitry. Metasurface is considered a desirable choice for this layer, which is a two-dimensional arrangement of subwavelength scatterers that controls the propagation of optical waves. The

planar structure of metasurface is significantly more suitable for integration with wearable antennas than traditional L-C RF signal blocking devices. In recent research, metasurface has been applied to reduce mutual coupling between antenna elements in [1], and applied as a retroreflector in [2].

So far, the e-textile antennas proposed in this work have mainly focused on HF (high frequency) (13.56 MHz), UHF (ultra-high frequency) band from 860 MHz to 960 MHz and microwave frequencies up to 5 GHz. However, with the vast development of 5G technology, it can be predicted that most of the future wireless communication will operate in higher frequency bands such as EHF (extremely high frequency) band from 30 GHz to 300 GHz. Therefore, it would be constructive to expand the research of e-textile antenna design in this work to higher frequency bands. Due to the compact structure of antennas working at such frequencies, the precision of embroidery in the fabrication process would require a higher standard.

There are limitations existing in the research of RF energy harvesting system proposed in Chapter 7. First of all, the ambient RF power is unstable regarding different locations which cannot ensure the constant functionality of the harvesting device. To solve this problem, a small-sized supercapacitor [3] can be integrated at the load of the harvesting system as a power collecting battery, which ensures wearable electronics powered by this device to work stably and constantly. This method would greatly benefit future integration of low power body sensors in this system and how the sensors perform while powered by the harvester. Secondly, the simulation and experimental results of the rectifier efficiency are not consistent with each other as well as expected. This is because the SPICE parameter and packaging parasitic elements of the ADS diode model were created for small signals with a limited frequency range, which are not perfectly suitable for the case where the frequency and power of the signals vary significantly. In future research, real-data based diode model loaded with the voltage over current (I/V) and electric charge over voltage (Q/V) functions can be developed in order to obtain more accurate simulation results.

Furthermore, due to low power level of ambient sources, the energy harvested by an e-textile rectenna is limited and only able to supply electronics with low input power requirements. For future improvements, the RF energy harvester could be combined with other types of e-textile powering devices, such as the e-textile triboelectric energy harvesting system proposed in [4]. Finally, the rectifier currently proposed for the RF harvester is a conventional PCB

circuit. In further research, an e-textile rectifier is expected to be developed where the electrical components are interconnected using seamlessly embroidered conductive threads on textile substrate, which would realize full textile applications. The main challenge exists in this idea is that such e-textile circuits can be easily broken in the connection points.

8.4. References

[1] M. Badawe, T. Almoneef and O. Ramahi, “A True Metasurface Antenna”, Sci Rep 6, 2016, doi:10.1038/srep19268

[2] Arbabi, Amir et al. "Planar Metasurface Retroreflector". Nature Photonics, vol 11, no. 7, 2017, pp. 415-420. Springer Science And Business Media LLC, doi:10.1038/nphoton.2017.96.

[3] Shown, Indrajit et al. "Conducting Polymer‐Based Flexible Supercapacitor". Energy Science & Engineering, vol 3, no. 1, 2014, pp. 2-26. Wiley, doi:10.1002/ese3.50.

[4] G. Medrano and Li, Xian, and Ye Sun. "WearETE: A Scalable Wearable E-Textile Triboelectric Energy Harvesting System For Human Motion Scavenging". Sensors, vol 17, no. 11, 2017, p. 2649. MDPI AG, doi:10.3390/s17112649.